Author Queries

AQ1	OK as changed?
AQ2	Should this be “Chapter 1”?
AQ3	Delete? This is ch. 2. Chapter 7 is on the solar interior.
AQ4	Please check the chapter number.
AQ5	Chapter 1 is on the solar wind.
AQ6	Please check if this should be “Chapter 5.”
AQ7	Should this be “Chapter 3”? This is Chapter 2.
AQ8	Should this be “Chapter 6”?
AQ9	Should this be “Chapter 1”? Chapter 1 is on solar flares.
AQ10	Should this be “Chapter 1”?
AQ11	Should this be “Chapter 1”?
AQ12	Please include the article titles for all the missing entries.
AQ13	Authors name added. Check.
AQ14	Authors name added. Check.
AQ15	Authors name added. Check.
AQ16	Authors name added. Check.
AQ17	Authors name added. Check.
AQ18	Authors name added. Check.
AQ19	Authors name added. Check.
AQ20	Provide publisher and place of publication.

2

The Heating of the Solar Corona

N. M. Viall[1], I. De Moortel[2,3], C. Downs[4], J. A. Klimchuk[1], S. Parenti[5], and F. Reale[6]

ABSTRACT

The solar corona, the outer atmosphere of the Sun, is heated to millions of Kelvin. This is several orders of magnitude hotter than the photosphere, the optical surface of the Sun, below, and a mystery that has baffled scientists for centuries. The answer to the question of how the solar corona is heated lies in the crucial magnetic connection through the atmosphere of the Sun. The magnetic field that threads the corona extends below the solar photosphere, where convective motions drag the magnetic field footpoints, tangling and twisting them. The chromosphere is the atmospheric layer above the photosphere, and the magnetic field provides an important connection between these layers. The exchange of mass and energy between the chromosphere and the corona is an essential piece of this puzzle. The connection between the chromosphere and the corona is a challenging piece of the puzzle both observationally and computationally, as it is highly complex in space and time. We describe the history of the observations and the theoretical understanding of the heating of the solar atmosphere, and end with future prospects of solving the coronal heating problem.

2.1. HISTORICAL VIEWPOINT ON THE CORONAL HEATING PROBLEM

The outer atmosphere of the Sun starts at the photosphere, the optical surface of the Sun, followed by the chromosphere, a thin transition region, and ends in a hot corona above. Understanding the heating of the solar atmosphere is important for understanding the fundamental physical processes governing our star, and also for understanding the space weather effects on Earth's atmosphere and ionosphere. Planetary ionospheres in general are created by the ionization of their atmosphere by ultraviolet (UV) and X-ray emissions from their parent star. This makes understanding these emissions important for understanding stellar coronae and exoplanetary systems in general, as well as space weather at other planets in our solar system. Radiation at UV and X-ray wavelengths also heats Earth's mesosphere, impacting the drag on spacecraft orbiting at these altitudes. Solar emission at these wavelengths exhibit large changes over short timescales in the case of flares (see Chapter 4), or more slowly, as the solar atmosphere and its heating evolve over the 11-year sunspot cycle (see Chapter 3). Lastly, the acceleration of the solar wind (see Chapter 7) plasma that fills the solar system is closely tied to the physics of the heating of the solar atmosphere and the hot corona.

[1] *NASA Goddard Space Flight Center, Greenbelt, Maryland, United States*

[2] *School of Mathematics and Statistics, University of St Andrews, St Andrews, Fife, United Kingdom*

[3] *Rosseland Centre for Solar Physics, University of Oslo, Norway*

[4] *Predictive Science Inc., San Diego, California, United States*

[5] *Université Paris-Saclay, CNRS, Institut d'Astrophysique Spatiale, Orsay, France*

[6] *Dipartimento di Fisica & Chimica, Universitá di Palermo, Palermo, Italy*

Space Physics and Aeronomy Collection Volume 1: At the Doorstep of Our Star: Solar Physics and Solar Wind, Geophysical Monograph 258, First Edition. Edited by Nour E. Raouafi and Angelos Vourlidas.

DOI: 10.1002/9781119507512.ch2

Figure 2.1 A total solar eclipse viewed in white light from Earth. (*Source*: S. Habbal, M. Druckmüller and P. Aniol, NASA/GSFC, taken on 20 March 2015 from Svalbard, Norway.)

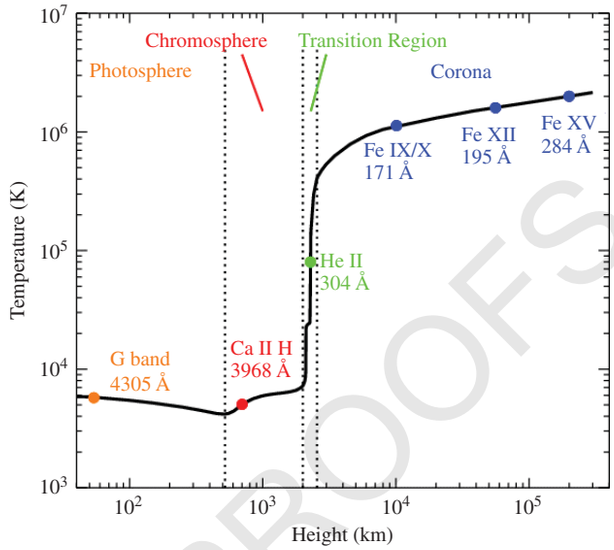

Figure 2.2 Plotted is a typical temperature as a function of height defining the different layers of the solar atmosphere. The mean formation heights of several commonly used spectral bands and lines are shown for reference. (*Source*: Yang et al., 2009. © 2009.)

The corona has been observed for millennia from total solar eclipses, such as the total solar eclipse observed from Svalbard, Norway, on 20 March 2015, shown in Figure 2.1. Total solar eclipses occur when the Moon crosses in between the Sun and Earth, blocking the emission from the Sun's photosphere, which is 10^5–10^6 times brighter in white light emission than the Sun's corona. Amazingly, only in the last centuries was it realized that the corona belongs to the Sun, and not to the Moon. In 1605, Hannes Kepler speculated that the corona surrounded the Sun, and after a total solar eclipse in 1724, Giacomo Filippo Maraldi concluded that the corona was indeed part of the Sun, because the Moon was observed to traverse the Sun.

With the advent of spectroscopy, important aspects of the solar atmosphere were revealed. Work by Grotrian (1939) and Edlén (1943) identified forbidden lines in the emission spectra of the corona, and it was recognized that these lines required highly ionized species. See Peter and Dwivedi (2014) for a review of these measurements and their historical context. Helium was later identified in a yellow spectral line in the optical spectrum in a prominence observation in 1868 (Kochhar, 1991), 10 years before it was identified on Earth (Palmieri, 1881). Also, a strong green emission line emerged in the optical spectrum, identified during the 1869 solar eclipse by Young and Harkness, which was of unknown origin. It was temporarily identified as a new element, coronium, in analogy to helium. It took nearly 60 years for scientists to conclude that the corona is not made in the same way as the underlying chromosphere and photosphere: the green line was ultimately identified as a forbidden line of the highly ionized iron (Fe XIV). This highly ionized state of iron requires extremely high temperatures, and so it was then realized that the corona is extremely hot, at temperatures above 1 million K, more than a hundred times the temperature of the photosphere. Although the energy source must be the flows in the convection layer of the Sun (see Chapter ~~2~~; solar interior), the heat cannot be simply conducted from below. AQ3

In Figure 2.2, we illustrate this extreme temperature gradient by showing a typical temperature gradient as a function of height (adapted from Yang et al., 2009). Also plotted are several commonly used spectral bands and lines at their mean formation height. The photosphere is the lowest layer, where the gas transitions from optically thick to optically thin; most solar optical light is from this layer. The next layer is the solar chromosphere, followed by a thin transition region and, finally, the solar corona, which is several orders of magnitude hotter than the chromosphere and photosphere below.

Thus, the problem of coronal heating was born. The questions became: What makes the corona so hot? What is the carrier that transports the solar energy to the corona? Once that energy reaches the corona, how is it dissipated? At temperatures above 1 million K most of the energy is radiated in the extreme ultra violet (EUV) and X-ray band, but these wavelengths cannot be observed from the ground, because they are absorbed by the terrestrial atmosphere. Before technology allowed the launch of telescopes with the capabilities of observing these wavelengths in outer space, the first hypotheses for coronal heating were made. The transport and subsequent dissipation of energy by waves was first considered

as a potential heating mechanism for the solar atmosphere. Both Biermann (1946) and Schwarzschild (1948) realized that the "noise" (acoustic waves) emitted by the convection zone would propagate into the solar atmosphere and could be a possible energy source to heat the chromosphere and corona (see, e.g., Narain & Ulmnschneider 1990, 1996; Stein & Leibacher, 1974, for a review). The idea was that acoustic waves coming up from the solar surface and generated by the solar granulation are similar to a field of pistons. According to this theory, the waves steepen into shock waves while traveling in the chromosphere and eventually dissipate, releasing their energy in the corona. Detailed steady-state models were developed that treated the whole corona as a uniformly stratified medium, also known as a plane-parallel atmosphere. At this point, it was thought that the magnetic field had only the role of shaping the visible structures because of preferential heat conduction along the field lines (see review by Kuperus, 1969). Although it seems that acoustic waves do play a role in chromospheric heating, their energy is dissipated before they reach the corona, and they do not directly contribute to coronal heating. Alfvén (1947), on the other hand, suggested that magnetohydrodynamic (MHD), or Alfvén, waves could be a prime candidate for supplying energy to the solar atmosphere (see, e.g., Hollweg, 1978, or Wentzel, 1974). MHD waves remain prime candidates for heating throughout the solar atmosphere and into the solar wind.

The breakthrough for the coronal heating problem came from solar X-ray observations during the Space Age, when it first became clear that the active region (AR) and quiet Sun (QS) corona comprise magnetically confined plasma, and that a plane-parallel atmosphere is not an accurate model. The first observations were made from rocket flights above the atmosphere. Pinhole cameras had arcmin (arc minute = 1/60th of a degree) resolution and revealed that intense X-ray emission comes from localized and relatively small regions of activity. The localized regions of X-ray emission were observed to be correlated with H-alpha and Ca-K plages, which themselves are chromospheric bright patches associated with concentrations of magnetic field, and also correlated with radio emission (see review by Peres & Vaiana, 1990). The quantum leap occurred with the development of grazing incidence optics for X-ray astronomy by Riccardo Giacconi's group in the 1960s (e.g., Giacconi & Rossi, 1960). X-ray photons were reflected by grazing metallic coaxial and confocal surfaces at very small angles of a few degrees. Grazing incidence observations improved continuously and in the late 1960s achieved a spatial resolution below the arcmin threshold to a few arcseconds (1 arcsec = 1/60th arcmin). This was sufficient to localize the most intense emission between concentrated regions of opposite magnetic polarity, ARs, showing the crucial role that the magnetic field plays in coronal heating.

Already from the early extensive rocket program, the morphology of the corona was firmly established: bright arch-like structures connecting regions of opposite photospheric magnetic polarity—called coronal loops—are the fundamental features of the corona (Vaiana et al., 1968, 1973). However, coronal magnetic field measurements were not yet possible, and so this alignment could not be established directly. Later it was largely confirmed by models that extrapolate the photospheric field into the corona (Poletto et al., 1975). With the extrapolation, it became clear that the magnetic pressure is much higher than the thermal pressure in the corona, high enough to confine the hot coronal plasma (see Chapter 3). AQ4

Further progress was made when the observations from telescopes onboard satellite missions allowed for temporal coverage in the X-ray and EUV beyond a few minutes. This was the case of the Skylab mission in 1973–1974, which allowed the study of the evolution of ARs, coronal holes, and very small bright points (Golub et al., 1975). It was confirmed that the bright corona is entirely made up of magnetic loops of all sizes confining hot plasma. Coronal holes correspond instead to ~~unipolar~~ regions in the photosphere, where the magnetic field opens to interplanetary space, and are therefore the natural source of the high-speed solar wind (Krieger et al., 1973, and see Chapter ~~7~~). AQ5

X-ray observations of the solar corona opened a new scenario for the physics of the solar corona and the problem of coronal heating: modeling the atmosphere as individual loops. Figure 2.3 shows a comparison of an X-ray image taken in 3–60 Å on 7 March 1970 from an Aerobee rocket (VanSpeybroeck et al., 1970) with an X-ray image of the Sun taken with Hinode XRT (Golub et al., 2007) in the Al-mesh filter on 26 February 2014, to illustrate the advancement of X-ray imaging. A first classification of loops was attempted to connect the maximum plasma temperature and the pressure at the base of the corona with the size of the loops, and the underlying photosphere and chromosphere structures. It was determined that coronal loop heights are typically in the range between 1,000 km up to more than 100,000 km. With observations in different filters, it became possible to measure densities in the corona of 10^7–10^{10} cm^{-3}, and temperatures of 1 to 4 million K, exceeding 10 million in flares. The intensity of the observed X-ray emission is directly correlated with the field complexity of the underlying magnetic field. These conditions determined the basis for a new investigation of coronal heating. Although the energy from the mechanical motions in the convection zone below the photosphere is crucial, the magnetically structured corona indicates that the key is

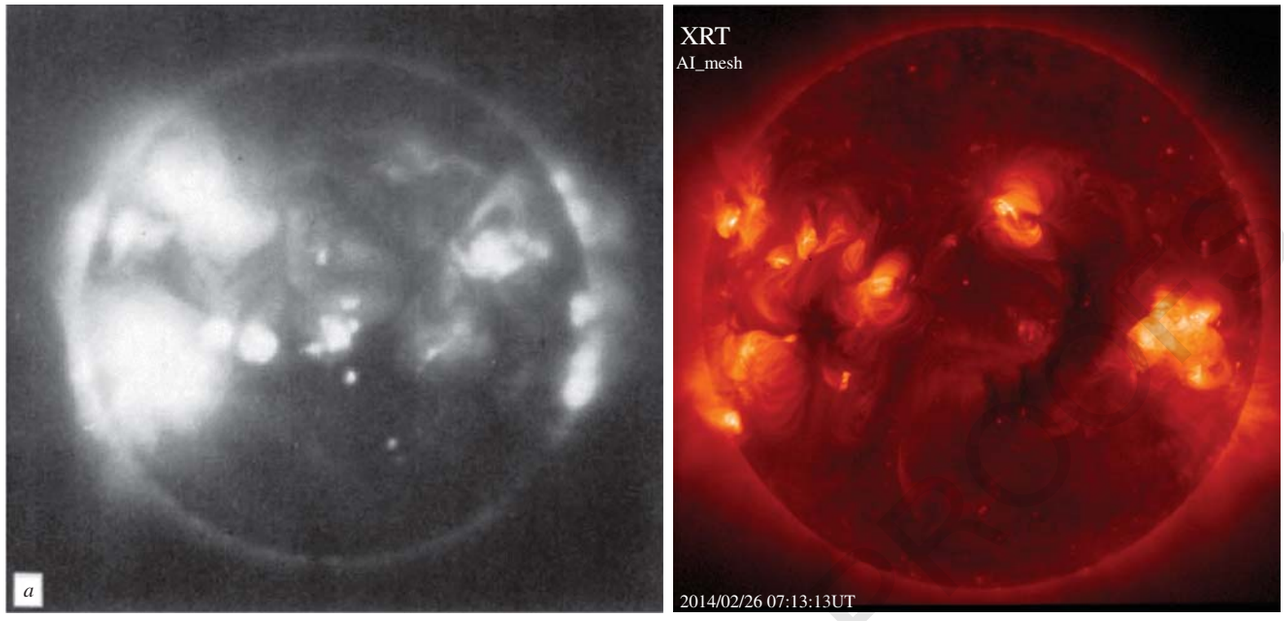

Figure 2.3 Left shows an X-ray image taken on 7 March 1970 from an *Aerobee* rocket; right shows an X-ray image taken on 26 February 2014, with Hinode XRT in the Al-mesh filter. (*Source*: (Left) Image from Van Speybroeck et al., 1970; (Right) Image courtesy of Smithsonian Center for Astrophysics, JAXA, and NASA.)

the conversion of magnetic energy into heat. Indeed, estimates of the Poynting flux associated with photospheric magnetic footpoint motions indicate there is more than enough energy available to account for both the chromospheric and coronal energy requirements. For example, Parnell and De Moortel (2012) estimate the Poynting flux to be on the order of 2.5×10^7erg cm^{-2} s^{-1} to 2.5×10^9 erg cm^{-2} s^{-1} in QS and AR corona, respectively (see also, e.g., Klimchuk, 2006).

In coronal conditions, the plasma is highly ionized and magnetized. Plasma particles spiral around the field lines with a typical gyroradius of about 10 cm, and their mean free path at 1 million K and a density of 10^9 cm^{-3} is about 100 km, both shorter than the typical length of coronal structures. The particles are therefore free to move only along the field lines, and the confined plasma can be described as a compressible fluid. At a million K, thermal conduction for a fully ionized gas is strongly guided by the magnetic field; that is, it is very efficient along the field lines, but strongly inhibited across them (Spitzer, 1962). The thermal conduction coefficient has a steep dependence on the temperature ($T^{5/2}$) and becomes extremely efficient above 1 million K. Therefore, if we consider a closed magnetic structure, the plasma confined in it moves and transports energy mostly along the magnetic field lines. Each loop is therefore dynamically and thermally insulated from the others. This was a radical change of view for the solar atmosphere: the corona is no longer described by a single stratified atmosphere, but it is structured into a collection of a myriad of independent atmospheres, each contained in single coronal loop flux tubes.

Recent progress has been more gradual and extensively employed physical models of the loop atmosphere. One difficulty has been the inability to localize the heating. The efficient thermal conduction (possibly combined with mass flows) immediately redistributed energy along the magnetic field, so evidence of localization is rapidly lost. The coronal plasma is optically thin, and its emission is a function of the product of the temperature and the square of the density, so the bright regions are typically the densest regions, not necessarily the hottest, though the two parameters are related. Figure 2.4 shows a composite image of the solar corona taken by the Solar Dynamics Observatory's Atmospheric Imaging Assembly. The images were taken at nearly the same time in the 211 Å (red), 193 Å (green), and 171 Å (blue) filters. The 211 Å channel peak sensitivity is to plasma around 2 MK; the 193 Å channel peak sensitivity is around 1.5 MK; and the 171 Å channel peak sensitivity is around 0.8 MK. Bright, dense ARs are visible, as well as darker, cooler coronal holes at the poles of the Sun.

As a starting point for modeling a coronal loop, long-term X-ray observations showed that the lifetimes of the X-ray bright coronal loops are generally significantly larger than the cooling times for radiation and thermal conduction. The implication is that the heating powering the loops must be rather continuous. As a result,

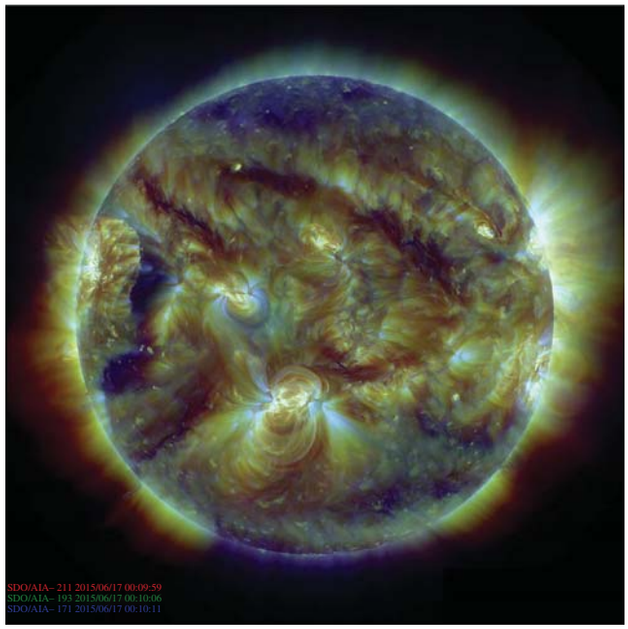

Figure 2.4 Shown is a composite image from the ~~Solar Dynamics Observatory~~. Three images of the Sun taken at nearly the same time with the ~~Atmospheric Imaging Assembly~~ are superimposed. From hotter to cooler plasma, images taken in the 211 Å (red), 193 Å (green), and 171 Å (blue) channels are shown. Bright, dense active regions (ARs) are visible, as are darker, cooler coronal holes at the poles of the Sun. (*Source*: Courtesy of NASA/GSFC.)

coronal loops were systematically described with hydrostatic models, with each loop having unique parameters independent of the others. As a first approximation, gravity can be neglected, so the loop internal structure is essentially dictated by the energy balance between the losses by radiation and thermal conduction and the heating, which can be described as an empirical function of the coordinate along the loop. By solving the equation of energy conservation under the simplifying assumption of a heating distributed uniformly along the loop, it is possible to derive scaling laws connecting important loop parameters, that is, the maximum temperature, the length, the pressure at the loop base, and the heating rate per unit volume (Rosner et al., 1978). These so-called RTV scaling laws were compared with observations and have been a reference point for loop physics for decades.

The first challenge to the RTV scaling laws was that they generally do not apply to the most highly impulsive coronal events: coronal flares. Flares are highly localized explosions where the plasma is heated above 10 million K for a few minutes and often reaches and even overtakes the brightness of the whole remaining corona (see Chapter 4). The observed evolution generally consists of a fast brightening followed by slower decay. Flares are often observed on many other stars, where they can be orders of magnitude more intense that on the Sun. Because their duration is generally small, and the physics is very complex, their investigation required the development of time-dependent hydrodynamic models of plasma confined in a single flux tube. This is the basis for one-dimensional (1D) nanoflare models of coronal heating, described further in section 2.3.2.

From theoretical considerations, Parker hypothesized that the same mechanism that produces solar flares, but with a factor-of-10^9 less energy, could be responsible for heating the corona. In these nanoflares, as they were named, the X-ray corona is heated by dissipation at the many small current sheets forming as a consequence of the continuous shuffling of the footpoints of the field in the photospheric convection (Parker, 1988). Rapid small-scale reconnection of the magnetic field across the discontinuities destroys them as fast as they are created by the motions of the footpoints. The critical angle between the magnetic fields across the current sheet when reconnection occurs can be estimated by relating the Poynting flux associated with the photospheric footpoint motion of the magnetic fields with the energy budget of the corona (Klimchuk, 2006). If the reconnection occurs before this critical angle, then the corona would be cooler than observed, and if the reconnection occurs after this critical angle, then the corona would be hotter than observed. Much attention has then been devoted to studying coronal magnetic reconnection (Priest, 1996) through modeling with detailed magnetic treatment and simplified coronal atmosphere. After first attempts in 2D geometry, it was soon realized that reconnection must be modeled in a 3D geometry to be realistic (Priest, 1999).

The other leading theory of coronal heating, as mentioned above, is through the dissipation of MHD waves. The presence of waves and oscillations of magnetic structures throughout the solar atmosphere has been firmly established by observational evidence. Indeed, recent high-cadence and high-resolution observations have revealed an abundance of waves, oscillations, and other quasi-periodic disturbances present in the solar atmosphere (see, e.g., reviews by Arregui et al., 2012; Arregui, 2015; Banerjee et al., 2007; De Moortel & Nakariakov, 2012; Jess et al., 2015; Mathioudakis et al., 2013; Nakariakov & Verwichte, 2005; Zaqarashvili & Erdélyi, 2009). In most instances, the perturbations have been interpreted in terms of MHD modes, and in many cases, these observed waves are reported to contain a substantial amount of energy.

In the next section, we describe the evidence for different heating mechanisms in the chromosphere and corona and describe the observational diagnostics used.

2.2. OBSERVATIONAL CONSTRAINTS ON CHROMOSPHERIC AND CORONAL HEATING

Currently, observations of the chromosphere and closed-field corona are limited to remote measurements of the Sun. No current or planned mission will reach the predicted height of the closed corona (below ~2.5 solar radii) with in situ measurements. As described above, spectroscopic measurements and images taken in different wavelengths are the primary way that information on the chromosphere and corona is obtained. See Del Zanna and Mason (2018) for a thorough review on spectral diagnostics, especially in combination with imaging techniques, in the UV and X-ray ~~for~~ the solar atmosphere. Magnetic field measurements in the photosphere are regularly obtained; however, chromospheric and coronal magnetic fields are more difficult, though radio observations provide a measure (Shibasaki et al., 2011). The standard practice is to extrapolate the magnetic field from the photospheric measurements into the solar atmosphere, either assuming a potential field source surface (PFSS), or a nonlinear force-free (NLFF) model
AQ7 of the magnetic field (see Chapter ~~2~~ and the review by Wiegelmann & Sakurai, 2012). Recently, the Coronal Multi-Channel Polarimeter (CoMP) instrument (see Tomczyk et al., 2007) has been measuring the coronal magnetic field with a full latitudinal field of view (FOV) in the low corona (~1.03 to 1.5 Rsun), providing important constraints on the magnetic field. Modeling is still required to make a direct comparison between the 3D magnetic field structure and the plasma properties observed in the chromosphere and corona.

From observations, it is clear that the chromosphere is highly complex, ultimately set in motion from the convection below. Figure 2.5, from Judge (2006), Wedemeyer-Böhm et al. (2009), and Wiegelmann et al. (2014), shows the complexity in the atmosphere of a quiet region of the Sun.

The convection zone drives granulation and supergranulation flows that concentrate the magnetic field into network lanes. The plasma beta (the ratio of the plasma pressure to the magnetic pressure) shows that the photosphere and chromosphere are dominated by plasma pressure, whereas the corona is dominated by magnetic pressure. Finally, much of the magnetic field in the chromosphere closes in low-lying loops, and does not connect up into the corona. So, although the connection to the chromosphere is crucial for understanding the corona, there are regions of the chromosphere where the opposite is not always true.

Withbroe and Noyes (1977) estimated the energy required to sustain the chromosphere and corona in the QS, ARs, and coronal holes, based on their typical observed emissions. These are the baseline requirements for the solar atmosphere. It is what observers and theorists have been working to explain for decades. In Table 2.1, we show these estimates of energy in erg cm^{-2} s^{-1} from the chromosphere and the corona.

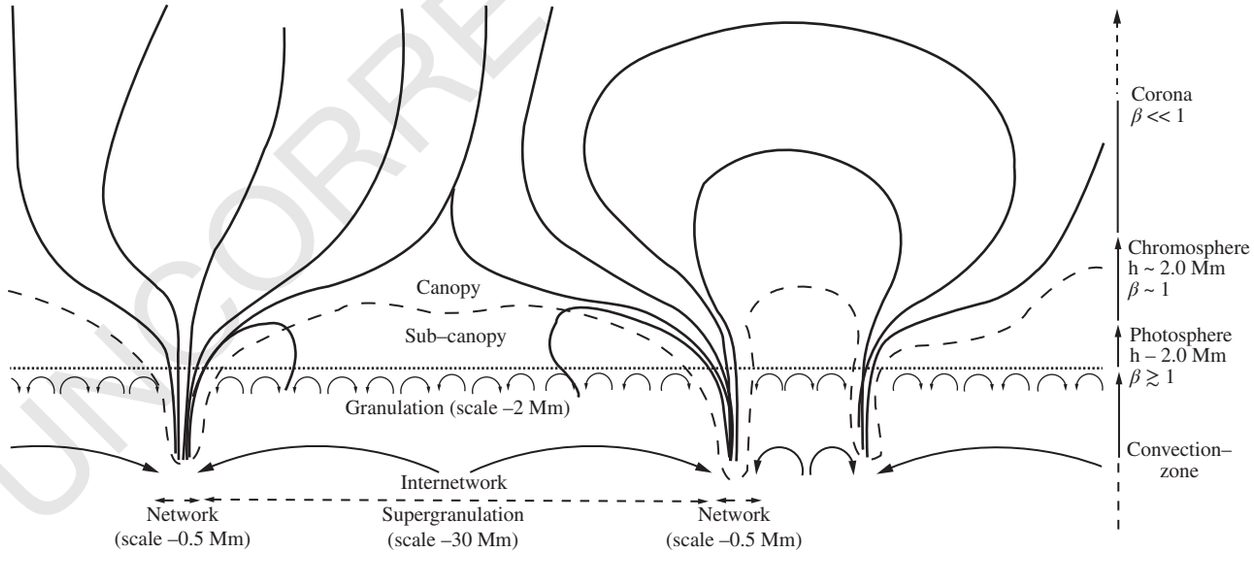

Figure 2.5 This cartoon shows the atmospheric layers of the Sun. Large-scale, supergranular cells concentrate magnetic field in the network, and smaller granulation cells stirs up the internetwork fields. The strongest concentrations of magnetic field in the network expand outward into the corona, whereas the weaker fields close below the corona. Plasma betas at different heights are shown on the right. (*Source*: Wiegelmann et al. 2014. Licensed under CCBY.)

In much of the chapter, we differentiate "wave" heating from "reconnection" heating. The distinction between the two is determined by the timescale of driving and whether the flux tube experiences that driving as a wave or as a slow buildup of energy. The relevant time scale for the flux tube is the length of the flux tube divided by the Alfvén speed in the loop. Energy buildup and dissipation that is shorter than this timescale is an "AC" mechanism, whereas energy buildup and dissipation on longer timescales is "DC" (e.g., Cranmer, 2009; Zirker, 1993). This is a simplified version of the complex physics that occurs in the actual Sun, as we will see in much of the discussion that follows. That is, the two concepts are not mutually exclusive, as magnetic reconnection launches waves, and waves can bring field lines together, forcing the onset of reconnection. Many of their observational signatures are not easily distinguishable, which is one reason why progress has been difficult. Nevertheless, it is still a useful conceptual tool to separate waves from reconnection, and so, where useful, we have done so in what follows.

Table 2.1 Coronal Temperature and Energy Requirements of the Solar Atmosphere.

Location	Quiet Sun (QS)	Coronal Hole	Active Region (AR)
Coronal temperature (K)	1.1–1.6 × 10^6	10^6	2.5 × 10^6
Coronal energy loss (erg/cm^{2}s)	3×10^5	8×10^5	10^7
Chromospheric energy loss (erg/cm^{2}s)	4×10^6	4×10^6	2×10^7

Source: Withbroe and Noyes, 1977. © 1977 by Annual Reviews, http://www.annualreviews.org.

2.2.1. Observations of Chromospheric Heating

The first thing that is immediately obvious from the Withbroe and Noyes (1977) result is that the chromosphere has a much greater energy requirement than the corona, even though the corona is strikingly hotter. The chromosphere is partially ionized, making ion-neutral effects important, and radiates strongly in Lyman alpha, CaII, MgII, and the H^- continuum.

In a more complex version of Figure 2.5, in Figure 2.6, we show a figure adapted from Wedemeyer-Böhm and Wöger (2008) and Wedemeyer-Böhm et al. (2009). This version includes many of the complex observational aspects of the chromosphere. See Wedemeyer-Böhm et al. (2009) for an excellent summary of these phenomena. An important takeaway is that the zoo of phenomena and dynamics that occur in the chromosphere is largely a function of the magnetic domain. For example, fibrils and spicules are associated with the concentrated network fields and intergranular lanes, whereas the wave dynamics and small, weak magnetic loops are associated with the internetwork. Wave propagation connects the

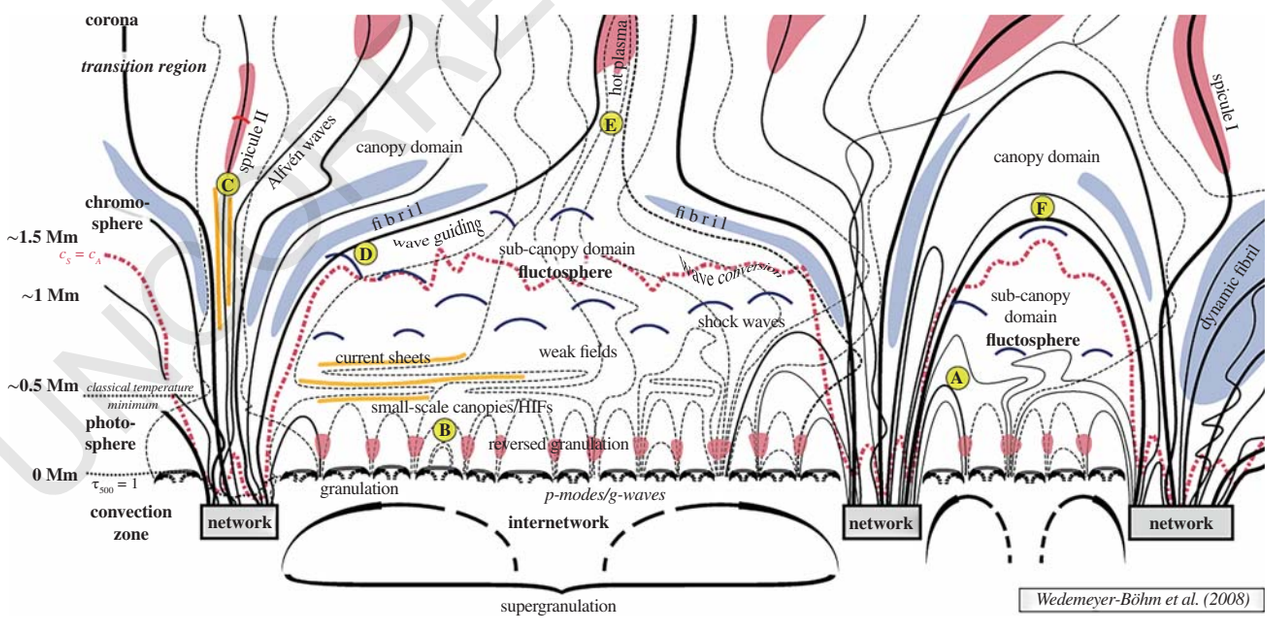

Figure 2.6 Similar to Figure 2.5, with additional complexity of the observations added. (*Source*: Wedemeyer-Böhm et al., 2009. © 2009 Springer Nature.)

different regions in ways that are not immediately clear when looking at the magnetic field connections of Figure 2.5 alone.

2.2.1.1. Observations of Chromospheric Waves

In the chromosphere, magneto-acoustic waves arising from convective flows propagating upward into the solar atmosphere are expected to shock readily, which would lead to strong brightenings and heating as demonstrated, for example, by Carlsson and Stein (1992, 1997). Using Interface Region Imaging Spectrograph (IRIS) and Swedish Solar Telescope (SST) observations of bright grains in internetwork regions in the quiet chromosphere, Martinez-Sykora et al. (2015) suggested that such upward propagating acoustic waves can even reach the transition region as, on occasion, the characteristic sawtooth shock signature can be found in the IRIS Si IV spectra.

In addition to the acoustic mode shocks, observations have revealed a multitude of both compressive and incompressive waves in photospheric and chromospheric structures (see, e.g., Carlsson et al., 1997; Judge et al., 2001; Wikstøl et al., 2000 for early examples using TRACE and SUMER). Here, we will focus on examples that provide direct evidence relevant to heating rather than an exhaustive review of wave observations.

Chromospheric spicules and dynamic fibrils have been widely reported to support a variety of different and complex wave modes. For example, using Hinode data, De Pontieu et al. (2007) reported transverse oscillating ("swaying") spicules with amplitudes of around 10–25 km/s and periods on the order of 100–500s. These "Alfvénic" waves contain a substantial amount of energy flux, potentially sufficient to heat the QS corona and/or accelerate the solar wind (assuming a transmission coefficient of energy from the chromosphere to the corona of about 3%). Numerical simulations by Martinez-Sykora et al. (2017) show a natural association between (type II) spicules and transverse waves from the rapid release of magnetic tension. Analyzing transverse motions along a large number of spicules, Okamoto and De Pontieu (2011) found a complex interplay between upward and downward propagating waves as well as standing waves, where it is suggested that the upward propagating waves are produced near the solar surface and the downward propagating waves are the result of reflection off the transition region. Analyzing Rapid Oscillations in the Solar Atmosphere (ROSA) data of chromospheric mottles, Kuridze et al. (2013) also report a combination of propagating and standing transverse oscillations, where they suggest that the sudden decrease in phase speed and transverse velocity could be due to the waves becoming nonlinear near the canopy. Morton et al. (2014) analyzed the evolution of the transverse wave properties for a spicule observed with Hinode/Solar Optical Telescope (SOT) and found a rapid initial increase in the wave amplitude due to the large changes in density and magnetic field strength, followed by a decrease in amplitude at larger heights, which the authors attributed to wave damping.

Figure 2.7 shows an example of transverse waves observed in Hinode SOT Ca II H 3968 Å, adapted from De Pontieu et al. (2007). Panel A is an image of the limb of the Sun showing that the spicules dominate the chromosphere. Panels B and D show space-time plots of the Ca intensity at the slits marked "1," and "2," respectively, in Panel A. Swaying back-and-forth motions are clear in the plots. Panels C and E show the results of a Monte Carlo simulation of spicules carrying Alfvén waves.

As well as the incompressive (transverse) waves and oscillations described so far, compressive modes have been observed in photospheric and chromospheric structures, usually by combining observations of modulations in intensity and variations in the width of the observed structures. For example, using ROSA observations of magnetic pores in the photosphere, Morton et al. (2011) interpreted out-of-phase periodic variations in pore size and intensity in terms of compressive MHD sausage modes, with periods ranging from 30 s to 450 s. Due to the similarity in periods, these authors suggested that the observed sausage modes could be driven by the global acoustic modes of the solar interior. Analyzing Dunn Solar Telescope (DST) observations in wavelengths covering the photosphere to the base of the Transition Region, Grant et al. (2015) found evidence of damping of sausage modes in a magnetic pore. Keys et al. (2018) again analyzed sausage modes in magnetic pores and found that surface modes were present more frequently in the data and that the sausage modes appeared to carry more energy than body modes. Frequencies were found to be in the range of 2–12 mHz (although the authors find no evidence of surface modes above 10 mHz).

Morton et al. (2012) provided observational evidence of concurrent compressive (sausage) and incompressive (kink) modes in chromospheric fibrilar structures. Estimating that 4%–5% of chromospheric magnetic flux tubes penetrate into the corona, the total energy flux able to reach the corona is estimated to be on the order of $1.7 \times 10^5 \pm 1.1 \times 10^5$ erg cm^{-2} s^{-1}for incompressible transverse waves and about $4.6 \times 10^5 \pm 1.5 \times 10^5$ erg cm^{-2} s^{-1} for compressive waves. Jafarzadeh et al. (2017a) and Gafeira et al. (2017) similarly report on ubiquitous transverse and compressive waves in slender Ca II H fibrils in SUNRISE data. Jafarzadeh et al. (2017b) also find compressible and incompressible (transverse) waves in small-scale magnetic features observed with SUNRISE.

Although harder to observe, torsional perturbations have also been reported in the lower solar atmosphere

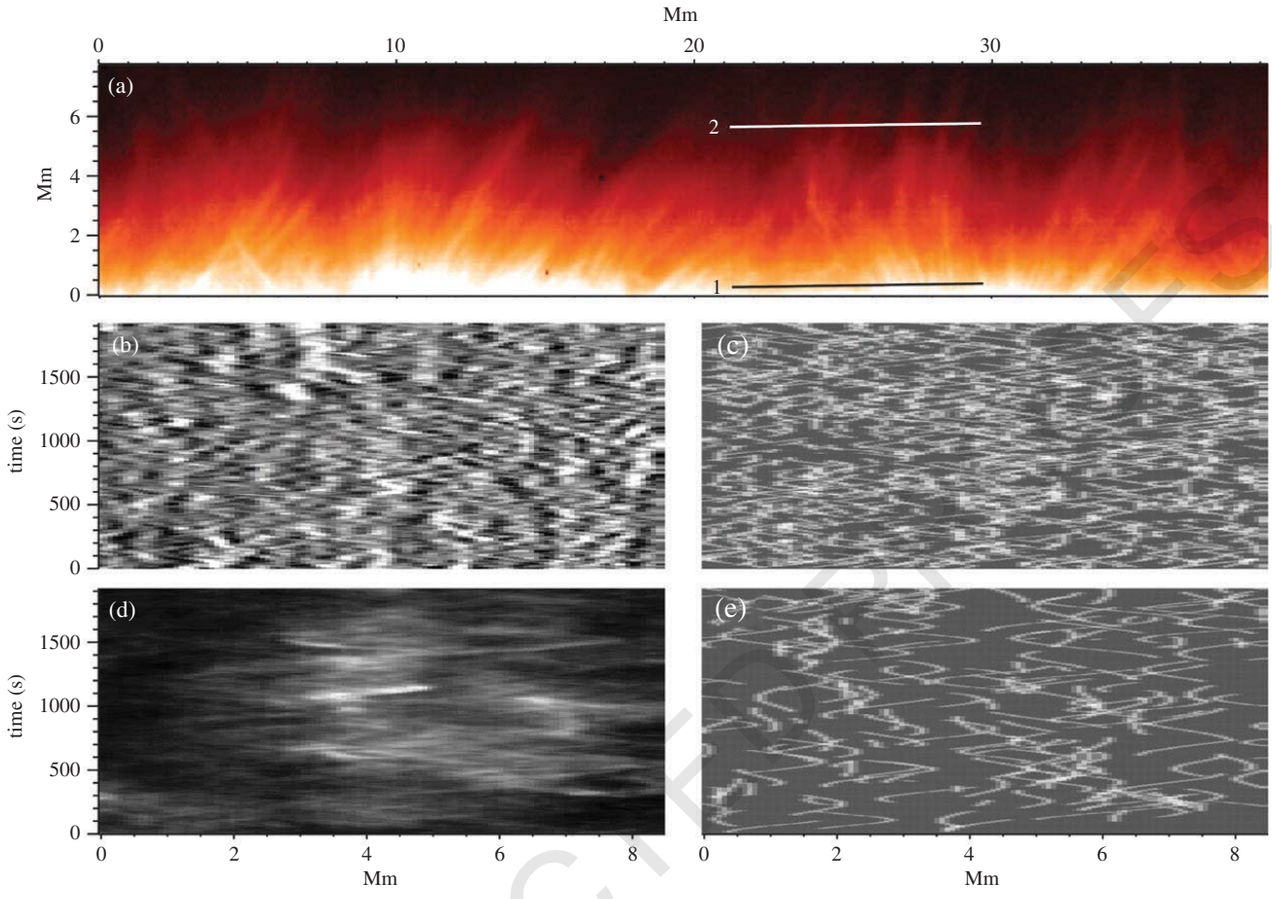

Figure 2.7 Alfvén waves observed in the chromosphere. (A) Spicules in Hinode SOT Ca II H 3968 Å image. (B) A space-time plot of the Ca intensity at the slit marked "1" in Panel A. (D) Same as B, but at slit location "2." C and E show Monte Carlo simulations in which spicules carry Alfvén waves. (*Source*: From De Pontieu et al., 2007).

from analyzing line width and Doppler velocities. For example, based on variations in line width in H_a, Jess et al. (2009) suggested the presence of torsional Alfvén waves in a large photospheric bright point group. The global average energy associated with these oscillations was estimated to be on the order of 2.4×10^5 erg cm^{-2} s^{-1}. Such torsional motions could be associated with surface vortex motions (e.g., Bonet et al., 2008; Wedemeyer-Böhm et al., 2009), propagating up into the solar atmosphere. Spicules (and dynamic fibrils) have also been found to undergo rotational motions (e.g., De Pontieu et al., 2012, 2014; Rouppe van der Voort et al., 2015; Skogsrud et al., 2015), further increasing the wave energy budget associated with spicules. Detailed analysis of the spectra revealed evidence of heating, potentially associated with the rapid torsional motions. Analyzing SST observations, Srivastava et al. (2017) found evidence for high-frequency (~12–42 mHz) torsional motions in thin spicular structures in the chromosphere. Combining the observations with numerical modeling, they suggest that even after partial reflection off the transition region, a substantial amount of energy (~10^5 erg cm^{-2} s^{-1}) is transferred to the overlying corona, providing sufficient Poynting flux to both heat the overlying corona and accelerate the solar wind. Again using SST observations, Stangalini et al. (2017) find evidence for the presence of helical perturbations in chromospheric small-scale magnetic elements, which the authors interpret as kink-like oscillations with an elliptic polarization.

The (selective) examples described above provide a flavor of the many types of observations of waves and oscillations in the lower solar atmosphere. For a more comprehensive overview, we refer the interested reader to Jess et al. (2015) and the excellent introductions in many of the papers cited above. However, even from the small selection of observational examples presented here, it is clear that many of the observed waves and oscillations are reported to contain substantial amounts of energy. Given the ubiquitous nature of some of the described waves and oscillations, observations have now established that the

chromosphere is a reservoir of wave energy contained in compressive, incompressive, and torsional motions. Although gravitational stratification is expected to lead to a "cutoff" frequency, the inclination of the magnetic field reduces the effect of gravity and hence allows for a broader spectrum of waves to propagate from the photosphere into the atmosphere (e.g., Bel & Leroy, 1977; De Pontieu et al., 2005; Jefferies et al., 2006). Analyzing the energy contained in different parts of the wave spectrum, Fossum and Carlsson (2005) and Carlsson et al. (2007) found that the energy contained in the low-frequency part of the spectrum (<5 mHz) was substantially larger than in high-frequency waves (see also more recent work by Rajaguru et al., 2019, who estimate the acoustic energy flux in the 2–5 mHz frequency range to be on the order of 2.25–2.6×10^6 erg cm^{-2} s^{-1} between the upper photosphere and the lower chromosphere).

There is plenty of wave energy to play a significant role in heating of the chromosphere. The next question is whether or not that wave energy is dissipated, and if so, where. A number of authors have looked at the change in wave energy in height by comparing observations of waves and oscillations in different wavelengths. For example, Grant et al. (2015) interpreted the gradual decrease in energy flux with height in upward propagating sausage modes in a magnetic pore as evidence of wave damping. Looking at Hinode and IRIS observations in a sunspot umbra, Kanoh et al. (2016) estimate upward energy fluxes associated with slow magneto-acoustic waves on the order of 2×10^7 erg cm^{-2} s^{-1} at the photosphere, decreasing to 8.3×10^4 erg cm^{-2} s^{-1} at the level of the lower transition region. If all of this "missing" wave energy is dissipated, it would be more than what is required to maintain chromospheric temperatures in the sunspot umbra. The remaining upward energy flux in the transition region, however, is too small to make a significant contribution to coronal heating. Similarly, Krishna Prasad et al. (2017) study the damping characteristics of slow magneto-acoustic waves at multiple heights in a sunspot umbra and find an energy flux ~1.3×10^7 erg cm^{-2} s^{-1} at the photosphere, decreasing to about 40 erg cm^{-2} s^{-1} at a height of about 2 Mm (observed in IRIS 1330 Å), again indicating significant damping. These authors also find a frequency dependence in the energy decrease, with shorter damping lengths observed for oscillations with higher frequencies. A similar dependence on frequency was found by Morton et al. (2014) for the damping of chromospheric kink waves when comparing ROSA and CoMP data. Complexities and uncertainties such as line formation heights, opacity, and wave mode identification, among others, make estimating the changes in wave energy fluxes with height less than straightforward. Despite this, these examples highlighted here clearly show a significant decrease in wave energy flux with height where the "lost" energy could make a substantial contribution to heating the local plasma.

Sunspots are known to exhibit myriads of waves and oscillations. The above were instances where energy estimates show compelling evidence that the waves contributed to the heating in the umbra. See reviews by Khomenko and Collados (2015) and Bogdon and Judge (2006) on sunspot waves. Penumbra and umbra have different wave properties and propagation, related to the highly inclined magnetic field of the penumbra and the largely vertical field of the umbra. There is also a connection between dynamics in each, with a possible connection between umbral flashes and running penumbral waves (van der Voort et al., 2003). There are global oscillations with periods as long as hours to days, but the dominant modes are several minutes. The atmospheric layers above the umbra, from the chromosphere up to the corona, all exhibit 3-min oscillations.

Directly associating the damping of observed wave energy with dissipation and heating remains elusive, though. The observations of wave modes in spicules cited above come tantalizingly close, as do the observations and modeling of prominence oscillations by Okamoto et al. (2015) and Antolin et al. (2015). There is a very rich literature of observations of oscillations in prominences with a comprehensive review provided by Arregui et al. (2012). Okamoto et al. (2007) reported on transverse waves in Hinode observations of prominences with a significant Poynting flux but with no direct evidence of heating. Using IRIS observations in multiple wavelengths and numerical modeling, Okamoto et al. (2015) and Antolin et al. (2015) combined the measurements of transverse (plane of the sky) displacements with line-of-sight (Doppler) measurements in multiple wavelengths to show evidence of significant heating from chromospheric to transition region temperatures. The authors suggest that the observed phase differences of about 180° between transverse motions in the plane-of-sky and line-of-sight velocities of the oscillating prominence threads are consistent with resonant absorption and the triggering of the Kelvin–Helmholtz instability (KHI) at the boundaries of the oscillating threads, where the instability creates thin current sheets, allowing the wave energy to be dissipated. Further evidence of wave-based heating is presented by Grant et al. (2018), who interpret DST IBIS observations in terms of Alfvén wave dissipation in the form of shock fronts close to chromospheric umbra boundaries, consistent with observed local temperature enhancement of about 5%.

2.2.1.2. Observations of Reconnection Heating in the Chromosphere

As seen in the previous section and Figure 2.6, the chromosphere is highly complex with many different types of waves and shocks that heat the chromosphere. In

this section, we discuss compelling observations that magnetic reconnection is likely playing a role in the heating of the chromosphere too.

One of the most striking observations of reconnection heating of the chromosphere is the observations of jets. We refer the reader to Chapter ~~5~~ for a full discussion of these phenomena, and discuss here the resulting atmospheric heating that is observed. Hinode observations have revealed that almost all parts of the AR chromosphere are covered by numerous tiny jets or jetlike features, which are thought to be caused by magnetic reconnection. Shibata et al. (2007) presented observations of chromospheric anemone jets, which are observed abundantly in Hinode SOT measurements. The average energy flux of anemone jets is 7×10^3 erg cm^{-2} s^{-1}. Observations suggest that anemone jets contribute to heating the chromosphere, but that not much of the associated energy heats the corona. Other types of jets observed to heat the atmosphere that are thought to be associated with magnetic reconnection include penumbral microjets (Katsukawa et al., 2007) and jets in the network regions observed with IRIS (Tian et al., 2014). Many jets are observed to heat up to at least 10^5 K in IRIS, confirming that they are involved in heating the chromosphere and transition region, and possibly even contribute to the solar wind.

Another striking observation that is highly suggestive of magnetic reconnection is the observation of flux cancellation in photospheric magnetic field measurements. The very high-resolution Imaging Magnetograph eXperiment (IMaX) instrument on two flights of the SUNRISE balloon mission (Solanki et al., 2010, 2017) show that photospheric flux cancellation, and therefore reconnection, is happening at a much higher rate than previously thought. IMaX has a factor-of-six higher resolution compared to the resolution of the Helioseismic and Magnetic Imager (HMI) measurements on SDO. The QS flux emergence and cancellation rate was recently shown by Smitha et al. (2017) to be 1100 Mx cm^{-2} day^{-1} which is an order of magnitude larger than previously thought, and parasitic polarities in nearby AR footpoints have a flux cancellation rate of 10^{15} Mx cm^{-2} s^{-1} (Chitta et al., 2017b). Following these observations, Priest et al. (2018) showed analytically that magnetic reconnection driven by such photospheric flux cancellation releases heat in the chromosphere and that the reconnection heights they model are consistent with those from magnetic field extrapolations for the observed chromospheric bursts (e.g., Chitta et al., 2017a; Tian et al., 2018). Chitta et al. (2019) studied plages in the vicinity of ARs with ~~the Swedish 1-m Solar Telescope~~ (SST~~)~~ and AIA. Using their 3D radiation MHD simulation of magnetoconvection, they estimate that the observed flux emergence and cancellation events are associated with a transfer of energy in excess of 1×10^9 erg cm^{-2} s^{-1} through the photosphere.

Another place where reconnection occurs is in the photospheric network and internetwork magnetic fields. Gošić et al. (2018) provides a nice discussion of recent attempts to determine whether magnetic flux cancellation events in the photospheric network and internetwork fields provide enough energy to heat the chromosphere. Determining whether there is enough energy is only the first step; estimates of how much energy is transferred to chromosphere and corona are extremely difficult and typically involve data-model comparisons. Wiegelmann et al. (2013) and Chitta et al. (2014) used temporal evolution of the magnetic connectivity extrapolated from IMaX observations and concluded that there is not enough energy released in the chromosphere from photospheric network and internetwork fields of the QS. Gošić et al. (2018) used coordinated IRIS and SST observations of cancellations of internetwork magnetic fields to make another estimate of chromospheric heating from reconnection. They found that the cancellation events are associated with clear evidence of local heating in the atmosphere, with chromospheric temperature increases of more than 10^3 K. However, the global estimate based on the cancellation events averaged over time and area is $\approx 1 \times 10^{-2}$ erg cm^{-3} s^{-1}, which is an order of magnitude too low to power the global chromosphere.

It is now believed that chromospheric "bombs" and "bursts" are due to magnetic reconnection as well. Ellerman bombs were the first of such events observed. They are brightenings at temperatures of ~10,000 K that seem to be due to reconnection events from emerging flux. Ellerman bombs are estimated to release between 10^{23} and 10^{26} ergs of radiative energy per event (Reid et al., 2016). Georgoulis et al. (2002) studied the statistical properties of Ellerman bombs and found that they generally exhibit power-law distribution functions. They occur preferentially near magnetic neutral lines and are associated with photospheric downflows. Georgoulis et al. (2002) estimated Ellerman bombs to have total energies (not just the radiated energy) in the range (10^{27}, 10^{28}) ergs, and temperature enhancements of $\sim 2 \times 10^3$ K.

With IRIS, bomb and burst events are now observed low in the solar atmosphere in the UV with temperatures up to 8×10^4 K. Peter et al. (2014) present an event observed with IRIS that they compare to an Ellerman bomb. These bombs are also believed to be due to magnetic reconnection; however, the IRIS bombs are much hotter than Ellerman bombs, and are observed to heat to at least chromospheric, and even transition region temperatures. The plasma in the photosphere is observed to be heated to almost 100,000 K, and there is a bidirectional flow channeled by the magnetic field. The normal temperature stratification (a very hot corona above a hot transition region gas above the chromosphere) is turned upside down. Figure 2.8 shows a cartoon

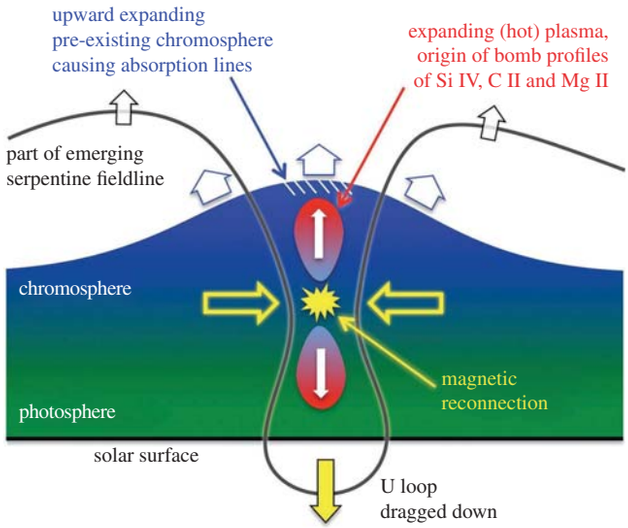

Figure 2.8 A cartoon representation of a magnetic reconnection event generating hot plasma embedded in cooler material in the chromosphere. (*Source*: Peter et al., 2014. © 2014 The American Association for the Advancement of Science [AAAS].)

representation of the reconnection event and plasma heating, adapted from Peter et al. (2014).

In addition to the similarity to Ellerman bombs, chromospheric bombs and bursts in UV show additional evidence for intermittent magnetic reconnection. Rouppe van der Voort et al. (2017) used the CHROMIS instrument Ca II K line at the SST and found blob-like features at Alfvénic speeds followed by the heating of plasma to transition region temperatures in IRIS, which is consistent with predicted signatures of reconnection (Innes et al., 2015). A unifying picture is coming together. Hansteen et al. (2017) showed with a 3D radiative MHD simulations of magnetic flux emergence that reconnection between emerging bipoles triggers Ellerman bombs in the photosphere, UV bursts in the middle and low chromosphere and small nanoflares and microflares that occur in the upper chromosphere but produce 10^6 K plasma. Depending on where the reconnection occurs, the energy released through flux cancellation can produce a range of "bomb" and "burst" signatures, such as the Ellerman bomb in the wings of Hα in the QS and around sunspots (Hansteen et al., 2017; Rouppe van der Voort et al., 2016), ultraviolet (UV) bursts in the chromosphere (Peter et al., 2014) and explosive events in the transition region (Brueckner & Bartoe, 1983; Innes et al., 2011).

The transition region is a layer where thermal conduction is a heating term, in contrast to the corona, where it is a cooling term. Although the transition region is geometrically thin, it spans temperatures from chromospheric (~10^4 K) to coronal (~10^6 K). A long-standing problem has been that the observed emission at temperatures below about 10^5 K is much greater than that predicted through thermal conduction from the hot corona alone (Gabriel, 1976). Feldman (1983) proposed that this excess "transition region" emission could be due to structures that were not resolvable at that time, "unresolved fine structures" or UFS. This emission is not "transition region" emission in the thermal conduction definition of transition region; rather, these would be structures whose peak temperatures were on the order of 100,000 K. Figures 2.5 and 2.6 show that, in the QS, a large amount of magnetic flux is expected to close back to the surface of the Sun before reaching coronal heights. Trujillo et al. (2010) showed that modeling of observations taken with the Chromospheric Lyman-Alpha Spectro-Polarimeter (CLASP) are indeed consistent with a highly corrugated magnetic field structure in the transition region. Antiochos and Noci (1986) showed that loops with heights above the chromosphere that are lower than 5000 km have static solutions with a temperature maximum of less than 100,000 K. An alternate explanation is required for the large unipolar areas (plage) in ARs, where the small UFS loops do not exist. Type II spicules are another possibility (Klimchuk, 2012).

Though there has been observational evidence that these low-lying structures contribute to the emission at these temperatures for years (e.g., Dowdy et al., 1986; Feldman et al., 1999; Vourlidas et al., 2010), it was the high-resolution IRIS observations that confirmed low-lying structures that are likely the UFS. Magnetic reconnection is likely involved in their heating (Hansteen et al., 2014). These IRIS low-lying loops are highly dynamic; both heating and cooling have been observed. They are heated to hundreds of thousands of K, but never reach coronal temperatures, and have scales of only about 2–6 Mm. Hansteen et al. (2014) demonstrated that their high densities cause very rapid radiative cooling, and hence these loops cool before they reach coronal temperatures. Interestingly, Pereira et al. (2018) used SST and showed a lack of chromospheric heating associated with the IRIS low-lying loops. They argued that magnetic reconnection created the loops based on the observations of Y-shaped jets above the loop.

As described earlier, waves and reconnection are not mutually exclusive, and in fact there seem to be very compelling examples where magnetic reconnection results in waves, and where waves drive magnetic reconnection. Song et al. (2017) concluded that magnetic reconnection events in a light bridge triggered oscillations in the nearby sunspot umbra. Tian et al. (2014) presented IRIS observations of magnetic reconnection jets that launched upward propagating waves. With causality going the other direction, many explosive events are observed to occur at intervals of 3–5 min, close to the periodicities produced by solar granulation (Chae

et al., 1998; Doyle et al., 2006; Ning et al., 2004). Heggland et al. (2009) simulated wave-induced magnetic reconnection in the solar atmosphere and reproduced many aspects of the observations of periodic reconnection in chromospheric jets.

2.2.2. Observations of Coronal Heating

Coronal heating cannot be understood without understanding of the coupling from the photosphere through the chromosphere and transition region into the corona (see review by Wedemeyer-Böhme et al., 2009). The complexity of this connection is illustrated in Figure 2.6. The atmosphere is dynamic on many spatial and temporal scales, and therefore the coupling is dynamic too. The exchange of mass between the chromosphere and corona through chromospheric evaporation is crucial to understanding the coronal observations. Most coronal heating occurs on spatial scales that are not resolved by current instrumentation. The corona is optically thin, so even with perfect resolution, there would still be line-of-sight effects that make heating events that are physically separate appear to overlap. As with the chromospheric studies described above, images and spectroscopy in the X-ray and UV are the primary observational tools for understanding coronal heating.

Both waves and reconnection are predicted to produce impulsive heating. As reviewed in Klimchuk and Hinode Review Team (2019), there are several independent lines of evidence that point to the existence of impulsive heating events. TRACE data combined with the extensive X-ray observations with the Yohkoh mission were among the first to show that many coronal loops are not in a steady state. In particular, many coronal loops are diagnosed in the EUV to be denser than predicted by scaling laws of hydrostatic equilibrium conditions for their temperature. Presumably, this means that they are observed while they are cooling, and therefore the heating of each magnetic strand is not continuous, but rather irregular, or impulsive (Klimchuk, 2006). Other evidence for impulsive heating includes the fact that loop intensities as a function of height are not in agreement with the hydrostatic scale height, emission measure distributions with shallow slopes coolward of their peak, time lags between emissions formed at different temperatures, asymmetries in the distribution of intensity fluctuations, footpoints (transition region) not sufficiently bright, and the existence of very hot (>5 MK) plasma. A review of these observational aspects is found in Reale (2014) and Klimchuk (2006, 2015).

However, as we will show in the descriptions of observational coronal heating constrains that follow, many observations are consistent with steady heating too. Because impulsive and steady heating both seem to be consistent with observations at certain times and locations, current research focuses on the frequency distribution of the heating events and requires a range of frequencies, rather than either steady heating or impulsive heating (e.g., Bradshaw & Viall, 2016; Cargill, 2014; Reep et al., 2013). Low-frequency heating events occur at cadences that allow plasma cooling and evolution between them, and high-frequency heating is effectively steady heating in terms of the plasma evolution (see discussion in section 2.3 on modeling), and produces observations consistent with steady heating, though they too are impulsive. Note that much of the current literature uses "impulsive heating events" and "nanoflares" interchangeably, even in situations where the mechanism is not necessarily magnetic reconnection, though we only use "nanoflare" in the reconnection sense in this chapter.

Direct evidence of wave heating or reconnection heating is the exception, not the rule. Due to the unresolved nature of the events, most observations of coronal heating do not conclusively or immediately point to either waves or reconnection. Rather, they put constraints on the characteristics of the mechanisms' timing and spatial distribution, which then must be compared to forward-modeled simulations of coronal heating (section 2.3). Also, as described for the chromosphere, magnetic reconnection and waves in the corona are observed and predicted to occur in concert, complicating the observations further. Due to these limitations, the current state of the art is to use observations to determine the spatial and temporal distribution of coronal heating. We next describe such observational constraints that do not yet point conclusively to waves or reconnection.

2.2.2.1. Individual Brightenings

One observational constraint is transient brightenings observed in the UV and X-ray. The nanoflare concept introduced first by Parker (1988) was the result of these observed properties of the X-ray, UV corona, and transition region, which showed a space and time variability at small scales. Typical events that Parker considered are those with an X-ray illumination variation between 20% and 100% over characteristic timescales of 20–60 s. Such observations suggested a "heat input composed of many localized impulsive bursts of energy." By this time there was already observational evidence that brightenings from larger events were less frequent than from the smaller ones. Parker proposed the name *nanoflare* for any of these events having an associated inferred energy below the microflare value ($\leq 10^{27}$ ergs). Already in his paper Parker had introduced concepts such as impulsive, unresolved events, clusters of nanoflares, and statistics of nanoflares with the idea that the corona is the result of a large number of nanoflares happening all the time. He showed that

quantitatively they could roughly explain the existence of the corona. However, it is still unclear how many of these brightenings are indeed reconnection events.

Observations of individual brightenings show that they have power-law distributions. This has been measured in the Fourier spectra of the radiance (Ireland et al., 2015), the spatial and temporal scales of the brightenings, and the inferred thermal energy. In particular, the index of the slope in the energy distribution remains close to −2. Table 1 of Benz and Krucker (2002) summarizes estimated slopes from several studies, which range from −1.35 to −2.59. One important aspect to keep in mind is that soft X-ray and EUV observations infer the amount of energy of each event from the observed radiance. This is the plasma response to the injected energy. The hypothesis behind studying the plasma radiation is that all the energy injected in the loop in the form of heating by the magnetic field is radiated away to cool the system and that the plasma response to this heating preserves the heating statistical properties. However, Parenti et al. (2006, 2008) have tested these two hypotheses, and they showed that in general they do not hold: only the very high-temperature emission (~10 MK) retains memory of the statistical properties of the energy heating the system, whereas at lower temperatures, including the average 1–3 MK corona, such information is lost. See also Benz and Krucker (2002), Buchlin et al. (2005), and Jess et al. (2019) for a description of the difficulties in estimating the geometry and energies associated with brightening, and therefore estimating power-law slopes from them. It is clear that the direct relation made from radiance to heating properties is not straightforward, and other diagnostic methods should be used to investigate small-scale heating.

2.2.2.2. Loop Fine Structure

When subarcsec monitoring of the solar corona in the extreme UV (EUV) was made with the TRACE mission, it was clear that the coronal loops observed with prior instrumentation consist of bundles of even thinner coronal loops, or strands (Lenz et al., 1999). The data arising from high-resolution instruments in the soft-X-ray (HINODE/XRT) and EUV-UV (TRACE, AIA/SDO and IRIS), as well as the few observations from sounding rockets (Hi-C, pixels of about 75 km), have confirmed that loops have substructure at least down to less than 1000 km (e.g., Reale et al., 2007; see discussion in Klimchuk, 2015). Such detected strands may contain even finer structure.

There is a long history of literature concerning observational results of the thermal structure of loops, which is an indication of the elemental cross-scale heating scale. If an observed coronal loop shows isothermal plasma, then this could be evidence that the heating mechanism deposited energy over the entire width of the loop at the same time, whereas multithermal plasma indicates heating events occurring on substructures within the loop. The results are controversial, particularly concerning warm loops (see Del Zanna and Mason, 2003; Cirtain et al., 2007; Reale, 2014; and Tripathi et al., 2009 for a full review). Some observations indicate that even a single observed coronal loop is typically a compilation of many subresolution magnetic field strands, each independently undergoing heating and cooling cycles and are multithermal (Schmelz et al., 2001), whereas other observations indicate monolithic, resolved, or almost-resolved loops (Aschwanden & Nightingale, 2005; Aschwanden & Peter, 2017; Brooks et al., 2012). Some of these differences come from the different diagnostic techniques used, instrumental limitations, and the uncertainties in the data. There is also a possibility that there exist different classes of loops subject to different heating mechanisms and/or different frequency of heating events. Warm, ~1 MK loops have been found to be either isothermal or multithermal at a given time, ~~and~~quite time variable. Hotter, ~3 MK loops in AR cores are multithermal but more stable in time.

Spectroscopic filling factors measured in the EUV are another indication of substructures. They are a measure of how much the observed structure is filled with plasma at the temperature of the emission, and are another indication of substructure. Warren et al. (2008) measured filling factors in AR coronal loops, and Hahn and Savin (2016) measured QS and coronal hole filling factors; both papers found filling factors of around 10%, a strong indication of substructure.

2.2.2.3. Differential Emission Measure (DEM)

The DEM is a measure of the amount of plasma at a given temperature. In ARs in general, the DEM has a triangular shape (in the log-log scale), with the two sides of the peak being fitted with power-law functions that can change depending on the AR. Figure 2.9 shows one example of the DEM in the core of an AR derived from Hinode/EIS. The power-law index (α) computed over the lower temperatures was found to vary in the range $1.6 \leq \alpha \leq 5.2$ (e.g., see review of the observations in Bradshaw et al., 2012). This range is likely due to physical variations between different ARs, with some AR cores having slopes more consistent with high-frequency heating (Warren et al., 2011), and a possible dependence on the AR age (Ugarte-Urra & Warren, 2012). Warren et al. (2012) surveyed 15 ARs, and found that steeper slopes are correlated with the total unsigned photospheric magnetic flux as well as the relative amount of hot plasma along the line of sight. Note, however, that there are also instrumental uncertainties in the calculation of DEMs (Guennou et al., 2013).

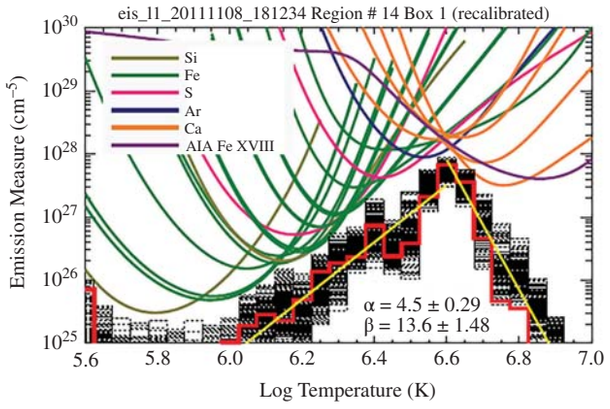

Figure 2.9 Active region (AR) differential emission measure curve. The emission measure distribution is the red curve. The black curves are solutions that use perturbed intensities. The parameters α and β are the unsigned slopes of the emission measure below and above log T = 6.6. (*Source*: Warren et al, 2014. © 2014 IOP Publishing.)

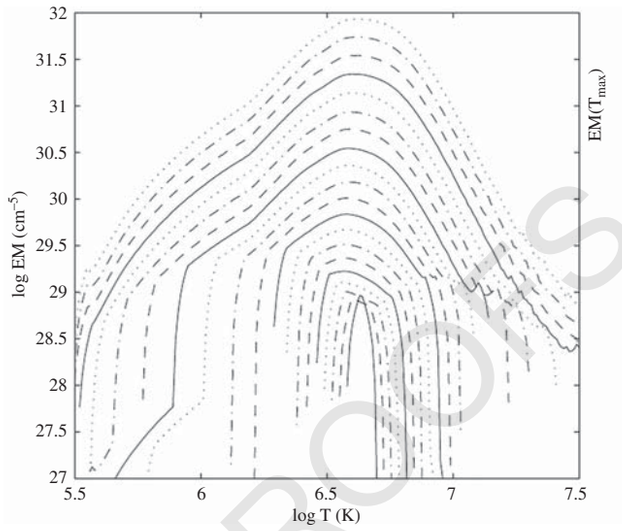

Figure 2.10 Emission measure as a function of temperature for nanoflare trains with constant energy nanoflares. The 20 curves are associated with different delay times between the nanoflares (between 250 and 5000 s). The lowest curve corresponds to a delay time of 250 s and the highest to 5000 s. Each curve is shifted vertically by 0.2 on a log scale with respect to the previous one as the delay time increases. The four line styles break the delay time up into groups of 1000 s. (*Source*: Cargill, 2014. © 2014 IOP Publishing.)

Models of impulsive heating (i.e., where the heating as a function of space and time is assumed, but a particular mechanism is not; see section 2.3.2) have shown that the cross-field thermal structure (represented by a DEM, for instance) carries important information about how the heating energy is distributed and released within a flux tube. Figure 2.10, shows an example where many flux tubes are in the simulated observation, which would result due to either line-of-sight effects and/or because the flux tube diameters are smaller than the resolution of the instrument. The plasma temperature of the many flux tubes changes depending on the frequency of the heating events, assuming a constant total injected energy. High-frequency events produce an almost isothermal plasma along the line of sight. As the heating frequency decreases, the plasma becomes more multithermal. It is important to note that in simulations of impulsive heating, such as this one, the coronal emission is dominated by plasma in its cooling phase (Klimchuk, 2006).

2.2.2.4. Light Curves

Another way to understand the properties of the heating in loops is to characterize their life cycle through their light curves, or emission at different wavelengths, as a function of time. These can give an estimate of the temporal distribution of the heating. The temporal stability over a few hours of the emission and the temperature of hot loops in the core of the AR are consistent with high-frequency heating which prevents the plasma from cooling ~~down~~ (e.g., Porter & Klimchuk, 1995; Schrijver et al., 2004; Warren & Winebarger, 2006; Warren et al., 2011).

In contrast, the cooling of loops has been detected through light curves since, at least, the Yohkoh and Skylab era (see Reale, 2014, for a full review), but only recently was it possible to measure the full lifecycle temperature range (from a few megakelvins to chromospheric temperatures), which provides a better constraint on the theories. Some of the coronal loops are seen to be cooling from hotter loops (e.g., Ugarte-Urra et al., 2009; Viall & Klimchuk, 2011; Winebarger & Warren, 2005). The observation of a stable emission over several hours together with the associated small, but detectable fluctuations (~15%), are compatible with a loop made of a substructures where each substructure is heated and cools fully, but the loop in aggregate is continuously heated (e.g., Sakamoto et al., 2008; Terzo et al., 2011). In support of this general picture has been the arrival of the SDO/AIA high spatial and temporal resolutions EUV data. Viall and Klimchuk (2012, 2015, 2016) have developed and used a time lag method (a delay in the peak of emission seen in the different AIA channels) to highlight the full cycle of plasma cooling, both in observable loops and in the diffuse surrounding unstructured areas. Analyzing the same 15 ARs dataset used by Warren et al. (2012), Viall and Klimchuk (2017) measured different classes of cooling cycles that could be explained using trains of impulsive heating events with a range of different

frequencies, high and low. Combining forward modeling with the observations, (Bradshaw & Viall, 2016) suggested that the majority of the plasma was heated by impulsive heating events at a range of frequencies, with a typical frequency of several thousand seconds.

2.2.2.5. Non-Thermal Broadening

Another observational signature expected from impulsive heating is spectral line broadening due to the high-speed plasma evaporating from the chromosphere into the coronal loop. High velocities, on the order of 100 km/s or more, are predicted in the early phase of the cooling cycle, when the strand is still weakly filled by plasma. Patsourakos and Klimchuk (2006) showed that this signature could be measured by observing the profiles of hot lines, such as Fe XVII, whereas cooler lines are less affected by the heating. However, when looking at the observations, no clear evidence has been found ~~until now~~ (e.g., Brooks and Warren 2016). It is possible that the present instrumentation does not have a high enough spectral resolution and sensitivity to isolate such weak signatures from the bulk coronal emission. Wave motion, even in the absence of heating, will also contribute to non-thermal line widths, with broadening of the non-thermal line width attributed to unresolved wave motions instead of flows. Brooks and Warren (2016) investigated non-thermal line broadening in Hinode/EIS observations in the core of 15 non-flaring ARs and find that their results are inconsistent with all current models of heating: Alfvén wave turbulence, reconnection jets in the corona, and chromospheric evaporation induced by coronal nanoflares. A straightforward conclusion of non-thermal broadening cannot be inferred from the current model predictions.

2.2.2.6. Coronal Rain

Another observational constraint on coronal heating is coronal rain. Coronal rain consists of cool, chromospheric temperature plasma observed to fall down from the corona along magnetic field lines (Antolin & Rouppe van der Voort, 2012; Auchere et al., 2014; Froment et al., 2015, 2017; Müller et al., 2005). When it is observed outside of flaring regions, coronal rain seems to require a condition called thermal non-equilibrium, which requires high-frequency heating that is concentrated toward the footpoints (see section 2.3.2 for a discussion of the theory of thermal non-equilibrium and how it is constrained by observations). Theoretically, thermal non-equilibrium is described with steady heating; however, the heating that produces coronal rain can also be impulsive, provided that the heating is at a high enough frequency relative to the plasma cooling time (Karpen & Antiochos, 2008). Antolin and Rouppe van der Voort (2012) measured the statistical properties of coronal rain outside of flares using the CRisp Imaging Spectro Polarimeter (CRISP) instrument on the SST. They found that, on average, they are 310 km wide, 710 km long, and at temperatures of below 7000 K. It is estimated that the fraction of the coronal volume with coronal rain is between 7% and 30%. An ~~additionalobservational~~ constraint on their formation is that sometimes coronal rain occurs periodically and in conjunction with periodic intensity enhancements (Auchère et al., 2018).

2.2.2.7. Doppler Shifts

Observed Doppler shift patterns generally show that lower-temperature plasma is red-shifted, whereas higher-temperature plasma is blue-shifted. The Doppler shifts show center-to-limb variations consistent with a cosine (theta) variation (Peter & Judge, 1999), and the general interpretation of the red shifts is that they are downflows from a hotter corona on the flux tube (Chae et al., 1998). The transition between up- and down-flowing plasma is measured to be somewhere between 0.5 and 1.0 MK (e.g., Chae et al., 1998; Dadashi et al., 2011; Peter & Judge, 1999).

2.2.2.8. Elemental Fractionation

Spectral observations show that elements with a low first ionization potential (FIP)—below 10 eV—are enhanced in abundance in the closed-field corona relative to their photospheric abundances. The chromosphere, where these low-FIP elements would be ionized whereas higher-FIP elements remain neutral, is thought to be the location where this difference in relative abundance is set, due to forces acting on ions but not on neutral elements. FIP abundance is an important tracer for solar wind formation because it is "frozen" into the solar wind plasma, and does not evolve in the solar wind as it travels away from the Sun. See the review by Laming (2015) for a thorough survey of the topic, and Chapter ~~7~~ for the use of ~~solar wind FIP measured in situ~~ to make a connection with the solar atmosphere. AQ9

2.2.2.9. Footpoints and Moss

Due to the crucial chromosphere–transition region–corona connection, the footpoints of coronal field lines can be an important diagnostic of coronal heating. Diagnostic techniques include comparing emissions formed at different temperatures, and therefore connections between different heights (e.g., Vourlidas et al., 2001), as well as its time variability, which is an indication of the heating frequency (Antiochos et al., 2003; Testa et al., 2014). Moss, an example of footpoint emission, is a low-height (3000 km), 1 MK plasma that was originally identified with the TRACE imager. Moss is now known to be the footpoints of hotter, 3–10 MK loops, with a brightness that scales with loop pressure

and filling factor (e.g., Berger et al., 1999; De Pontieu et al., 1999; Fletcher & De Pontieu, 1999; Martens et al., 2000; Schrijver et al., 1999).

2.2.2.10. Observations of Coronal Wave Heating

Although periodic variations were detected in early observations (see, e.g., Antonucci et al., 1984; Aschwanden, 1987; Deubner & Fleck, 1989; Rosenberg, 1970; Trottet et al., 1979; or Tsubaki, 1988; Vernazza et al., 1975, for an overview), it was the increased spatial resolution and wavelength coverage of SOHO and TRACE that provided spatially resolved observations of waves and oscillations in the solar atmosphere. Observations of standing and propagating waves were discovered in a wide range of coronal structures such as, for example, intensity (density) variations in coronal fan loops (see, e.g., De Moortel, 2009, for an overview), transverse loop oscillations (e.g., Aschwanden et al., 1999; Nakariakov et al., 1999), and perturbations in coronal plumes (e.g., DeForest & Gurman, 1998; Ofman et al., 1997).

Present-day observations by a range of imaging and spectroscopic instruments have allowed us to establish the presence of waves and oscillations in almost all parts of the solar corona and out into the solar wind. We have been able to directly measure the oscillatory displacement of coronal loops, intensity variations in magnetic structures, and variations in Doppler velocities, line widths, and periodic radio signatures. The study of MHD waves has two major applications within solar physics, namely, coronal (or magneto) seismology (Uchida, 1970; Roberts et al., 1984—see, e.g., Nakariakov & Verwichte, 2005, or De Moortel & Nakariakov, 2012, for a review on coronal seismology) and as a potential coronal heating mechanism (see reviews by, e.g., Arregui, 2015; De Moortel & Browning, 2015; Klimchuk, 2006, 2015; Parnell & De Moortel, 2012; Walsh & Ireland, 2003), and for comprehensive overviews of observations of waves and oscillations, we refer the reader to the reviews listed above. We will restrict ourselves here to looking at a few particular examples and their potential relation to coronal heating.

Early observations by SOHO and TRACE revealed the presence of quasi-periodic intensity perturbations propagating along coronal fan loops, mostly at the edges of ARs (see, e.g., Berghmans & Clettea, 1999; De Moortel et al., 2000; Robbrecht et al., 2001; Schrijver et al., 1999). These propagating coronal disturbances (PCDs) were found to have amplitudes on the order of a few percent compared to the background intensity, periods of a few minutes (typically 2–10 min although periods on the order of 15 min have been reported in polar plumes) and propagation speeds ~100 km/s (when observed in wavelengths such as 171 A, i.e., around 1 MK). The combination of these properties, and in particular the propagation speed close to the local sound speed, gave rise to the interpretation of PCDs as propagating slow magneto-acoustic waves (De Moortel et al., 2002a, 2002b), although others suggested an alternative interpretation in terms of flows. Combining the imaging observations with spectroscopic measurements (e.g., from Hinode/EIS) led to a more complicated picture than was first apparent. The spectroscopic observations showed that the low-amplitude, periodic PCDs were present not only in the intensity but also in the Doppler velocity measurements, and both the wave (e.g., Banerjee et al., 2009; Kitagawa et al., 2010; Krishna Prasad et al., 2011; Mariska & Muglach, 2010; Marsh et al., 2011) and flow interpretation (e.g., Bryans et al., 2010; Doschek et al., 2007; Guo et al., 2010; Hara et al., 2008; He et al., 2010; Peter, 2010; Sakao et al., 2007; Ugarte-Urra & Warren, 2011) became abundant in the literature. The ambiguous interpretation was highlighted by two papers analyzing the same dataset but putting forward a different interpretation (De Pontieu & McIntosh, 2010; Wang et al., 2009). Wang et al. (2009) compare the intensity and Doppler shift perturbations and, finding that these are approximately in phase, interpret the PCDs as slow magneto-acoustic waves. However, De Pontieu and McIntosh (2010) also look at the line widths and line asymmetries and, after comparing with model results suggest that the in-phase oscillations in intensity, Doppler velocity, line widths, and line asymmetries are consistent with an interpretation in terms of quasi-periodic upflows.

Distinguishing between the interpretations in terms of the propagation of slow magneto-acoustic waves and quasi-periodic upflows is less straightforward than it perhaps might seem. When looking at the asymmetries in the spectral line profiles, PCDs are often accompanied by quasi-periodically occurring enhancements of the same order of magnitude in the blue wing of the spectral line. De Pontieu and McIntosh (2010) and Tian et al. (2011) show that fitting line profiles that exhibit such an enhancement in the blue wing with a single Gaussian (rather than with a double Gaussian) mimics the properties of the intensity perturbations in the imaging data. However, Verwichte et al. (2010) argue that the periodically varying double-Gaussian fit could be composed of an oscillating dominant (core) component and an additional small, stationary blue-wing component, consistent with an interpretation in terms of slow magneto-acoustic waves. De Moortel et al. (2015) used forward modeling to derive observational signatures associated with simple models of slow magneto-acoustic wave or periodic flow propagation. Although there were a number of observational differences between the flow and wave scenarios, it was not possible to establish clear, robust observational characteristics that can be used in isolation (i.e., without needing a like-for-like comparison

between the models). The identification problem is further exacerbated by the fact that any distinguishing characteristics require extensive analysis of the spectroscopic data, which is nontrivial with the low signal-to-noise levels of these small-amplitude perturbations.

Recent work by De Pontieu et al. (2017), based on the numerical simulations by Martinez-Sykora et al. (2017), demonstrated that the interpretation of PCDs as either propagating slow waves or episodic flows might be too simplistic. Similarities in properties have previously hinted at a close relationship between PCDs and type II spicules (De Pontieu et al., 2005; De Pontieu & Erdélyi, 2006), which was firmly established by De Pontieu et al. (2017) by combining IRIS and AIA observations with numerical modeling. It was found that PCDs in plage region loops are not simply a signature of slow waves or flows but are part of a complex set of events linking the generation of spicular flows with shock waves that propagate into the corona as well as plasma heating through the dissipation of electrical currents and magnetic waves. Here, PCDs are not just a small-amplitude perturbation of the background intensity but the result of the formation of new coronal strands (an aspect missed by the often-used running difference analysis of PCDs). The complexity naturally explains the wide range of PCD propagation speeds reported in the literature, as the observed speeds are the result of a mixture of real flows, remnants of shock waves, and dissipation of currents in the coronal volume (i.e., local heating followed by thermal conduction). In addition, this model also resolves the ambiguous interpretations in terms of periodic flows (usually observed lower down in the loops) and slow magneto-acoustic waves (observed along a greater extent of the loops). Despite their small energy budget (~300 erg cm^{-2} s^{-1}—see, e.g., De Moortel et al., 2002a), their omnipresence in the solar atmosphere and their close link with spicule-driven heating imply that PCDs potentially play an important role in the mass and energy flow in the solar corona.

The increased spatial and temporal resolution of TRACE also gave us the first imaging observations of standing transverse loop oscillations induced by a nearby impulsive event (Aschwanden et al., 1999; Nakariakov et al., 1999). Since then, transverse oscillations have been reported in many of the solar atmosphere's magnetic structures such as prominences (e.g., Okamoto et al., 2007), magnetic bright points and intergranular lanes (Jess et al., 2012), chromospheric spicules (e.g., De Pontieu et al., 2007) and mottles (e.g., Kuridze et al., 2012), coronal loops (e.g., McIntosh et al., 2011), coronal rain (e.g., Antolin and Verwichte, 2011), and jets (e.g., Cirtain et al., 2007). Similar transverse perturbations were reported in Doppler shift observations of large, off-limb, coronal loops by Tomczyk et al. (2007) and Tomczyk and McIntosh (2009). Many other examples can be found in the literature. We will focus on the potential relevance of these perturbations for coronal heating.

Estimates of the energy associated with the observed propagating transverse waves vary substantially. For example, McIntosh et al. (2011) analyze SDO/AIA and report on small-amplitude transverse displacements in a coronal hole region, QS and AR loops. They suggest that these ubiquitous low-amplitude oscillatory displacements are footpoint driven and contain sufficient energy to account for the heating requirements of the QS and coronal holes (~$1–2 \times 10^5$ erg cm^{-2} s^{-1}). In the AR loops, however, the energy is estimated to be about 10^5 erg cm^{-2} s^{-1}, which is at least two orders of magnitude too small (where Withbroe & Noyes estimate that about 2×10^7 erg cm^{-2} s^{-1} is needed to account for the heating of ARs). In contrast to the energy budget reported by McIntosh et al. (2011), Tomczyk et al. (2007) report a much smaller energy budget estimated from CoMP observations of propagating disturbances in off-limb coronal loops. However, McIntosh and De Pontieu (2012) find that the off-limb line-of-sight superposition of Doppler velocities "hides" most of the wave energy flux, which is instead present in the large, observed non-thermal line broadening. Using 3D numerical simulations of oscillations in cylindrical flux tubes, De Moortel and Pascoe (2012) demonstrated that the superposition of randomly directed oscillating transverse displacements does indeed result in "observed" line-of-sight integrated Doppler velocities with an energy budget that is at least an order of magnitude smaller than the energy present in the three-dimensional coronal (numerical) volume. Therefore, the energy budget estimated by McIntosh et al. (2011) in the AR loops is likely to be a lower limit due to the superposition of a large number of oscillating loop strands. Off-limb, one would also expect a large number of loops with randomly directed transverse displacements along the line of sight, which could account for the low-energy budget reported by Tomczyk et al. (2007). In addition, mode identification further complicates the derivation of an estimated energy budget from observed waves and oscillations (Goossens et al., 2013).

To be relevant in the context of coronal heating, observed waves and oscillations not only need to contain a substantial amount of energy, but this energy needs to be dissipated on the appropriate time scales and in the right places. It is important to note here that damping (of the perturbation amplitudes) and dissipation are not necessarily the same. For example, waves can undergo "damping" due to a change in the background medium or by transferring energy to a different wave mode. The standing transverse loop oscillations induced by

impulsive events (see, e.g., Aschwanden et al., 1999, and Schrijver et al., 1999, for an early overview) are observed to undergo very rapid damping, within a few oscillation periods, but their contribution to (local) heating, if any, remains unclear. They do not occur frequently enough to really be relevant for coronal heating and in addition, their rapid damping is likely due to resonant absorption (see, e.g., Goossens et al., 2006; Goossens et al., 2011; Ruderman & Erdélyi, 2009; Ruderman & Roberts, 2002), which transfers energy from the observed transverse loop oscillation to azimuthal Alfvén waves in the loop boundary. Although subsequent phase mixing of the Alfvén waves in the loop boundary region could lead to local heating, this is unlikely to sustain the loop at coronal temperatures (Cargill et al., 2016). Aschwanden and Terradas (2008) find that the timescales on which the oscillating loops cool through the EUV passbands are compatible with heating and subsequent cooling, but this heating cannot necessarily be attributed to wave heating from the transverse loop oscillation.

The situation is different, however, for the propagating transverse (Alfvénic) waves observed by, for example, Tomczyk et al. (2007) and McIntosh et al. (2011). The CoMP observations not only show that these perturbations are ubiquitous through the solar corona, Tomczyk and McIntosh (2009) suggest that the waves must undergo rapid, in situ damping to explain the observed disparity between outward (propagating upward toward the loop apex) and inward (propagating down from the loop apex) wave power. The rapid damping of the transverse perturbations can be explained by mode coupling, again transferring energy from the observed oscillating displacements to small-scale azimuthal Alfvén waves in the tube boundary (see, e.g., De Moortel et al., 2016, for a review) but the contribution to local heating from the subsequent phase mixing in the loop boundary has so far not been found to be viable (Pagano & De Moortel, 2017, 2019). However, Morton et al. (2015) reported on the observation of counter-propagating Alfvénic waves which could lead to the development of turbulence and enhanced wave dissipation, which was not included in the model by Pagano et al. (2018) . Morton et al. (2016) suggested that regardless of local topology, the CoMP spectra reveal the presence of enhanced power around 3 mHz, suggesting a global link between the observed coronal transverse perturbations and the global p-modes. In addition, analyzing CoMP data from a number of different dates during 2012–2015, Morton et al. (2019) recently suggested the possible presence of a basal Alfvénic flux throughout the solar cycle. On the other hand, Morton and McLaughlin (2013) exploit the high resolution provided by Hi-C to try and confirm the ubiquitous nature of wave activity in the solar corona but find that low-frequency (50–200 s) wave activity in the coronal loops is generally of low energy and that some structures do not show any periodic transverse displacements at all.

The observations of waves and oscillations in the solar corona described so far are all direct measurements of periodic variations in observables such as intensity or Doppler velocity. Indirect evidence of the presence of waves can also be derived from observations of non-thermal line widths, with broadening of the non-thermal line width attributed to unresolved wave motions. For example, McClements et al. (1991) demonstrated that if Alfvén waves are present, there should be a center-to-limb broadening of the observed line widths, a concept that was used to suggest the presence of Alfvén waves based on observed changes in the line broadening by, for example, Hassler et al. (1990) or Erdélyi et al. (1998). As pointed out by McIntosh and De Pontieu (2012), a considerable amount of wave energy could be "hiding" in the non-thermal line widths. Changes in observed line widths could therefore be indicative of changes in the wave amplitude. Such variations have been analyzed by, for example, Harrison et al. (2002), who found a decrease in EUV line width with height above the limb, which they suggested could be due to wave damping (see also, e.g., O'Shea et al., 2003; Sakurai et al., 2002; Zaqarashvili, 2003; Wilhelm et al., 2004). A similar decrease in the non-thermal line widths was found by, for example, Hahn et al. (2012), Bemporad and Abbo (2012), and Hahn and Savin (2013) in polar coronal holes, which these authors also attribute to damping of Alfvén waves (see also, e.g., Banerjee et al., 1998, 2009b). In coronal holes, dissipation of wave energy is not only relevant for coronal heating but also for the acceleration of the fast solar wind (see review by, e.g., Banerjee et al., 2011; Cranmer, 2009). Hahn et al. (2012) suggest that the observed rapid decrease in line width could account for up to 70% of the energy required to heat the polar coronal hole and drive the solar wind acceleration (where Hahn & Savin, 2013, estimate the initial energy flux density present as $6.7 \pm 0.7 \times 10^5$ erg cm^{-2} s^{-1}). Hahn and Savin (2014) find that the spatial profile of the wave damping is correlated with the loop length, suggesting that the mechanism responsible for the damping of the waves depends on the global loop properties. Oscillating transverse displacements have also been measured directly in coronal plumes from SDO/AIA observations by, for example, Thurgood et al. (2014), who find that the energy budget contained within these resolved oscillations is insufficient to account for the acceleration of the solar wind.

2.2.2.11. Observations of Coronal Heating from Magnetic Reconnection

Parker proposed that the origin of nanoflares is the dissipation of magnetic tangential discontinuities

(reconnections) that are created by the photospheric random motion of a bundle of magnetic field footpoints. Hard X-ray observations show that the detected events in the flare-microflare energy range ($\geq 10^{27}$ ergs, over about three decades) are distributed in energy following a power law with an index greater or close to, −2 (see, e.g., Crosby et al., 1993; Lin et al., 1984, and references therein). Similar studies have also been addressed observing small impulsive transients in the soft X-ray (using Yohkoh/SXT) and EUV (SOHO/EIT, SUMER, and TRACE data) both in QS and ARs (Aletti et al. 2000; Aschwanden & Parnell, 2002; Bazarghan et al., 2008; Benz et al. 2005; Berghmans et al., 1998; Buchlin et al., 2006; Krucker & Benz, 1998; Parnell & Jupp, 2000; Pauluhn & Solanki, 2007). Hudson (1991) pointed out that a power law steeper than −2 is required for nanoflares to be energetically important (compared to larger flares). Since nanoflares are not directly observable, this requires extrapolation from the observed events, which are much more energetic. There are two problems with this extrapolation. First, as mentioned previously, there are large uncertainties in the measured power-law slope. Second, an extrapolation from flare energies to nanoflare energies may not be appropriate. Yashiro et al. (2006) have found that the slopes for flares that are and are not associated with CMEs are different, with the confined flare slope being steeper than −2. Nanoflares are more likely related to confined flares than to eruptive flares.

Even in resolved flares, it is the consequences of reconnection on the plasma that is observed, such as bidirectional jets (Innes et al., 1997). Such signatures are expected to be especially difficult to detect in nanoflare-associated jets. For example, reasons that it may be difficult to detect nanoflare jets are if jet energy is converted to thermal energy rapidly, if the jet interacts with the surrounding plasma, if the filling factor is $<<1$, 3D effects, tearing islands, and if thermal conduction cools the associated shocks rapidly (e.g., see Cargill, 1996; Klimchuk, 1998, for a discussion of these effects).

As with chromospheric heating, one way to estimate the amount of reconnection is through the change in the magnetic field and estimated flux cancellation. Using a potential field model calculated from SUNRISE/IMaX data, Wiegelman et al. (2013) found that the connectivity in the upper solar atmosphere changes rapidly, suggesting magnetic reconnection. However, both Wiegelman et al. (2013) and Chitta et al. (2014) estimated an upper limit of the free magnetic energy that would be available to magnetic reconnection, and found that it was too small to explain the coronal heating in the QS. We note that the above estimates do not take into account the free magnetic energy associated with tangling and twisting of the field on small scales. Such energy could easily be enough to power the QS (Klimchuk, 2006, 2015).

Evidence and theory suggest that X-ray bright points are produced by flux cancellation (e.g., Archontis & Hansteen, 2014; Falconer et al., 1999; Longcope, 1998; Martin et al., 1985; Parnell & Galsgaard, 2004; Parnell & Priest, 1995; Priest et al., 1994, and review by Priest et al., 2018). Flux cancellation has been associated with coronal loop brightenings, also implicating magnetic reconnection (Tiwari et al. 2014; Huang et al. 2018). Chitta et al. (2018) observed fluctuations in the footpoint of a coronal loop observed in the171 Å channel of SDO/AIA, concurrent with flux cancellation. They concluded that the flux cancellation could provide energy to heat the corona to temperatures over 5 MK. Braiding followed by reconnection has been observed recently in the Hi-C, high-resolution observations of an AR in the EUV (Cirtain et al., 2007). The event observed is shown in Figure 2.11. Panel e shows an image observed with Hi-C, while c shows an unsharp mask version of the image. Panels a, b, d, and f show concurrent SDO/AIA images of the same region. The event was a C1.7 flare, which might share similar physics to smaller nanoflares.

One important observation that is unique to magnetic reconnection is very hot, >5MK plasma. The DEM of ARs generally decreases quite sharply above the peak at 3MK, and it is difficult to quantify the highest detectable temperature emission, though attempts have been made. The very hot plasma is emitted in the very early phase of the cooling (e.g., Cargill, 1994; Cargill et al., 1995). For this reason, it can possibly preserve more information on the heating properties (Parenti et al., 2006). In the recent decade, several efforts have been made to detect such plasma. It has been identified in on-disk AR using EUV, soft X-ray, and hard X-ray (e.g., Brosius et al., 2014; Hannah et al., 2016; Marsh et al., 2018; Patsourakos & Klimchuk, 2009; Reale & Ciaravella, 2006; Reale et al., 2009a, 2009b; Schmelz et al., 2016; Testa et al., 2011; Warren et al., 2012; Figure 2.12), even though the quantification with respect to the background, 3 MK plasma has been a very difficult task. EUV data rely in the detection of Fe XVIII-XIX emission (formed around logT=6.9) in deep exposures. The general agreement is that it is present in an amount consistent with nanoflares. Most recently (Parenti et al., 2017) quantified the hot plasma in off-limb AR data using very deep exposures of Fe XIX: up to ~0.1% of the plasma from the bulk corona could reach ~10 MK. For the first time, it was shown that this hot plasma was persistently present almost everywhere in the core of the AR up to about 9 Mm above the limb (Figure 2.13). A smaller amount of hot plasma was detected on the disk by the rocket FOXSI-2 in hard X-ray (Ishikawa et al., 2017).

Table 2.5 (from Parenti et al., 2017) summarizes from the literature the index (β) of the inferred power-law slope above 5 MK, which shows an important variability

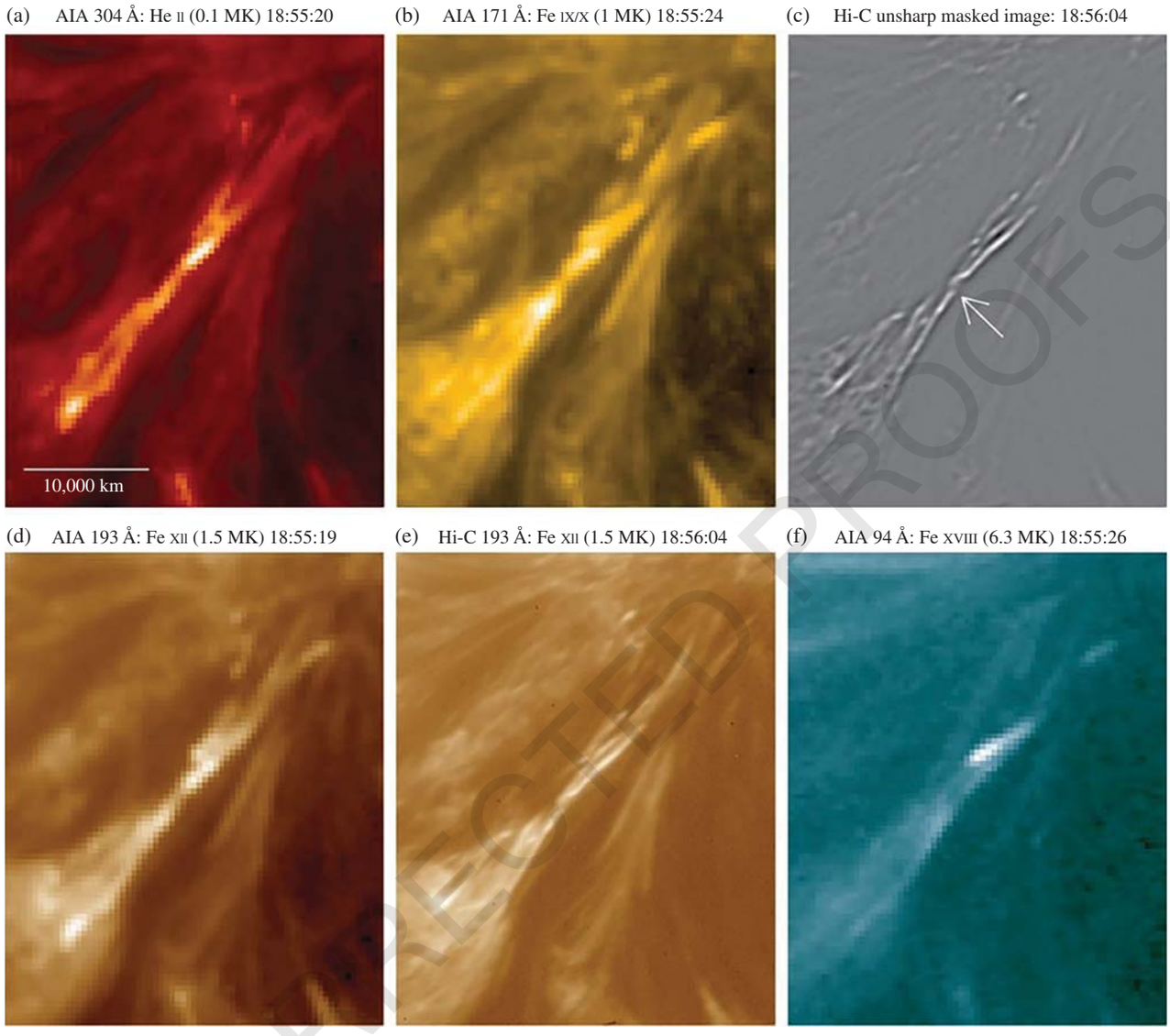

Figure 2.11 Magnetic reconnection observed after braiding in Hi-C for a C1.7 flare. A, b, d, and f show the event viewed in different AIA passbands. E shows the Hi-C image, and c shows an unsharp mask version of the Hi-C. (*Source*: Adapted from Cirtain et al., 2007.)

($-14 < \beta < -4.4$). At high temperatures, the EUV and X-ray emissions become weak, inferring the slope becomes very difficult, and the uncertainties in the measure increase. In some cases, the power-law shape has not been confirmed (Barnes et al., 2016). It is also possible that changes in the DEM shape (and so in the power-law index) may occur during the AR lifetime (e.g., Ko et al. 2016). More work has to be done in this respect. Indeed, the properties of this very high-temperature plasma are not yet completely understood. The physics involved may be more complex as at the very high temperature this tenuous plasma can be in non-equilibrium conditions (Bradshaw & Cargill 2006; Bradshaw, 2009). Ionization non-equilibrium, as well as departures from Maxwellian distributions in general, are important to consider in the interpretation of observations (Dudík et al., 2017).

More generally, the presence of hard X-rays (HXR) indicate hot >5MK plasma and can be used to identify nanoflares. HXR emission can also be used to test whether nanoflares have similar physical processes as larger flares, namely, magnetic reconnection that results in particle acceleration. Microflares are observed to have HXR emission and hot plasma. RHESSI observations (review by Hannah et al., 2011) show that microflares resemble more energetic flares in many respects, including that they occur only in AR, have high temperatures and

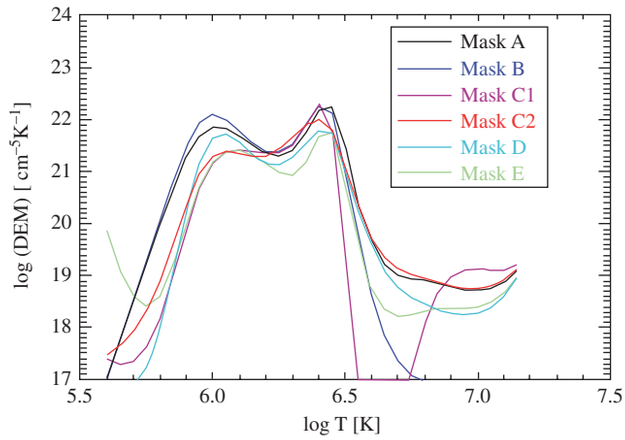

Figure 2.12 Results from the DEM inversion for different areas (indicated by Mask letter) in an off-limb active region (AR). Only Mask B does not reach a very high temperature. (*Source*: Parenti et al. (2017). © 2017 IOP Publishing.)

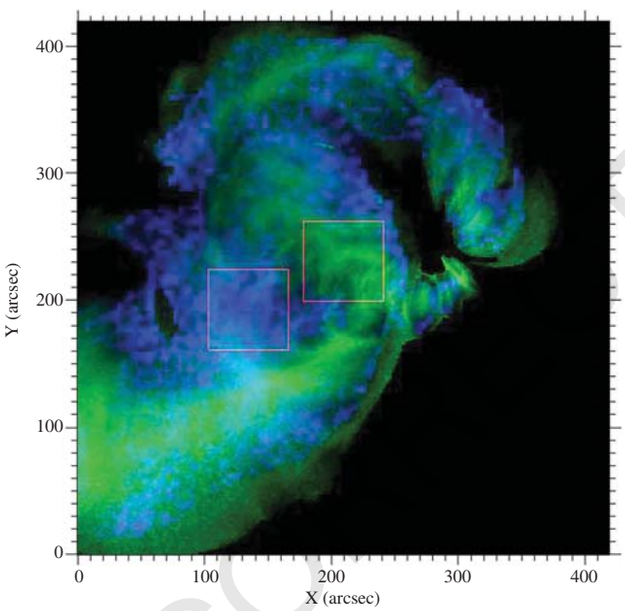

Figure 2.13 Map of temperature in an active region (AR). The Green scale refers to an average of 3 MK, and the blue scale localizes the plasma above 5 MK. (*Source*: From Reale et al., 2009).

non-thermal emission, and non-thermal energy deposition for microflares was confirmed with Nuclear Spectroscopic Telescope Array (NuSTAR; Glesener et al., 2017; Wright et al., 2017). Although the amount of energy in microflares does not account for the global coronal heating budget, the observations show that they supply substantial coronal heating in the locations where they occur.

Because microflares are part of a distribution of flares, it is possible that flares smaller than microflares could supply the energy for the global coronal. In order to see if even smaller events, which could explain coronal heating, exist, data from the ~~Focusing Optics X-ray Solar Imager~~ (FOXSI) rocket and the NuSTAR have been used. Marsh et al. (2018) showed that these HXR data were consistent with nanoflares and ruled out steady heating. Kuhar et al. (2018) showed evidence of three "flares" in NuSTAR that are eight orders of magnitude fainter than flares—smaller than microflares. However, even these smaller flares are larger than the canonical nanoflare. Importantly, they had substructure within them, indicating that they ~~werecomprised~~ of many smaller fundamental magnetic reconnection events.

A final piece of evidence of magnetic reconnection and coronal nanoflares is beams of non-thermal electrons. Such particles are observed in association with larger flares. Type III radio emission is a possible diagnostic of electron beams that may be associated with nanoflares (e.g., Saint-Hilaire et al., 2013; Alissandrakis et al., 2015; Bouratzis et al., 2016; James & Subramanian, 2018~~;~~). Chen et al. (2013) showed with larger flares that Type III emission can even be used as a diagnostic to localize the magnetic reconnection site. It is even possible that nanoflare-accelerated electron beams leave signatures in the solar wind electron velocity distribution function (e.g., Che & Goldstein, 2014). High-resolution IRIS observations also show evidence of non-thermal electrons. IRIS observed intensity and velocity variability at the footpoint of a hot, dynamic coronal loop, which Testa et al. (2014) concluded were consistent with beams of non-thermal electrons in a nanoflare. The beams were estimated to have deposited ~~⊠~~10^{25} erg of energy into the chromosphere and TR. Indeed, the energy deposited by the non-thermal particles in the chromosphere could be an important contribution to the coronal plasma response in a nanoflare (Brown et al., 2000).

2.3. MODELING OF THE SOLAR ATMOSPHERE

The ultimate goal of theory and modeling is to understand the fundamental physics well enough to quantitatively predict the observables described above. Modeling the relevant physics for the entire solar atmosphere is not possible with current computational resources. For example, it is not possible to resolve the thin current sheets and their dissipation regions up through the global corona scales or even active region scales simultaneously. Within these computational limitations and the available observations, there are three main modeling strategies for studying coronal heating, each with its strengths and weaknesses. The important point is that they all must approximate or represent some aspects of the physics. In

some, it is immediately apparent, and in some, the approximations are more subtle. In all cases, there are situations and interpretations that are appropriate, and conclusions and applications that are not.

The first modeling approach is to perform detailed simulations of the energy release process (broadly categorized as magnetic reconnection or waves, though as we have outlined above, they are not mutually exclusive). To do this accurately requires zooming in on a very small region of the solar atmosphere, such as an individual current sheet. Resistive MHD is generally adequate for coronal conditions, though kinetic effects may become important as smaller and smaller structures develop. A key requirement is achieving a high enough resolution, because the numerical resolution affects the dissipation and heating (e.g., Galsgaard & Nordlund, 1996). The disadvantage of this approach is that coupling to larger scales and to the lower atmosphere cannot be easily included. Such coupling can affect the energy release itself, because there is often a feedback between large-scale stresses and the reconnection that allows the field to evolve. Equally important is the energetic and dynamic coupling between the corona and transition region/chromosphere, which dramatically impacts the plasma properties and radiative output of the corona. This can cause serious problems when comparing predicted observations with actual observations to evaluate the models.

The second approach to studying coronal heating is to treat the heating in an ad hoc manner by simply specifying its spatial and temporal dependencies. Then, the response of the plasma, including the crucial coupling with the lower atmosphere, can be simulated with great accuracy. These are the so-called hydrodynamic loop models discussed in section 2.1. The advantage here is that meaningful comparisons with observations can be made. The spatial and temporal dependencies of the heating can be changed to determine which ones give the best agreement. Because they are computationally less expensive than global models (model type three), the massive parameter space of the possible heating mechanisms and their associated spatial and temporal dependencies can be investigated efficiently. The disadvantage is that the properties of the heating are assumed and not necessarily motivated by a particular physical mechanism. Nevertheless, the observationally derived properties place valuable constraints on any theories for the mechanism, current or future.

The third approach attempts to combine the first two by treating both the energy release process and the response of the plasma, including the production of observational signatures. This is sometimes called *ab initio*, or first principles, modeling. Impressive models of active regions and even the global corona have been obtained. However, present-day computers are not capable of accurately simulating simultaneously the energy release process and the coupling to the lower atmosphere and the global scales. The dominant heating mechanism in these simulations is ohmic dissipation of relatively large-scale currents, and it is not yet understood if this is a reasonable proxy for what is heating the solar atmosphere. Measurements of kG elemental flux tubes in the photosphere lead to the conclusion that an individual AR contains on the order of 100,000 current sheets or more (Klimchuk, 2015). Simulations of the range of physical effects relevant for the reconnection of even a single current sheet is highly challenging (Daughton et al., 2011; Huang & Battacharjee, 2016; Leake et al. 2020), let alone for 100,000. The actual heating mechanism operating on the Sun (fundamentally involving small-scale structures and viscosity, according to models of type 1) has not yet been established. A crucial aspect is the onset of reconnection. As discussed by Klimchuk (2015), reconnection must remain switched off to allow magnetic stresses to build, and switch on to release the stored energy only after a sufficient level of stress has been reached. If reconnection were to happen too soon, the corona would be cooler than observed.

All three approaches to the coronal heating problem provide useful information. Eventually, they will converge on a common solution. But the limitations of each approach must be recognized at all times.

2.3.1. Approach One: Local MHD Models

2.3.1.1. Wave Heating

As is evident from the observations described above, the key question for wave-based heating of the solar atmosphere is no longer whether waves and oscillations are present but whether they contain sufficient energy and whether wave dissipation occurs on the right timescales and in the right locations. Alfvén(ic) waves, in particular, are seen as a highly effective way to transport energy from below the Sun's surface out into the solar atmosphere, and the suggestion of Alfvén-wave-based heating of the solar atmosphere was already made by Alfvén (1947) (see also, e.g., Wentzel, 1974; Wentzel, 1976; or Hollweg, 1978). However, classical resistive or viscous dissipation of the Alfvén wave energy is slow, as it is proportional to the viscous and magnetic Reynolds numbers (both >>1). For example, Porter et al. (1994) pointed out that even though observed non-thermal line broadenings might imply sufficient wave fluxes, this does not necessarily mean that this wave energy is readily converted into heat. Arregui (2015) argued that given the rapid damping of many of the observed (standing) transverse loop oscillation (generally within a few oscillation periods), it is not at all clear that the time scales involved even allow for heating to occur during the actual oscillations.

To enhance the dissipation rate of Alfvén waves, mechanisms such as resonant absorption (Ionson, 1978; Tataronis & Grossman, 1973) and phase mixing (Heyvaerts & Priest, 1983) were proposed. Both resonant absorption and phase mixing depend on the presence of a variation in the local Alfvén speed and the fact that individual field lines can oscillate with their own Alfvén frequency. Resonant absorption occurs when, on a specific magnetic surface, a "global" mode (reflects the large-scale plasma and magnetic structure) is in resonance with local oscillations. This will lead to the transfer of energy from large-scale perturbations to small length scales at a rate that is independent of the diffusion coefficients, giving effective damping of the large-scale mode (see, e.g., Hollweg & Sterling, 1984; Poedts et al., 1989; Poedts et al., 1990; Ofman et al., 1995, or Goossens et al., 2011, for a review of resonant absorption). Resonant absorption itself is a damping rather than a dissipation mechanism; to provide heating, dissipation of the wave energy must still occur within the resonant layer, which is often implicitly assumed to happen on timescales similar to the damping of the original global perturbation.

Phase mixing occurs when Alfvén waves gradually move out of phase on neighboring field lines with different Alfvén speeds (due to a transverse inhomogeneity in the density and/or the magnetic field strength), generating increasingly large transverse gradients, again leading to more efficient dissipation. This leads to a significant enhancement of the dissipation, which under the assumption of strong phase mixing becomes proportional to the cube root of Rm (the magnetic Reynolds number) and Re (the viscous Reynolds number) (Heyvaerts & Priest, 1983). Although theoretical models of the individual mechanisms are usually presented, there is a natural close interplay between resonant absorption and phase mixing, where the small-scale oscillations in the resonant layer are expected to undergo phase mixing due to the local variation in the Alfvén speed (see, e.g., Ruderman et al., 1997a, 1997b). Apart from resonant absorption and phase mixing, other mechanisms such as mode conversion (to modes that might more readily dissipate) and ion-cyclotron resonance have also been proposed (see reviews by, e.g., Aschwanden, 2004; Erdélyi & Ballai, 2007; Goedbloed & Poedts, 2004; Klimchuk, 2006, and references therein). Ion-cyclotron waves in particular are likely important for heating coronal holes and the acceleration of the fast solar wind (see Cranmer et al., 2017, and
AQ10 Chapter ~~7~~on the solar wind).

There is a very substantial body of literature on the theoretical and numerical development of wave-based heating models, particularly in the 1980s and early 1990s (see, e.g., Aschwanden, 2004; Goedbloed & Poedts, 2004, or Goossens et al., 2011, for more detailed reviews). For resonant absorption and/or phase mixing to occur, a gradient in the Alfvén speed has to be present. Also implicit in the models is the presence of an ignorable coordinate, where Parker (1991) argues that this might not readily be the case in the solar atmosphere, leading to coupling to other modes. The most often-used equilibrium configuration for wave-heating models is a straight (and uniform) magnetic field with a transverse density gradient (balanced by a change in temperature to maintain cross-field pressure balance), although see, for example, Poedts et al. (1990) for resonant absorption in a sheared magnetic field. Most modeling then injects waves into this equilibrium (either through imposing a perturbation on the equilibrium or through boundary driving) and investigates the heating through dissipation of the wave energy. However, this is where wave-based heating mechanisms face a fundamental problem. In magnetically closed loops, the density is related to the magnitude of the heating (see, e.g., Klimchuk, 2006, or Reale, 2014), which immediately begs the question of whether wave heating can self-consistently sustain the assumed (equilibrium) density profile or if ~~it~~ is an additional (alternative) heating mechanism needed to sustain the high-density region and prevent draining (e.g., Bradshaw & Cargill, 2010). If the former, then the imposed density structure must be compatible with the spatial profile of the wave heating. If the latter, then there are new questions to answer, such as: what is the required (background) heating mechanism, how does it affect the wave-based heating, and does this automatically imply that the contribution from wave-based heating must be small?

Cargill et al. (2016) assessed the self-consistency of assuming a fixed (preexisting) density gradient by examining the evolution of the coronal density when wave heating takes place. They found that heating due to phase mixing of Alfvén waves cannot sustain the assumed density. Conceptually, this is relatively easy to understand. Phase mixing leads to enhanced dissipation (local heating) where the gradient in the Alfvén speed, that is, in the density, is largest. However, cooling and draining are proportional to the density (not to the gradient of the density) and therefore will occur faster where the density is highest. In other words, the imposed density profile (which leads to phase mixing) cannot be sustained self-consistently by the wave heating. The same basic conclusion holds for resonant absorption (Ofman et al., 1998). Cargill et al. (2016) also look at the related question of whether density changes induced by the wave heating affect the imposed (equilibrium) density profile sufficiently to alter the wave propagation and dissipation (see also Ofman et al., 1998). It is found that including feedback of the heating on the density gradient can lead to significant local structuring but that this occurs only on timescales longer than the thermal evolution of the loop (i.e., the changes to the density profile due to cooling

and draining are more significant that the local structuring due to the wave heating). In addition, the authors point out again that transport coefficients need to be substantially enhanced to obtain effective heating. Pagano and De Moortel (2017) study heating due to phase mixing in 3D MHD simulations where transverse footpoint displacements trigger kink modes that mode couple to torsional Alfvén modes in the boundary shell of the cylindrical flux tube. As expected, the Alfvén waves phase mix in the boundary layer of the loop but even with the use of (excessively) high values of magnetic resistivity and strong footpoint drivers, the heating due to phase mixing is insufficient to be relevant for coronal heating. Further work by Pagano et al. (2018) and Pagano and De Moortel (2019) extended this study to include multi-harmonic loop oscillations and an observed power spectrum, but the basic conclusion remains unchanged.

So, can the slow dissipation rate of the Alfvén wave energy that seems to be inherent to the basic phase mixing and resonant absorption models be increased? One possibility is the development of the Kelvin–Helmholtz instability and/or the onset of turbulence (see, e.g., Browning & Priest, 1984; Lee & Roberts, 1986; Hollweg, 1986; Hollweg & Yang, 1988; or Hollweg & Johnson, 1988, for early discussions). A turbulent cascade of wave energy down to smaller length scales where dissipation becomes efficient might address the problem of the slow dissipation rate of Alfvén waves. A frequently studied model is turbulence induced by the (internal) reflection of waves (e.g., Matthaeus et al., 1999; Suzuki & Inutsuka, 2005; Verdini & Velli, 2007). Numerical modeling by van Ballegooijen et al. (2011) showed that reflections at the transition region could lead to such a turbulent cascade of Alfvén waves in the chromosphere down to dissipative length scales and could account for the required chromospheric heating rate (see also Asgari-Targhi et al., 2013, 2014; van Ballegooijen et al., 2014), though the present Alfvén wave turbulence modeling currently does not satisfy observational constraints (van Ballegooijen et al., 2017). However, the model uses reduced MHD and hence compressive effects such as the coupling between Alfvén waves and slow modes or the formation of (compressive) shocks cannot be evaluated (see also, e.g., Tu & Song, 2013). In the chromosphere, compressive effects are expected to be important, with several authors showing that shock heating might in fact be the dominant mechanism (e.g., Hollweg et al., 1982; Kudoh & Shibata, 1999; Matsumoto & Suzuki, 2012, 2014; Arber et al., 2016). In the corona however, the compressive effects might be less significant. A cascade of Alfvénic turbulence is also present in the global models of coronal heating and solar wind by, for example, Sokolov et al. (2013) and van der Holst et al. (2014), though it is parameterized (see section 2.3.3). A recent paper by Magyar et al. (2017) looked at the development of turbulence-like behavior for unidirectionally propagating Alfvénic waves, that is, without internal reflections, in a perpendicularly inhomogeneous plasma. The authors find that this generalized phase mixing model can lead to "uniturbulence" with complex, ribbon-like current structures throughout the 3D volume. Enhanced dissipation can also be associated with the presence of an instability such as the Kelvin–Helmholtz instability (KHI), and the strong shear motions at the edges of transverse oscillating loops have been shown to lead to the rapid development of the KHI (e.g., Antolin et al., 2014; Browning & Priest, 1984; Ofman et al., 1994; Terradas et al., 2008; Uchimoto et al., 1991). However, whether this is sufficient to make wave-based heating significant is still under debate (e.g., Howson et al., 2017a, 2017b; Guo et al., 2019; Karampelas et al., 2017).

If wave-induced turbulence (or unresolved Alfvénic motions) makes a viable contribution to heating of the solar atmosphere, this contribution should be evident in observed line broadening (see also, e.g., De Moortel et al., 2014; Liu et al., 2014; Morton et al., 2015 for indirect evidence for the possible presence of Alfvénic turbulence). For example, Carlsson et al. (2015) find that the width of the chromospheric O I 135.6 nm line implies non-thermal velocities less than 10 km/s, whereas De Pontieu et al. (2015) find that non-thermal line broadening at the transition region (IRIS Si IV) footpoints of coronal loops is limited to about 20 km/s. Such observations place constraints on the amount of unresolved Alfvénic turbulence in the (lower) solar atmosphere, and, so far it is not clear that sufficient power is present to play a significant role in coronal heating.

We note here that we have so far only described wave heating based on dissipation in a fully ionized plasma. Whereas this assumption is most likely valid for the solar corona, in the chromosphere, dissipation due to ion-neutral collisions becomes important (e.g., Khodachenko et al., 2004; Khomenko & Collados, 2012), and several authors have shown this can lead to efficient chromospheric heating (e.g., De Pontieu et al., 2001; Goodman, 2011; Leake et al., 2005; Song & Vasylunas, 2011; Tu & Song, 2013).

Modeling can establish whether wave heating can be efficient enough to obtain viable heating rates, and observations can place limits on the available wave energy flux. However, to assess whether any particular (wave) heating model is indeed operating in the solar atmosphere, observational signatures need to be established through forward modeling. For such observational characteristics to be meaningful, the full thermodynamic response of the plasma (including thermal conduction and radiation) needs to be included in the modeling.

So far, it has not proved easy to establish unique observational signatures associated with wave-based heating

mechanisms (see Taroyan & Erdélyi, 2009, for a review of heating diagnostics with MHD waves). For example, it is not clear whether wave-based heating would appear near-continuous or episodic ("bursty") and hence, difficult to distinguish from reconnection-based heating models (e.g., Antolin & Shibata, 2010; De Groof & Goossens, 2002; Klimchuk, 2006; Mendoza-Briceño et al., 2005; Mendoza-Briceño & Erdélyi, 2006; Moriyasu et al., 2004; Ofman et al., 1998). If resonant absorption and/or phase mixing leads to drifting of the heating layers (Cargill et al., 2016; Ofman et al., 1998), heating may appear impulsive (depending on the resolution) and could resemble a nanoflare storm. Indeed, based on 3D reduced-MHD numerical models of Alfvén wave propagation, van Ballegooijen and collaborators (Asgari-Targhi et al., 2013, 2014; van Ballegooien et al., 2011, 2014) found that the spatial and temporal distribution of heating events was similar to the profile of a nanoflare storm. Although these authors pointed out that the wave-based coronal heating rate was dependent on the loop parameters (with an increase in heating rate with coronal field strength and a decrease with loop length), this does not provide robust, observational characteristics that can be used in isolation as it relies on being able to make a direct comparison between different loops (as well as being able to reliably measure the field strength)—a limitation that is likely to be true for any parameterization of heating mechanisms in terms of loop parameters such as field strength or length. On the other hand, investigating the different observational signatures of heating by nanoflares or Alfvén wave dissipation, Antolin et al. (2008, 2010) suggested that coronal rain could provide insight into coronal heating mechanisms. Comparing observed estimated heating profiles with analytically and numerically obtained profiles, Van Doorsselaere et al. (2007) suggest that any wave-heating mechanism should be dominated by a resistive rather than a viscous phenomenon. Taroyan et al. (2007) demonstrated that the power spectrum of Doppler shift oscillations can be used to distinguish between uniform and footpoint heating of coronal loops and to estimate the average energy of a single heating event.

2.3.1.2. Magnetic Reconnection

The other types of simulations that fall under the heading of this first modeling approach are those that study dissipation during magnetic reconnection. The time-dependent nature of reconnection was hypothesized from the current sheet tearing mode instability (Furth et al., 1963), well before detailed numerical simulations demonstrated their existence. The Parker idea of nanoflares is that photospheric motions that twist and tangle the fields result in the formation of tangential discontinuities, which correspond to currents. Though braided fields are not often observed, elementary magnetic fields are not resolved by current instruments, and, given their aspect ratios, misalignments are not expected to be obvious in existing instrumentation (Wilmot-Smith, 2015). The process by which these field lines relax back into a force-free equilibrium has been the focus of many recent experiments. See Wilmot-Smith (2015) and Cargill et al. (2010) for excellent reviews on reconnection experiments. A general result is that thin current layers form, and a highly dynamic, but statistical steady state is achieved where the Poynting flux and dissipation are coupled on long timescales, but decoupled on short timescales. In the numerical models, dissipation can be both ohmic and viscous, and is bursty and spatially localized.

Moving to 3D theory and numerical simulations of magnetic reconnection provided important new insight. In particular, Hornig and Priest (2003), Priest et al. (2003), and Pontin et al. (2005) demonstrated that it is not possible to follow individual field lines through the diffusion region. Instead, the reconnection in 3D takes a finite volume and amount of time and involves many field lines at any one instant (not just two). The coronal tectonics framework with driving from the magnetic carpet was advanced by Priest et al. (2002), with dissipation at the separatrix surfaces. Currents can form and reconnection can take place both at the central reversal and current sheets, but also separatrices (Priest & Forbes, 2000). These separatrix surfaces occur because of the motion and localization of the magnetic field (Schrijver et al., 1999). Related, quasi-separatrix layers (QSLs; Démoulin et al., 1997; Priest & Démoulin, 1995; Titov et al., 2002) are locations where the magnetic connectivity has steep gradients, rather than being truly discontinuous. Current sheets can also form at QSLs (Titov, 2007), and electric currents may dissipate there as well (Aulanier et al., 2005; Bellan, 2006; Pariat et al., 2009). Simulations have advanced to the point of applying the tectonics framework to loop models of magnetic reconnection. Such simulations model the magnetic field line as straight and occurring between two parallel plates, with velocities applied at the boundaries. There is no flux emergence or cancellation in these models; instead, they investigate how footpoint motions of different types (rotation, shears) result in reconnection and dissipation (De Moortel & Glasgaard, 2006a,b; Mellow et al., 2005; Wilmot-Smith & De Moortel, 2007; Knizhnik et al. 2018, 2019; Leake et al., 2020;).

Boundary shears, or flows oppositely directed across a neutral flow line, were applied first in a loop simulation by van Ballegooijen (1988). They found that shear driving produced QSLs (Titov et al., 2002), locations where magnetic reconnection is likely to occur. Resistive 3D MHD models show that shearing generates electric currents, and the strength of the currents grows

exponentially (Galsgaard & Nordlund, 1996). The current sheet fragments, the magnetic structure is complex, and the dissipation is bursty.

Moving on from simple shear motions, others have approximated solar granulation with rotational motions (e.g., Gomez et al., 2000; Longcope et al., 1993; Rapazzo et al., 2007), based on the principle that twisting the photospheric footpoints should produce dissipation at many current sheets (Tucker, 1973). Random circulation patterns at small scales can be linked to energetic heating events occurring with power-law frequency distributions (Knizhnik et al., 2018), and such experiments yield insights into the possible relationship of the coronal heating problem to the helicity injection and condensation processes that shape the large-scale corona (Antiochos, 2013). The kink instability (Hood & Priest, 1979) can also result in line-tied coronal field lines if they are twisted past a certain threshold. Once this threshold is reached and the kink instability sets in, strong current sheets develop, and energy is dissipated by magnetic reconnection (Browning et al., 2008; Hood et al., 2009).

In contrast to these footpoint-driving motions, loop simulation can begin with a braided loop (Longbottom et al. 1998). The conclusion of the braiding experiments is that the nature of the photospheric tangling and flows will impact the resulting heating (Wilmot-Smith et al., 2011). Recent advancements have included braiding with footpoint motions, and have produced models that account for the connection of the corona with the chromosphere and the important mass and energy exchanged between the two, through the transition region. These have resulted in predictions of realistic coronal temperatures that result from the energy dissipation of magnetic field stresses from rotating the magnetic footpoints (Reale et al., 2016) and from random footpoint motions (Dahlburg et al., 2016). Both cases produce EUV emission from hot, multi-million temperature plasma, which is crucial for testing theories with observations, and both find the heating rate in the loops to be highly structured in space and time.

Flux emergence and cancellation is another way for footpoint motions to generate magnetic reconnection (e.g., Parnell & Priest, 1995; Welsch, 2006). Priest et al. (2018) recently expanded the flux cancellation concept analytically in 3D for the case of coronal heating, though flux emergence and cancellation had been studied extensively for larger flares. Syntelis et al. (2019) modeled flux cancellation and showed that hot ejections with temperatures of coronal loops and/or cool ejections can be formed depending on the height of the reconnection. Chen et al. (2014) modeled flux emergence in the formation of a solar AR, and showed that footpoint braiding can be an inherent feature of flux emergence. The simulated emergence-braiding generates currents that dissipate and can heat the corona to temperatures of 1 MK. In a QS example, Meyer et al. (2013) estimated flux cancellation rates using the HMI/ SDO and showed that there is enough energy to maintain the radiative losses of the QS corona, with a lower limit of 8.7×10^4 erg cm^{-2} s^{-1}.

Under wave models, we described the onset of turbulence from waves. MHD turbulence can also be set in motion by slow footpoint motions under the same "DC" regime as magnetic reconnection (e.g., Mikić et al., 1989). The turbulence converts energy to ohmic heating; that is, the dissipation of electric currents (Hendrix & van Hoven, 1996), and again, the results show an intermittent distribution of events in space and time (e.g., Dmitruk et al., 1998; Einaud et al., 1996; Georgoulis et al., 1998; Rappazzo et al., 2008), with well-developed power laws in energy spectra ~~are~~ found in the simulations (Georgoulis et al., 1998; Rapazzo et al., 2010), even when driven by simple shear motion (Dahlburg et al., 2009). For a general background on MHD instabilities, turbulence, and magnetic reconnection, see Biskamp (1997); for a review of the impact of turbulence in the solar environment on reconnection and heating, see Matthaeus and Velli (2011); and for a review on MHD of magnetic reconnection in a turbulent media, see Browning and Lazarian (2013). Because particle acceleration may occur with nanoflare reconnection, it is an important aspect to capture in reconnection simulations as well. Particle acceleration is highly dependent on the nature of the current sheet, or current sheet fragments (Cargill et al., 2012), so turbulence may be an important path to accelerating non-thermal particles (Browning & Lazarian, 2013; Vlahos et al., 2016). Baumann and Nordlund (2012) discuss results from particle-in-cell simulations that couple the kinetic scales with MHD scales, which is an important advancement in linking particle acceleration with coronal heating.

Theories of avalanches and self-organized-criticality may also prove important for explaining nanoflare storms. They provide a useful description of larger solar flares (Lu et al., 1993; Vlahos et al., 1995), and extrapolating the application to nanoflares shows promise (Georgoulis et al., 1998). See Charbonneau et al. (2001) for a nice review on avalanche models. Detailed 3D MHD simulations of avalanches show that an individual unstable magnetic strand (elemental field line) can start an avalanche, triggering other strands to go unstable, even when they are below marginal stability (Hood et al., 2016; Tam et al., 2015).

2.3.2. Approach Two: Field-Aligned Hydrodynamic Modeling

We now discuss the second approach in more depth. It has received the most attention through the years.

Our discussion concerns the atmosphere in an individual magnetic flux tube for which the plasma is approximately uniform over the cross section. We refer to this as a strand. It is the fundamental building block of the magnetically closed corona. Observationally distinguishable loops in coronal images are bundles of unresolved strands. The diffuse component of the corona, which contains more plasma and produces more emission than distinct loops (Viall & Klimchuk, 2011), is also made up of strands. Because the plasma beta is large and thermal conduction is highly efficient along the magnetic field but inhibited across it, we can treat each strand as a rigid thermally insulated pipe. Strands are rooted in the photosphere at both ends and are often treated as semicircular. The shape has little influence as long as the maximum height is less than the gravitational scale height, which is usually the case in ARs.

We first consider steady (time-independent) heating. If both the heating and the cross-sectional area are symmetric about the loop midpoint, the loop atmosphere will be in static equilibrium. (An important exception is when the heating is highly concentrated at low coronal altitudes, which we discuss below.) Roughly one third of the energy deposited in the coronal portion is radiated directly to space. The remaining two thirds is thermally conducted down to the transition region at the footpoints and radiated to space from there. Although the transition region is very thin, its emissivity (ergs cm^{-3} s^{-1}) is far stronger than in the corona, so it can accommodate the downward energy flux. The equilibrium corona is thus characterized by a balance between the energy input from coronal heating and cooling from radiation and thermal conduction. The energy balance in the transition region is primarily between heating from thermal conduction and cooling from radiation. There may also be some direct heating that occurs locally, but it is usually thought to be small owing to the thin nature of the transition region. If we define the top of the transition region to be the place where thermal conduction switches from a cooling term above to a heating term below (Klimchuk et al., 2008), then it occurs at a temperature of roughly 60% of the maximum temperature in the strand. If the maximum is 3 MK (where the emission measure distribution peaks in ARs), the transition region will extend to 1.8 MK. Thus, much of the emission from ARs that is normally thought of as "coronal" actually comes from the transition region of the hot coronal loops.

Because both wave and magnetic reconnection heating are unlikely to be steady (Klimchuk, 2006), an important question concerns the frequency with which nanoflares repeat in a given strand. If they repeat on a time scale that is short compared to a cooling time, the state of the plasma is similar to what it would be if the heating were truly steady. This is called high-frequency heating. We now discuss the opposite case of low-frequency heating, where the plasma has time to cool fully between successive events.

When a heating event occurs in a strand that is otherwise experiencing minimal heating, the temperature rises suddenly. It can reach values approaching or even exceeding 10 MK. Thermal conduction is very strong at these elevated temperatures, and the coronal plasma cools quickly. The intense downward conduction flux heats the plasma in the transition region and top of the chromosphere, raising its pressure and causing it to expand rapidly into the corona. This is the well-known process of chromospheric evaporation.

As the coronal temperature falls and its density increases from evaporation, thermal conduction becomes less effective, and radiation takes over as the dominant cooling mechanism. The plasma continues to cool after evaporation ceases completely, and it begins to drain back down to the surface as the pressure support declines. This is known as chromospheric condensation, the inverse process of evaporation. Eventually the strand reaches a final state characterized by low temperature and density.

Because the thermodynamic variables (temperature, pressure, and density) are reasonably uniform along the coronal portion of the strand at any given time, it is meaningful to consider their field-line averages. The evolution of the average values can be well described by considering the effect of enthalpy (the flux of internal energy carried by flowing plasma). During evaporation, the excess of the downward thermal conduction flux compared to transition region radiation drives an upward enthalpy flux. During condensation, the radiation from the transition region exceeds the downward thermal conduction flux, and a downward enthalpy flux makes up the difference. This is the basis of the "0D" hydrodynamics code EBTEL (Cargill, Bradshaw, & Klimchuk, 2012; Klimchuk et al., 2008).

Observations seem most consistent with heating events that occur with a distribution of frequencies and for which the distribution is centered roughly on a frequency corresponding to an inverse cooling time (~1000 s) (Cargill et al. 2015). Some heating events have higher frequency, giving rise to quasi-steady conditions, and others have lower frequency, giving rise to the very hot, though faint, plasma that is often called the smoking gun of nanoflares (Cargill, 1994).

As mentioned above, symmetric steady heating does not always produce an equilibrium state. If it is concentrated at low coronal altitudes, a fascinating situation called thermal non-equilibrium (TNE) can occur (Antiochos & Klimchuk, 1991). With TNE, no solution to the steady-state fluid equations exists. The strand atmosphere is constantly evolving even though the heating is not. The strand is essentially searching for a

nonexistent equilibrium, and as it does so it periodically undergoes a thermal runaway, related to, but different from a thermal instability (Klimchuk, 2019). This usually results in the formation of a cold condensation of chromospheric temperature high in the corona. The condensation slides down the loop leg to the solar surface, and the cycle repeats. This is the generally accepted explanation of coronal rain (Antolin et al., 2010; Muller et al., 2004; Schrijver, 2001). If there is a dip in the magnetic field, that is, a region of upward concavity, the condensation may settle in the dip and grow. This is believed to be the process by which prominences form (Antiochos et al., 1999; Karpen et al., 2006; Luna et al., 2012). Long-period (multi-hour) loop pulsations (Auchere et al., 2014; Froment et al., 2015, 2017) and periodic reconnection events at null point topologies (Mason et al., 2019) have also been attributed to TNE. It is possible that TNE is even more widespread than just these relatively isolated phenomena, perhaps playing an important role in the diffuse component of the corona (Downs et al., 2016; Winebarger et al., 2016; ~~Yung~~ et al., 2016).

It has recently been recognized that asymmetries in the heating and/or cross-sectional area affect TNE (Froment et al., 2018; Mikić et al., 2013). If the asymmetries are modest, a cold condensation may not form. A thermal runaway begins, but the plasma reheats before it drops significantly below 1 MK. This is sometimes called incomplete condensation. However, if the asymmetries are larger than roughly a factor of 3, TNE is prevented from occurring altogether (Klimchuk & Luna, 2019). A steady-state end-to-end flow develops instead. The essence of TNE is that heating is too weak at high altitudes to balance the radiation, which is set by the strong heating at low altitudes. If the asymmetry-driven flow is fast enough, a gradient in the enthalpy flux is able to balance the excesses radiation, preventing TNE from occurring.

Before moving on to discuss models of the third type, we point out the existence of what might be called hybrid models. These take information on heating from "MHD-based" models that cannot accurately predict the plasma response and radiation signature, and feed that heating information into the hydrodynamic models that can. Examples include (e.g., Buchlin et al., 2007; Gontikakis et al., 2013; López Fuentes & Klimchuk, 2015; Moraitis, et al., 2016; Parenti et al., 2006; Reale et al., 2005; Walsh & Galtier, 2000).

2.3.3. Approach Three: Global Models of the Solar Atmosphere

One of the more challenging aspects of studying the coronal heating problem stems from the inherently multi-dimensional nature of the corona itself. This is somewhat paradoxical, considering how the dominance of the magnetic field and the great efficiency of field-aligned electron heat conduction has traditionally led to the corona being thought of as a collection of independent, stratified atmospheres collimated along flux tubes. It is precisely this character, however, that ensures a litany of magnetic conditions are simultaneously present in the coronal volume and baked into our remote-sensing diagnostics. From the hot plasma threaded by strong magnetic fields in ARs, to the warm, diffuse plasma in the meandering weak-field regions of the QS, to the colder, outflowing plasma that becomes the solar wind along open flux tubes, each system presents a different set of heating conditions and field geometries, each defining its own unique piece of the coronal heating puzzle.

As mentioned previously, we typically observe coronal plasma via optically thin emission lines. In this case, any intensities measured by a detector represent the integrated emission along the line of sight and thus include contributions from the entire coronal (and transition region) volume along it. Because the governing equations are strongly linked to the magnetic field geometry (loop length, areal expansion, and inclination), changes in the hydrodynamic character of coronal plasmas become particularly important as the magnetic field properties change along a given line of sight or from region to region. In this light, extending our intuition gleaned from analytic theory and single flux tube modeling to the myriad complex and inherently 3D conditions present in the corona is a nontrivial task.

One way to tackle this problem in models is to consider the "realistic," 3D nature of the coronal magnetic field by incorporating information from observations. Typically, this falls into two categories: employing 3D coronal magnetic field extrapolations, or using full 3D magnetohydrodynamic (MHD) computations, the latter of which capture the hydrodynamic and magnetic evolution simultaneously. In either case, such models typically incorporate measurements of the magnetic field in the photosphere as the inner boundary condition, enabling one to study the entire corona (or a subregion) at a particular point in time.

A popular use of magnetic field extrapolations in coronal heating studies has been to test empirical scaling laws of coronal heating, in particular, the relationship between the coronal heating rate and the magnetic field strength, field stratification, and loop length. As illustrated by Mandrini et al. (2000), one can relate the scaling of loop properties in a 3D magnetic field model with the predicted scaling of various coronal heating theories, narrowing the plausible range of theories. Furthermore, simple hydrostatic loop modeling along selected loop bundles can be combined with forward modeling of EUV and soft X-ray emission to test which

(if any) heating formulation may be most consistent with observations (e.g., Lundquist et al., 2008; Schrijver et al., 2004). A modern take on this technique is to simulate the hydrodynamic evolution of hundreds to thousands of loop bundles within a given field model using either 1D hydrodynamic models or a more efficient "0D" approach that captures the average evolution of loop plasma in response to a specified heat input (i.e., the EBTEL model; Klimchuk et al., 2008). In this way, the time-dependent evolution of a given subregion of the corona can be studied in the context of realistic geometries and observables, greatly extending our ability to characterize and contextualize coronal heating models (e.g., Bradshaw & Viall, 2016; Nita et al., 2018; Ugarte-Urra et al., 2017).

That being said, solving simplified 0D or 1D hydrodynamic loop models along realistic magnetic loop bundles is not without its disadvantages. Lines of sight passing through the corona will include emissivity contributions over a range of heights and loop bundles; therefore, selecting loop bundles in such a way that they sufficiently sample the variety of loop properties in the 3D volume that contribute to the emissivity is a matter of art. Often, the method used to fill the loop bundles results in empty voxels between filled loops, which is unphysical. At a certain point, if the spatially resolved hydrodynamic evolution is to be simulated accurately for many thousands of loop bundles, it may make more sense to do the calculation in 3D, where the full dynamic range of the magnetic field and volume-filling nature of the corona can be properly accounted for. The utility of doing so is nicely illustrated in Mok et al. (2016), which still uses a realistic magnetic field extrapolation but efficiently solves for the parallel hydrodynamic transport, including gradients and expansion in the magnetic field. In this case, they illustrated how a steady, but stratified coronal heating profile (concentrated at loop footpoints) could lead to rich heating and cooling signatures, exciting TNE, and coronal rain cycles in a significant portion of an AR.

Moving toward increasing sophistication, the standard approach for modeling the coupled hydrodynamic and magnetic evolution of astrophysical plasmas on large, macroscopic scales is to use some variant of the MHD equations in a numerical model. For capturing coronal heating in realistic field contexts, the ideal MHD equations must be extended (at a minimum) to include the relevant thermodynamic terms in the energy equation: coronal heating, optically thin radiative losses, and field-aligned electron heat conduction, a variant sometimes referred to as "thermodynamic" MHD (e.g., Lionello et al., 2009). Solving for these terms allows the plasma density and temperature to be computed with realistic thermodynamic energy balance along various magnetic structures in the corona. Solutions can also be benchmarked by the forward modeling of EUV and X-ray observables (including SDO/AIA bandpasses), allowing the solution to be compared directly with observations. Some more specialized "radiative" MHD models are expressly designed to connect the dynamics of the convection zone directly to the low corona, incorporating prescriptions for radiative transfer in the chromosphere and below (e.g., Abbett, 2007; Gudiksen et al., 2011).

It should be mentioned that solving for electron heat conduction substantially increases the difficulty of a given hydrodynamic or MHD computation. This is because of the stiff, parabolic nature of the term itself and the extremely small conduction length scales that are present in the transition region (dictated by the steep dependence of the conductivity with temperature). Resolving the conduction length scales in the transition region can be essential for describing the hydrodynamics of coronal plasmas (Bradshaw & Cargill, 2013), and this requirement implies strict limitations on the grid size and/or feasibility of multidimensional simulations. Various practical solutions include treating the transition region as an unresolved discontinuity (Johnston et al., 2017), broadening the conduction length scale in a manner that preserves the coronal hydrodynamics (Johnston et al., 2019; Lionello et al., 2009), or using an alternate form of the conduction term itself (Rempel, 2017)

For our purposes, it helps to divide MHD models that study coronal heating further into two broad categories: (a) Local, *ab initio* models that attempt to capture all or some of the physical mechanisms that cause heating on small scales, and (b) global models that capture both the large and small scales of the magnetized corona. The first category includes models that attempt to capture the connection between surface flows in the photosphere (where the plasma β is large) and energy dissipation in the corona. Seminal 3D simulations by Gudiksen and Nordlund (2005) illustrated how footpoint motions of the magnetic field in the photosphere could lead to Joule (resistive) dissipation in the coronal volume, and the formation of plasma structures that resemble the cool loop-like structures observed in EUV. Other simulations have further elucidated the Joule heating mechanism (Bingert & Peter, 2011), as have complementary scenarios involving Alfvénic fluctuations powering the corona and solar wind (De Pontieu et al., 2007). Simulations capturing the complete convection zone to corona connection are also crucial for detailing the way in which the local convective dynamo continually stresses the corona, and how the relevant energies convert and vary as a function of height in the solar atmosphere (Abbett, 2007).

As computational power grows, and methods for approaching this problem become more sophisticated, new details are emerging on exactly how such braiding or

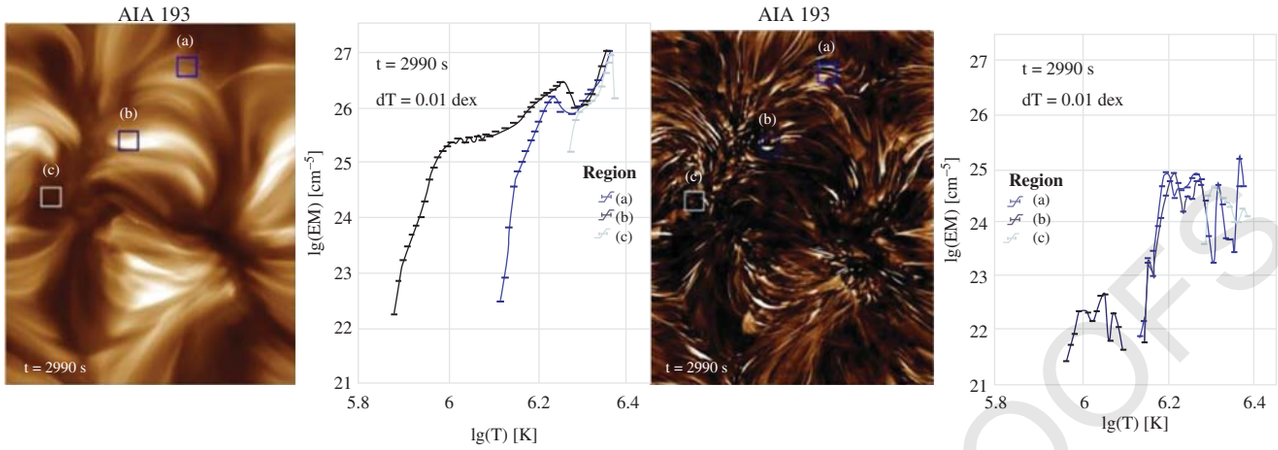

Figure 2.14 High-resolution radiative MHD simulation spanning the convection zone and corona for a 24×24 Mm patch of quiet Sun (from Kanella & Gudiksen, 2019). Here, forward-modeled SDO/AIA 193°A images are computed for the total volume (left) and sub-volumes with clearly identified heating events (right). The emission measure distributions (EM vs. T) are plotted for specific lines of sight. (*Source*: Kanella & Gudiksen, 2019. © 2019.)

"DC" heating mechanisms dissipate energy and how we observe it. For example, recent work by Rempel (2017) shows that when the magnetic Prandtl number of the simulation increases, viscous heating by strong Lorentz force induced flows may dominate direct Joule dissipation. Similarly, forward modeling of line-of-sight integrated plasma emissivities from high-quality, high-resolution simulations (e.g., Kanella & Gudiksen, 2019) are increasingly able to test and challenge our assumptions of how DC heating mechanisms should manifest observationally. An example of results from a high-resolution radiative MHD simulation spanning the convection zone and corona for a 24×24 Mm patch of QS (Kanella & Gudiksen, 2019) is shown in Figure 2.14. The left panel shows the predicted SDO/AIA emission in the 193 Å channel computed over the entire volume, while the right volume shows sub-volmes and identifies individual heating events. The emission measure distributions (EM vs. T) for specific lines-of sight are also shown, illustrating how a background of diffuse multithermal-thermal plasma may conceal individual heating events. In such a setup, Joule heating can be systematically characterized in space and time and connected to the evolution of plasma quantities and observables. In particular, these efforts inform us on how impulsively heated plasma structures in 3D relate to our nominal, simplified notions of loop geometry and cross sections.

The second broad category of MHD models capture the 3D, global volume of the solar corona, and provide a complementary and powerful tool for studying the coronal heating problem. Because it is not yet feasible to simultaneously capture the full volume of the corona (<1−20 R_s) and the scales where dissipation occurs in a single numerical model (<200 km and smaller), global models will generally specify the heating term directly, using either empirical scaling laws (Downs et al., 2010; Lionello et al., 2009) or by solving an additional set of equations that encapsulate the macroscopic effects of an unresolvable heating mechanism (van der Holst et al., 2014; Mikić et al., 2018).

Including the global structure of the corona has a number of key advantages. First, by including the full spherical volume of the solar corona, one naturally captures a large dynamic range of magnetic field strengths, loop geometries, and plasma β regimes. This ensures that a wide parameter space can be explored with a given heating formulation. Assessing the influence of a heating model on all morphological regions in the corona at the same time (ARs, QS, coronal holes) helps build a complete perspective on coronal heating and identify the missing or problematic aspects of a given approach. Second, by including the thermodynamic heating and transport processes, such models naturally provide a realistic background of temperatures and densities in the corona, providing a starting point for studying dynamic, large-scale phenomena such as CMEs, where forward modeling of coronal observables is an essential piece connecting theory to observations (Downs et al., 2012; Jin et al., 2016).

Third, an often-overlooked but important aspect of the coronal heating problem is the way in which the plasma heating and acceleration can directly influence the coronal magnetic field structure and morphology. Although ARs are typically thought of as magnetically dominated, this is not generally true in the extended corona and solar wind. In fact, it is the interplay between

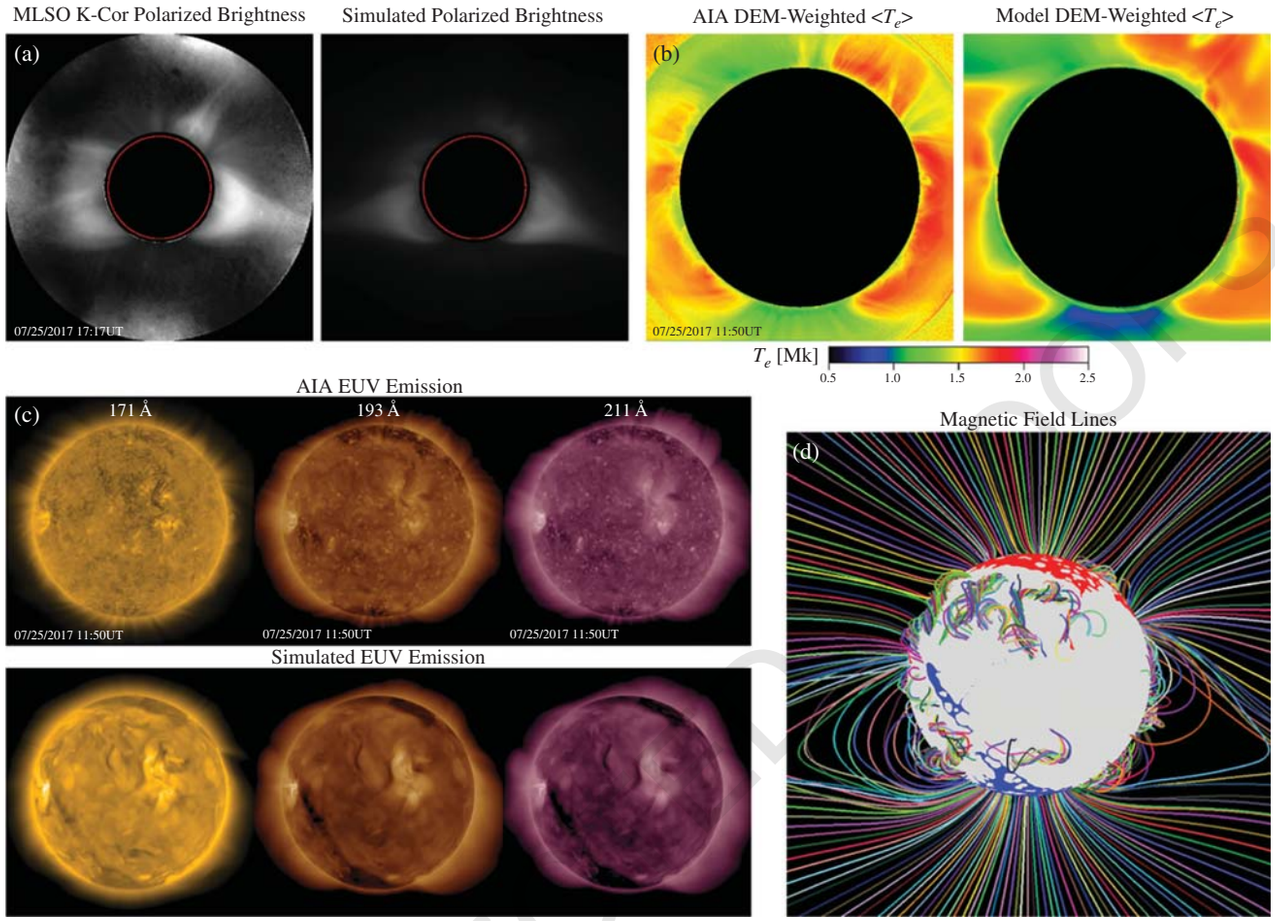

Figure 2.15 Diagnostics from a thermodynamic MHD model of the global corona and their comparison with observations. (a) Radially filtered K-Corona brightness in visible light. (b) Average electron temperatures. (c) EUV emission in three of the SDO/AIA imaging bandpasses. (d) The underlying magnetic field, visualized with traces near the plane of sky and a map of the open (blue/red) and closed (gray) flux at the inner boundary. (*Source*: Mikić et al., 2018.)

the thermal and ram pressures of the heated plasma with the overlying magnetic field that opens the coronal magnetic fields in the first place, creating bipolar helmet streamers and unipolar pseudostreamers (and perhaps continually modulating them; e.g., Mason et al., 2019). Assessing how and where a given heating model can affect the global coronal morphology in EUV (Downs et al., 2010) and white light (Mikić et al., 2018) can provide complementary information and constraints to the overall magnitude and scaling of coronal heating mechanisms. Figure 2.15 shows an example comparing the results of a 3D MHD global model with observations (from Mikić et al., 2018). Panel a shows the predicted radially filtered K-Corona brightness in visible light, which is sensitive to electron density, next to that observed at Mauna Loa Solar Observatory (MLSO). Panel b shows the predicted electron temperatures and those measured by SDO/AIA, determined by fitting EUV intensities off the limb. Panel c shows the observed and predicted EUV emission in three of the SDO/AIA imaging bandpasses. Panel d shows the underlying magnetic field, visualized with traces near the plane of sky and a map of the open (blue/red) and closed (gray) flux at the inner boundary

Along these lines, it is now possible to explore the unification of coronal heating and solar wind acceleration in such models. It has long been postulated that the turbulent fluctuations observed in the solar wind have a low coronal origin (at least in part), and a number of theories exist that link them (see review by Cranmer et al., 2015 and Chapter ~~7~~, on the solar wind). There has been a AQ11
recent trend to develop tractable formalisms that capture the macroscopic propagation, reflection, and dissipation of low-frequency Alfvénic turbulence, which is used to specify coronal heating and solar wind acceleration in

global models (Mikić et al., 2018; Usmanov et al., 2018; van der Holst et al., 2014). Although specific implementations vary, the key concept is to leverage the natural scaling of the Poynting flux of waves injected into the corona with the magnitude of the magnetic field at the base of a given flux tube. Nicely articulated by Sokolov et al. (2013), this provides the large dynamic range of heating required for the different morphological regions of the corona, and such formalisms have reasonable scaling properties for both open (Lionello et al., 2014), and closed-field regions of the corona (Downs et al., 2016). Exploring the extent to which phenomenological modeling can capture the basic properties of the corona and solar wind is key for delineating when or where the small-scale or stochastic aspects of coronal heating are (or are not) essential for describing the global state of the corona and inner heliosphere.

Ultimately, whether using extrapolations for hydrodynamic modeling, conducting sophisticated *ab initio* experiments, or simulating the global corona, all of these varied approaches incorporate the realistic multidimensional nature of the coronal magnetic field in some way. Perhaps the most important commonality of these multidimensional approaches is that they enable the forward modeling of coronal observables, and their interpretation in direct observational contexts. This latter aspect is key for characterizing heating mechanisms, and is becoming even more important as our remote-sensing diagnostics become more sensitive and varied.

For example, although static EUV and soft X-ray morphologies have been the primary focus of a number of coronal heating studies, it is now clear that the time dependence of coronal emission may pose an additional set of constraints on how, when, and where coronal heating is deposited. Capturing how certain formalisms may or (may not) explain the predominant heating and cooling cycles observed in line-of-sight integrated emission from ARs (e.g., time lags; Viall & Klimchuk, 2012) is an important next step in vetting competing heating scenarios (Bradshaw & Viall, 2016; Winebarger et al., 2016).

2.4. FUTURE PROSPECTS FOR MODELING AND OBSERVATIONS

The understanding of the heating and energization of the solar atmosphere has come a long way from the initial approximation of a plane parallel atmosphere with three static layers: chromosphere, transition region, and corona. The magnetic field is fundamental to the heating. Spatial and temporal dynamics on multiple scales resulting in impulsive heating seem to be unavoidable. Many improvements in understanding small-scale impulsive heating have been made in the past two decades, but there is plenty of room for further development.

Observations have now clearly established that waves and oscillations are prevalent throughout all structures of the solar atmosphere, and many of the observed oscillations are reported to contain a substantial energy budget, comparable to, for example, the QS heating requirements. However, establishing the actual contribution of the observed waves and oscillations to heating of the solar atmosphere remains an open challenge, as there are still substantial difficulties to be addressed for wave-based heating mechanisms to be viable, particularly in the corona of magnetically closed regions such as AR loops. Likewise, it is clear that magnetic reconnection provides heating to the solar atmosphere, but issues still need to be addressed before definitive conclusions can be made. A more accurate characterization of the very hot emission is also needed, as the hot, >5 MK temperature plasma is a unique indication of magnetic reconnection. The connection between the layers of the atmosphere is crucial, and further quantitative observational constraints on the relation between the chromosphere and corona are needed, as the new high-resolution IRIS results seem to be just the tip of the iceberg. It is clear now that in the highly structured and dynamical solar atmosphere, multiple heating mechanisms will be at work (most likely simultaneously), and the true "coronal heating question" is to determine the relative contribution of different mechanisms in different structures and under different circumstances.

New telescopes and instrumentation that are poised to provide new and/or high-fidelity measurements of the solar atmosphere now or in the near future include Solar Orbiter (February 09, 2020), and the ground-based telescopes Daniel K. Inoue Solar Telescope (DKIST), the European Solar Telescope (EST), and The Atacama Large Millimeter/submillimeter Array (ALMA). The SPICE spectrometer on Solar Orbiter will provide measurements of electron temperatures in the outer corona; DKIST has been designed to make polarimetric measurements of the magnetic field of the off-limb low corona at 0.1 arcsec spatial resolution, which will be an important advancement in the understanding of the AR magnetic configuration; and ALMA primarily probes chromospheric temperatures and heating at high spatial, temporal, and spectral resolution (Wedemeyer et al., 2016).

Coordinating these synergistic observations with each other and with models is crucial for further advancement and understanding. For example, because the DKIST magnetic field diagnostic involves line-of-sight convolutions of the temperature and density as well as the magnetic field strength and/or orientation, interpreting such measurements will increasingly require context provided by models that capture both realistic coronal heating mechanisms and magnetic field geometries.

Solar Orbiter has the unique characteristics of approaching the Sun down to 0.3 AU and moving out of

the ecliptic. Measurements of the photospheric magnetic field (instrument PHI), together with the UV-EUV imaging (full sun at medium resolution with EUI/FSI and high resolution with EUI/HRI) and spectroscopic data (SPICE) from a unique point of view will be made. For the first time, ARs will be observed outside of the ecliptic, providing additional information on their topology, magnetic field, and plasma flow directions. Occasionally, depending on the spacecraft–Sun–Earth angle, coordinated observations will be made with other observatories. These include, for instance, DKIST and SDO. Different LOS measurements of the photospheric magnetic field (PHI, DKIST, and SDO/HMI), combined with UV imaging (SDO/AIA and EUI/FSI) will provide important constraints to the 3D geometry of ARs. If still available, STEREO could also contribute with different orbit configurations with Solar Orbiter, and would provide white light images of the corona and solar wind outflow. For the first time, it will be possible to perform stereo-spectroscopy using, if still available, HINODE/EIS and IRIS and DKIST, with SPICE. We could achieve a more precise diagnostics of plasma flow and constrain the line-of-sight effects on the density and temperature measurements.

Looking toward the near future for modeling, the potential unification of models that simultaneously describe heating and solar wind acceleration opens up new ways to study the coronal heating problem. It has been known for some time that the relative charge states, elemental abundances, fluctuation content, and speed distribution of the solar wind (measured in situ by spacecraft) encode key details of the underlying heating mechanism. Ensuring that a given model satisfies not only remote-sensing diagnostics but in situ measurements as well provides tighter constraints on the models (e.g., Oran et al., 2015) and forces us to broaden our perspective beyond the low corona when studying this classic problem. The in situ plasma measurements made with Parker Solar Probe and Solar Orbiter compared with the remote-sensing spectral diagnostics with the SPICE spectrometer on Solar Orbiter will provide important constraints in this way (Del Zanna & Mason, 2018). Likewise, the connection between coronal heating solar wind and particle acceleration could be also probed with spectroscopic observations.

In summary, the heating of the solar atmosphere involves universal, fundamental physical processes such as waves, magnetic reconnection, turbulence, and particle acceleration. In addition, it is important for understanding the solar wind that fills the solar system, and space weather interactions with Earth and other solar system planets, as well as for understanding stellar atmospheres and how they create and modulate the space environment around their exoplanets.

ACKNOWLEDGMENTS

N.M.V and J.A.K. are supported by the NASA Heliophysics Internal Scientist Funding Model. I.D.M. has received support from the European Union Horizon 2020 research and innovation program (grant agreement No. 647214) and the Research Council of Norway through its Centres of Excellence scheme, project number 262622. S.P. acknowledges the funding by CNES through the MEDOC data and operations center. CD was supported by the NASA Heliophysics Supporting Research program, grant 80NSSC18K1129.

REFERENCES

Abbett, W. P. (2007). *The Astrophysical Journal*, *665*, 1469. doi: 10.1086/519788. AQ12

Aletti V., Velli, M., Bocchialini, K., Einaudi, G., Georgoulis, M., & Vial, J.-C. (2000). *The Astrophysical Journal*, *544*, 550.

Alfvén, H. (1947). *Monthly Notices of the Royal Astronomical Society*, *107*, 211–219.

Alissandrakis, C. E., Nindos, A., Patsourakos, S., Kontogeorgos, A., & Tsitsipis, P. (2015). *Astronomy & Astrophysics*, *582*, 52.

Antiochos, S. K. (2013). *The Astrophysical Journal*, *772*, 72.

Antiochos, S. K., & Klimchuk, J. A. (1991). *The Astrophysical Journal*, *378*, 372.

Antiochos, S. K., MacNeice, P. J., Spicer, D. S., & Klimchuk, J. A. (1999). *The Astrophysical Journal*, *512*, 985.

Antiochos, S. K., & Noci, G. (1986). *The Astrophysical Journal*, *301*, 440.

Antiochos, S. K., Karpen, J. T., DeLuca, E. E., Golub, L., & Hamilton, P. (2003). *The Astrophysical Journal*, *590*, 547.

Antolin, P., Okamoto, T. J., De Pontieu, B., Uitebroek, H., Van Doorselaere, T., & Yokoyama, T. (2015). *The Astrophysical Journal*, *809*, 72. doi: 10.1088/0004-637X/809/1/72

Antolin, P., & Rouppe van der Voort, L. (2012). *The Astrophysical Journal*, *745*(2), article id. 152, 21 pp.

Antolin, P., & Shibata, K. (2010). *The Astrophysical Journal, 712*, 494–510.

Antolin, P., Shibata, K., & Vissers, G. (2010). *The Astrophysical Journal*, *716*, 154.

Antolin, P., & Verwichte, E. (2011). *The Astrophysical Journal, 736*, 121.

Antolin, P., Shibata, K., Kudoh, T., Shiota, D., & Brooks, D. (2008). *The Astrophysical Journal*, *688*, 669–682.

Antolin, P., Yokoyama, T., & Van Doorsselaere, T. (2014). *Astrophysical Journal Letters*, *787*, L22.

Antonucci, E., Gabriel, A. H., & Patchett, B. E. (1984). *Solar Physics, 93*, 85–94.

Arber, T. D., Brady, C. S., & Shelyag, S. (2016). *The Astrophysical Journal*, *817*, 94.

Arregui, I., Oliver, R., & Ballester, J. L. (2012). *Living Reviews in Solar Physics*, *9*, 2.

Arregui, I. (2015). *Philosophical Transactions of the Royal Society A*, *373*, 20140261.

Aschwanden, M. J. (1987). *Solar Physics*, *111*, 113–136.

Aschwanden, M. J. (2004). *Physics of the solar corona. An introduction*. Chichester, UK: Praxis Publishing Ltd.
Aschwanden, M. J., Fletcher, L., Schrijver, C. J., & Alexander, D. (1999). *The Astrophysical Journal*, *520*, 880.
Aschwanden, M. J., & Nightingale, R. W. (2005). *The Astrophysical Journal*, *633*, 499.
Aschwanden, M. J., & Peter, H. (2017). *The Astrophysical Journal*, *840*, 4.
Aschwanden, M.J., & Parnell, C.E. (2002). *The Astrophysical Journal*, *572*, 1048.
Aschwanden, M. J., & Terradas, J. (2008). *Astrophysical Journal Letters*, *686*, L127–L130
Asgari-Targhi, M., van Ballegooijen, A. A., Cranmer, S. R., & DeLuca, E. E. (2013). *The Astrophysical Journal*, *773*, 111.
Asgari-Targhi, M., van Ballegooijen, A. A., & Imada, S. (2014). *The Astrophysical Journal*, *786*, 28.
Auchere, F., Bocchialini, K., Solomon, J., & Tison, E. (2014). *Astronomy & Astrophysics*, *563*, A8.
Auchère, F., Froment, C., Soubrié, E., Antolin, P., Oliver, R., & Pelouze, G. (2018). *The Astrophysical Journal*, *853*, 176.
Banerjee, D., Erdélyi, R., Oliver, R., & O'Shea, E. (2007). *Solar Physics*, *246*, 3.
Banerjee, D., Pérez-Suárez, D., & Doyle, J. G. (2009b). *Astronomy & Astrophysics, 501*, L15–L18.
Banerjee, D., Gupta, G. R., & Teriaca, L. (2011). *Space Science Reviews*, *158*, 267–288.
Banerjee, D., Teriaca, L., Doyle, J. G., & Wilhelm, K. (1998). *Astronomy & Astrophysics, 339*, 208–214.
Banerjee, D., Teriaca, L., Gupta, G. R., Imada, S., Stenborg, G., & Solanki, S. K. (2009a). *Astronomy & Astrophysics*, *499*, L29–L32.
Barnes, W.T., Cargill, P.J., & Bradshaw, S.J. (2016). *The Astrophysical Journal*, *833*, 217.
Baumann, G., & Nordlund, A. (2012). *The Astrophysical Journal*, *759*, 9.
Bel, N., & Leroy, B. (1977). *Astronomy & Astrophysics, 55*, 239.
Bemporad, A., & Abbo, L. (2012). *The Astrophysical Journal*, *751*, 110.
Benz, A. O., & Krucker, S. (2002). *The Astrophysical Journal*, *568*, 413.
Benz, A. O., Grigis, P. C., Csillaghy, A., and Saint-Hilaire, P. (2005) *Solar Physics*, *226*, 121. doi: 10.1007/s11207-005-5254-
Berger, T. E., De Pontieu, B., Schrijver, C. J., & Title, A. M. (1999). *The Astrophysical Journal*, *519*, 97.
Berghmans, D., Clette, F., & Moses, D. (1998). *Astronomy and Astrophysics*, *336*, 1039.
Berghmans, D., & Clette, F. (1999). *Solar Physics, 186*, 207–229.
Biermann, L. (1946). *Naturwissenschaften*, *33*, 118–119.
Bingert, S., & Peter, H. (2011). *Astronomy & Astrophysics*, *530*, A112. doi: 10.1051/0004-6361/201016019.
Bogdon, T. J., & Judge P. G. (2006). Observational aspects of Sunspot oscillations. *Philosophical Transactions of the Royal Society A: Mathematical, Physical and Engineering Sciences*, *364*. http://doi.org/10.1098/rsta.2005.1701
Bonet, J. A., Márquez, I., Sánchez Almeida, J., Cabello, I., & Domingo, V. (2008). *The Astrophysical Journal Letters*, *687*, L131.
Bouratzis, C., Hillaris, A., Alissandrakis, C. E., Preka-Papadema, P., Moussas, X., Caroubalos, C., et al. (2016). *Astronomy & Astrophysics*, *586*, 29.
Bradshaw, S. J., & Cargill, P.J. (2006). *Astronomy & Astrophysics*, *458*, 987.
Bradshaw, S. J. (2009). *Astronomy & Astrophysics*, *502*, 409.
Bradshaw, S. J., & Cargill, P. J. (2010). *The Astrophysical Journal*, *717*, 163
Bradshaw, S. J., & Cargill, P. J. (2013). *The Astrophysical Journal*, *770*, 12.
Bradshaw S. J., Klimchuk, J. A., & Reep, J.W. (2012). *The Astrophysical Journal 758*, 53.
Bradshaw, S. J., & Viall, N. M. (2016). *The Astrophysical Journal*, *821*, 63. doi: 10.3847/0004-637X/821/1/63.
Brooks, D. H., & Warren, P. (2016). *The Astrophysical Journal*, *820*, 63.
Brooks, D. H., Warren, H. P., & Ugarte-Urra, I. (2012). *Astrophysical Journal Letters*, *755*, 33.
Brosius, J. W., Daw, A. N., & Rabin, D. M. (2014). *The Astrophysical Journal*, *790*, 112.
Brown, J. C., Krucker, S., Güdel, M., & Benz, A. O. (2000). *Astronomy & Astrophysics*, *359*, 1185.
Browning, P. K., & Priest, E. R. (1984). *Astronomy & Astrophysics*, *131*, 283.
Browning, P. K., Gerrard, C., Hood, A. W., Kevis, R., & van der Linden, R. A. M. (2008). *Astronomy & Astrophysics*, *485*, 837.
Browning, P., & Lazarian, A. (2013). *Space Science Reviews*, *178*, 325.
Bryans, P., Young, P. R., & Doschek, G. A. (2010). *The Astrophysical Journal*, *715*, 1012–1020.
Buchlin, E., Vial, J.-C., & Lemaire, P. (2006), *Astronomy & Astrophysics*, *451*, 1091.
Buchlin, E., Galtier, S., & Velli, M. (2005). *Astronomy & Astrophysics*, *436*, 355.
Buchlin, E., Cargill, P. J., Bradshaw, S. J., & Velli, M. (2007). *Astronomy & Astrophysics*, *469*, 347.
Cargill, P. J. (1994). *The Astrophysical Journal*, *422*, 381.
Cargill, P. J. (1996). *Solar Physics*, *167*, 267.
Cargill, P. J. (2014), *The Astrophysical Journal*, *784*, 49.
Cargill, P. J., Mariska, J. T., & Antiochos, S.K. (1995), *The Astrophysical Journal*, *439*, 1034.
Cargill, P. J., Bradshaw, S. J., & Klimchuk, J. A. (2012). *The Astrophysical Journal*, *752*, 161.
Cargill, P. J., De Moortel, I., & Kiddie, G. (2016). *The Astrophysical Journal*, *823*, 31.
Cargill, P., Parnell, C., Browning, P., De Moortel, I., & Hood, A. (2010). *Astronomy & Geophysics*, *51*(3), 3.31–3.35. https://doi.org/10.1111/j.1468-4004.2010.51331.x
Cargill, P. J., Warren, H. P., & Bradshaw, S. J. (2015). *Philosophical Transactions of the Royal Society A: Mathematical, Physical and Engineering Sciences*, *373*(2042). https://doi.org/10.1098/rsta.2014.0260
Cargill, P. J., Vlahos, L., Baumann, G., Drake, J. F., & Nordlund, Å. (2012). *Space Science Reviews*, *173*, 223.
Carlsson, M., Judge, P. G., & Wilhelm, K. (1997). *The Astrophysical Journal*, *486*, L63–L66.
Carlsson, M., & Stein, R. F. (1992). *Astrophysical Journal Letters*, *397*, L59.

Carlsson, M., & Stein, R. F. (1997). *The Astrophysical Journal*, *481*, 500.

Carlsson, M., Hansteen, V. H., & De Pontieu, B. (2007). *Publications of the Astronomical Society of Japan*, *59*, S663–S668.

Carlsson, M., Leenaarts, J., & De Pontieu, B. (2015). *The Astrophysical Journal*, *809*, L30.

Cirtain, J. W., Golub, L., Lundquist, L., van Ballegooijen, A., Savcheva, A., Shimojo, M., et al. (2007). *Science*, *318*, 1580.

Chae, J., Yun, H. S., & Poland, A. I. (1998). *The Astrophysical Journal Supplement*, *114*, 151.

Charbonneau, P., McIntosh, S. W., Liu, H.-L., & Bogdan, T. J. (2001). *Solar Physics*, *203*, 321.

Che, H., & Goldstein, M. L. (2014). *The Astrophysical Journal*, *795L*, 38.

Chen, F., Peter, H., Bingert, S., & Cheung, M. C. M. (2014). *Astronomy & Astrophysics*, *564*, 12.

Chen, B., Bastian, T. S., White, S. M., Gary, D. E., Perley, R., Rupen, M., et al. (2013). *Astrophysical Journal Letters, 763L*, 21.

Chitta, L. P., Kariyappa, R., van Ballegooijen, A. A., DeLuca, E. E., & Solanki, S. K. (2014). *The Astrophysical Journal*, *793*, 112.

Chitta, L. P, Sukarmadii, A. R. C., Rouppe van der Voort, L., & Peter, H. (2019). *Astronomy & Astrophysics*, *623*, 176.

Chitta, L. P., Peter, H., Young, P. R. & Huang, Y. -M. (2017a) *Astronomy & Astrophysics*, *605*, A49, doi:10.1051/0004-6361/201730830

Chitta, L. P., Peter, H., Solanki, S. K., Barthol, P., Gandorfer, A., Gizon, L., et al. (2017b). *The Astrophysical Journal Supplement Series*, *229*, 4. doi:10.3847/1538-4365/229/1/4

Chitta, L. P., Peter, H., & Solanki, S. K. (2018). *Astronomy & Astrophysics*, *615*, 9. doi: 10.1051/0004-6361/201833404

Cranmer, S. R. (2009). *Living Reviews in Solar Physics*, *6*, 3. https://doi.org/10.12942/lrsp-2009-3

AQ13 Cranmer, S. R., Asgari-Targhi, M., Miralles, M. P., Raymond, J. C., Strachan, L., Tian, H. et al. (2015). *Philosophical Transactions of the Royal Society of London Series A*, *373*, 20140148. doi: 10.1098/rsta.2014.0148.

Cranmer, S. R., Gibson, S. E., & Riley, P. (2017). *Space Science Reviews*, *212*, 1345.

Crosby, N. B., Aschwanden, M. J., & Dennis, B. R. (1993). *Solar Physics*, *143*, 275.

Dadashi, N., Teriaca, L., & Solanki, S. K. (2011). *Astronomy & Astrophysics*, *534*, 90.

Dahlburg, R. B., Einaudi, G., Taylor, B. D., Ugarte-Urra, I., Warren, H. P., Rappazzo, A. F., et al. (2016). *The Astrophysical Journal*, *817*(1), article id. 47, 15 pp. doi: 10.3847/0004-637X/817/1/47.

Dahlburg, R. B., Liu, J.-H., Klimchuk, J. A., & Nigro, G. (2009). *The Astrophysical Journal*, *704*, 1059.

AQ14 Daughton, W., Roytershteyn, V., Karimabadi, H., Yin, L., Albright, B. J., Bergen, B., et al. (2011). *Nature Physics*, *7*, 539.

DeForest, C. E., & Gurman, J. B. (1998). *The Astrophysical Journal*, *501*, L217.

De Groof, A., & Goossens, M. (2002). *Astronomy & Astrophysics*, *386*, 691–698.

Del Zanna, G., & Mason, H. E. (2003). *Astronomy & Astrophysics*, *406*, 1089–1103.

Del Zanna, G., & Mason, H. E. (2018). *Living Reviews in Solar Physics*, *15*, 5. https://doi.org/10.1007/s41116-018-0015-3.

De Moortel, I., Antolin, P., & Van Doorsselaere, T. (2015). *Solar Physics, 290*, 399.

De Moortel, I., & Browning, P. (2015). *Philosophical Transactions of the Royal Society A*, *373*, 20140269.

De Moortel, I. (2009). *Space Science Review*, *149*, 65–81.

De Moortel, I., & Galsgaard, K. (2006a). Numerical modelling of 3D reconnection due to rotational footpoint motions. *Astronomy & Astrophysics, 451*, 1101–1115. doi:10.1051/0004-6361:20054587.

De Moortel, I., & Galsgaard, K. (2006b). Numerical modelling of 3D reconnection II. Comparison between rotational and spinning footpoint motions. *Astronomy & Astrophysics, 459*, 627–639. doi:10.1051/0004-6361:20065716.

De Moortel, I., Hood, A. W., Ireland, J., & Walsh, R. W. (2002a). *Solar Physics, 209*, 89–108.

De Moortel, I., Ireland, J., & Walsh, R. W. (2000). *Astronomy & Astrophysics*, *355*, L23.

De Moortel, I., Ireland, J., Walsh, R. W., & Hood, A. W. (2002b). *Solar Physics*, *209*, 61–88.

De Moortel, I., McIntosh, S. W., Threlfall, J., Bethge, C., & Liu J. (2014) *The Astrophysical Journal Letters, 782*, L34.

De Moortel, I., & Nakariakov, V. M. (2012). *Philosophical Transactions of the Royal Society A*, *370*, 3193.

De Moortel, I., & Pascoe, D. (2012). *The Astrophysical Journal Letters, 746*, 31.

De Moortel, I., Pascoe, D. J., Wright, A. N., & Hood, A. W. (2016). *Plasma Physics and Controlled Fusion*, *58*, article id 014001

De Pontieu, B., Berger, T. E., Schrijver, C. J., & Title, A. M. (1999). *Solar Physics*, *190*, 419.

De Pontieu, B., McIntosh, S. W., Carlsson, M., Hansteen, V. H., Tarbell, T. D., Schrijver, C. J. et al. (2007). *Science*, *318*, 1574–1577. AQ15

De Pontieu, B., Carlsson, M., Rouppe van der Voort, L. H. M., Rutten, R. J., Hansteen, V. H., & Watanabe, H. (2012). *The Astrophysical Journal Letters*, *752*, L12.

De Pontieu, B., De Moortel, I., Martinez-Sykora, J., & McIntosh, S. (2017). *Astrophysical Journal Letters 845*, L18.

De Pontieu, B., Martens, P. C. H., & Hudson, H. S. (2001). *The Astrophysical Journal*, *558*, 859.

De Pontieu, B., & McIntosh, S. W. (2010). *The Astrophysical Journal, 722*, 1013–1029.

De Pontieu, B., McIntosh, S., Martinez-Sykora, J., Peter, H., & Pereira, T. M. D. (2015). *The Astrophysical Journal*, *799*, L12.

De Pontieu, B., Erdélyi R., & De Moortel, I. (2005). *The Astrophysical Journal*, *624*, 61–64.

De Pontieu, B., & Erdélyi, R. (2006). *Philosophical Transactions of the Royal Society A*, *364*, 383.

De Pontieu, B., Title, A., & Carlsson, M. (2014). *Science*, *346*, D315.

Deubner, F.-L., & Fleck, B. (1989). *Astronomy & Astrophysics, 213*, 423–428.

Dmitruk, P., Gómez, D. O., & DeLuca, E. E. (1998). *The Astrophysical Journal*, *505*, 974.

Doschek, G. A., Mariska, J. T., Warren, H. P., Brown, C. M., Culhane, J. L., Hara, H., et al. (2007). *The Astrophysical Journal, 667*, L109–L112.

Dowdy, J. F., Jr., Rabin, D., & Moore, R. L. (1986). *Solar Physics*, *105*, 35.

Downs, C., Lionello, R., Mikic´, Z., Linker, J. A., & Velli, M. (2016). *The Astrophysical Journal*, *832*, 180. doi: 10.3847/0004-637X/832/2/180.

Downs, C., Roussev, I. I., van der Holst, B., Lugaz, N., & Sokolov, I. V. (2012). *The Astrophysical Journal*, *750*, 134. doi: 10.1088/0004-637X/750/2/134.

Downs, C., Roussev, I. I., van der Holst, B., et al. (2010). *The Astrophysical Journal*, *712*, 1219. doi: 10.1088/0004-637X/712/2/1219.

Dudík, J., Dzifčáková, E., Meyer-Vernet, N., Del Zanna, G., Young, P. R., Giunta, A. et al. (2017). *Solar Physics*, *292*, 100.

Edlén, B. (1943). Die deutung der emissionslinien im spektrum der sonnenkorona. Mit 6 abbildungen. *Zeitschrift für Astrophysik*, *22*, 30–64.

Einaudi, G., Velli, M., Politano, H., & Pouquet, A. (1996). *The Astrophysical Journal*, *457*, 113.

Erdélyi, R., & Ballai, I. (2007). *Astronomische Nachrichten*, *328*, 726–733.

Erdélyi, R., Doyle, J. G., Perez, M. E., & Wilhelm, K. (1998). *Astronomy & Astrophysics, 337*, 287.

Fletcher, L. & De Pontieu, B. (1999). *The Astrophysical Journal*, *520*, 135.

Fossum, A., & Carlsson, M. (2005). *Nature*, *435*, 919.

Froment, C., Auchère, F., Bocchialini, K., Buchlin, E., Guennou, C., & Solomon, J. (2015). *The Astrophysical Journal*, *807*, 158.

Froment, C., Auchère, F., Aulanier, G., Mikić, Z., Bocchialini, K., Buchlin, E., & Solomon, J. (2017). *The Astrophysical Journal*, *835*, 272.

Froment, C., Auchère, F., Mikić, Z., Aulanier, G., Bocchialini, K., Buchlin, E., et al. (2018). *The Astrophysical Journal*, *855*, 52.

Furth, H. P., Killeen, J., & Rosenbluth, M. N., (1963). *Physics of Fluids*, *6*, 459.

Gafeira, R., Lagg, A., Solanki, S. K., Jafarzadeh, S., van Noort, M., Barthol, P., et al. (2017). *The Astrophysical Journal Supplement*, *229*, 7.

Galsgaard, K., & Nordlund, Å. (1996). *Journal of Geophysical Research*, *101*, 13445.

Georgoulis, M. K., Rust, D. M., Bernasconi, P. N., & Schmieder, B. (2002). *The Astrophysical Journal*, *575*, 506.

Georgoulis, M. K., Velli, M., & Einaudi, G. (1998). *The Astrophysical Journal*, *497*, 957.

Glesener, L., Krucker, S., Hannah, I. G., Hudson, H., Grefenstette, B. W., White, S. M. et al. (2017). *The Astrophysical Journal*, *845*, 2.

Goedbloed, J. P. H., & Poedts, S. (2004). *Principles of Magnetohydrodynamics*. Cambridge, UK: Cambridge University Press.

Gontikakis, C., Patsourakos, S., Efthymiopoulos, C., Anastasiadis, A., & Georgoulis, M. K. (2013). *The Astrophysical Journal*, *771*, 126.

Goodman, M. L. (2011). *The Astrophysical Journal*, *735*, 45.

Goossens M., Andries J., & Arregui I. (2006). *Philosophical Transactions of the Royal Society A*, *364*, 433–446.

Goossens, M., Erdélyi, R., & Ruderman, M. S. (2011). *Space Science Reviews*, *158*, 289–338.

Goossens, M., Van Doorsselaere, T., Soler, R., & Verth, G. (2013). *The Astrophysical Journal*, *768*, 191.

Golub, L., Krieger, A.S., & Vaiana, G.S. (1975) Observation of a Non-Uniform Component in the Distribution of Coronal Bright Points. *Solar Physics 42*, 131.

Golub, L., DeLuca, E., Austin, G., Bookbinder, J., Caldwell, D., Cheimets, P., et al. (2007). *Solar Physics*, *243*, 63.

Gošić, M., de la Cruz Rodríguez, J., De Pontieu, B., Bellot Rubio, L. R., Carlsson, M., Esteban Pozuelo, S., et al. (2018). *The Astrophysical Journal*, *857*, 48.

Grant, S. D. T., Jess, D. B., Moreels, M. G., Morton, R. J., Christian, D. J., Giagkiozis, I., et al. (2015). *The Astrophysical Journal*, *806*, 132.

Grant, S. D. T., Jess, D. B., Zaqarashvili, T. V., Beck, C., Socas-Navarro, H., Aschwanden, M. J., et al. (2018) Alfvén wave dissipation in the solar chromosphere. *Nature Physics*, *14*, 480–483. https://doi.org/10.1038/s41567-018-0058-3 AQ16

Grotrian, W. (1939). Zur frage der deutung der linien im spektrum der sonnenkorona. *Naturwissenschaften*, *27*, 214.

Guennou, C., Auchère, F., Klimchuk, J. A., Bocchialini, K., & Parenti, S. (2013). *The Astrophysical Journal* , *774*, 31.

Gudiksen, B. V., Carlsson, M., Hansteen, V. H., Hayek, W., Leenaarts, J., & Martínez-Sykora, J. (2011). *Astronomy & Astrophysics*, *531*, A154. doi: 10.1051/0004-6361/201116520. AQ17

Gudiksen, B. V., & Nordlund, A. (2005). *The Astrophysical Journal*, *618*, 1020. doi: 10.1086/426063.

Guo, L.-J., Tian, H., & He, J.-S. (2010). *Research in Astronomy and Astrophysics*, *10*, 1307–1314.

Guo, M., Van Doorsselaere, T., Karampelas, K., Li, B., Antolin, P., & De Moortel, I. (2019). *The Astrophysical Journal*, *870*, 55.

Hahn, M., Landi, E., & Savin, D. W. (2012). *The Astrophysical Journal*, *753*, 36.

Hahn, M., & Savin, D. W. (2013). *The Astrophysical Journal*, *776*, 78.

Hahn, M., & Savin, D. W. (2014). *The Astrophysical Journal*, *795*, 111.

Hahn, M., & Savin, D. W. (2016). *The Astrophysical Journal*, *829*, 1.

Hannah, I. G., Hudson, H. S., Battaglia, M., et al. (2011). *Space Science Reviews*, *159*, 263. https://doi.org/10.1007/s11214-010-9705-4.

Hannah, I. G., Grefenstette, B. W., Smith, D. M., Glesener, L., Krucker, S., Hudson, H., et al (2016), *The Astrophysical Journal Letters*, *820*, L14

Hansteen, V. H., De Pontieu, B., Carlsson, M., Lemen, J., Title, A., Boerner, P., et al. (2014). *Science*, *346*, 6207. doi: 10.1126/science.1255757.

Hansteen, V. H., Archontis, V., Pereira, T. M. D., Carlsson, M., Rouppe van der Voort, L., & Leenaarts, J. (2017). *The Astrophysical Journal*, *839*, 1.

Hara, H., Watanabe, T., Harra, L. K., Culhane, J. L., Young, P. R., Mariska, J. T., et al. (2008). *The Astrophysical Journal*, *678*, L67–L71.

Harrison, R. A., Hood, A. W., & Pike, C. D. (2002). *Astronomy & Astrophysics*, *392*, 319–327.
Hassler, D. M., Rottman, G. J., Shoub, E. C., & Holzer, T. E. (1990). *The Astrophysical Journal*, *348*, L77–L80.
He, J.-S., Marsch, E., Tu, C.-Y., Guo, L.-J., & Tian, H. (2010). *Astronomy & Astrophysics*, *516*, A14.
Hendrix, D. L., & van Hoven, G. (1996). *The Astrophysical Journal*, *467*, 887.
Heyvaerts, J., & Priest, E. R. (1983). *Astronomy & Astrophysics*, *117*, 220–234.
Hollweg, J. V. (1978). *Solar Physics*, *56*, 305–333.
Hollweg, J., Jackson, S., & Gallaway, D. (1982). *Solar Physics*, *75*, 35.
Hollweg, J. V., & Sterling, A. C. (1984). *Astrophysical Journal Letters*, *282*, L31–L33.
Hollweg, J. V. (1986). *Journal of Geophysical Research*, *91*, 4111.
Hollweg, J. V., & Johnson, W. (1988). *Journal of Geophysical Research*, *93*, 9547.
Hollweg, J. V., & Yang, G. (1988). *Journal of Geophysical Research*, *93*, 5423.
Hood, A. W., Cargill, P. J., Browning, P. K., & Tam, K. V. (2016). *The Astrophysical Journal*, *817*, 5.
Hood, A. W., & Priest, E. R. (1979). *Solar Physics*, *64*, 303.
Hood, A. W., et al. (2009). *Astronomy & Astrophysics*, *506*, 913.
Hornig, G., & Priest, E. R. (2003). *Physics of Plasmas*, *10*, 2712.
Howson, T. A., De Moortel, I., Antolin, P. (2017b). *Astronomy & Astrophysics*, *607*, A77.
Howson, T. A., De Moortel, I., & Antolin, P. (2017a). *Astronomy & Astrophysics*, *602*, A74.
Huang, Y.-M., & Battacharjee, A. (2016). *The Astrophysical Journal*, *818*, 20.
Hudson, H. S. (1991). *Solar Physics*, *133*, 357
Innes, D. E., Cameron, R. H. & Solanki, S. K. (2011). *Astronomy & Astrophysics*, *531*, L13 DOI 10.1051/0004-6361/201117255
Innes, D. E., Inhester, B., Axford, W. I., & Wilhelm, K. (1997). *Nature*, *386*, 811.
Innes, D. E., Guo, L. -J., Huang, Y. -M., & Bhattacharjee, A. (2015) *The Astrophysical Journal*, *813*, 2, DOI 10.1088/0004-637X/813/2/86
Ionson, J. A. (1978). *The Astrophysical Journal*, *226*, 650–673.
Ishikawa, S., Glesener, L., Krucker, S., Christe, S., Buitrago-Casas, J. C., Narukage, N., et al. (2017). *Nature Astronomy*, *1*, 771.
Ireland, J. R., McAteer, T. J., & Inglis, A. R. (2015). *The Astrophysical Journal*, *798*, 1.
Jafarzadeh, S., Solanki, S. K., Gafeira, R., van Noort, M., Barthol, P., Blanco Rodríguez, J., et al. (2017a). *The Astrophysical Journal Supplement*, *229*, 9.
Jafarzadeh, S. Solanki, S. K., Stangalini, M., Steiner, O., Cameron, R. H., & Danilovic, S. (2017b). *The Astrophysical Journal Supplement*, *229*, 10.
James, T., & Subramanian, P. (2018). *Monthly Notices of the Royal Astronomical Society*, *479*, 1603.
Jefferies, S. M., McIntosh, S. W., Armstrong, J. D., Bogdan, T. J., Cacciani, A., & Fleck, B. (2006). *Astrophysical Journal Letters*, *648*, 151–155.
Jess, D. B., Dillon, C. J., Kirk, M. S., Reale, F., Mathioudakis, M., Grant, S. D. T., et al. (2019). *The Astrophysical Journal*, *871*, 133.
Jess, D. B., Mathioudakis, M., Erdélyi, R., Crockett, P. J., Keenan, F. P., & Christian, D. J. (2009). *Science*, *323*, 1582–1585.
Jess, D. B., Morton, R. J., Verth, G., Fedun, V., Grant, S. D. T., & Giagkiozis, I. (2015). *Space Science Reviews*, *190*, 103–161.
Jess, D. B., Shelyag, S., Mathioudakis, M., Keys, P. H., Christian, D. J., & Keenan, F. P. (2012). *The Astrophysical Journal*, *746*, 183.
Jin, M., Schrijver, C. J., Cheung, M. C. M., DeRosa, M. L., Nitta, N. V., & Title, A. M. (2016). *The Astrophysical Journal*, *820*, 16. doi: 10.3847/0004-637X/820/1/16.
Johnston, C. D., & Bradshaw, S. J. (2019). *Astrophysical Journal Letters*, *873*, L22.
Johnston, C. D., Hood, A. W., Cargill, P. J., & De Moortel, I. (2017). *Astronomy & Astrophysics*, *597*, A81.
Judge, P., (2006). Observations of the solar chromosphere. In J. Leibacher, R.F. Stein, & H. Uitenbroek (Eds.), Solar MHD theory and observations: A high spatial resolution perspective (Vol. 354, p. 259). Astronomical Society of the Pacific Conference Series, ASP, San Francisco.
Judge, P. G., Tarbell, T. D., & Wilhelm, K. (2001). *The Astrophysical Journal*, *554*, 424–444.
Kanella, C., & Gudiksen, B. V. (2019). *Astronomy & Astrophysics*, *621*, A95. doi: 10.1051/0004-6361/201833634.
Kanoh, R., Shimizu, T., & Imada, S. (2016). *The Astrophysical Journal*, *831*, 24.
Karampelas, K., Van Doorsselaere, T., & Antolin, P. (2017). *Astronomy & Astrophysics*, *604*, A130.
Karpen, J. T., & Antiochos, S. K. (2008). *The Astrophysical Journal*, *676*, 658.
Karpen, J. T., Antiochos, S. K., & Klimchuk, J. A. (2006). *The Astrophysical Journal*, *637*, 531
Katsukawa, Y., Berger, T. E., Ichimoto, K., Lites, B. W., Nagata, S., Shimizu, T., et al. (2007). *Science*, *318*, 1594.
Keys, P. H., Morton, R. J., Jess, D. B., Verth, G., Grant, S. D. T., Mathioudakis, M., et al. (2018). *The Astrophysical Journal*, *857*, 28.
Khodachenko, M. L., Arber, T. D., Rucker, H. O., & Hanslmeier, A. (2004). *Astronomy & Astrophysics*, *422*, 1073.
Khomenko, E., & Collados, M. (2012). *The Astrophysical Journal*, *747*, 87.
Khomenko, E., & Collados, M. (2015). *Living Reviews in Solar Physics*, *12*(1), 6. doi10.1007/lrsp-2015-6.
Kitagawa, N., Yokoyama, T., Imada, S., & Hara, H. (2010). *The Astrophysical Journal*, *721*, 744–749.
Klimchuk, J. A. (2000). *Solar Physics*, *193*, 53.
Klimchuk, J. A. (2006). *Solar Physics*, *234*, 41–77.
Klimchuk, J. A. (1998). Solar jets and coronal plumes. *Proceedings of an International meeting, Guadeloupe*, France, 23–26 February 1998, Publisher: Paris: European Space Agency (ESA), 1998, ESA SP-421. ISBN: 9290926848, p. 233.
Klimchuk, J. A. (2012). *Journal of Geophysical Research*, *117*, A12102. doi: 10.1029/2012JA08170.
Klimchuk, J. A. (2015). *Philosophical Transactions of the Royal Society A*, *373*, 20140256. http://dx.doi.org/10.1098/rsta.2014.0256.
Klimchuk, J. A. (2019). *Solar Physics*, *294*, 173. doi: 10.1007/s11207-019-1562-z.

Klimchuk, J. A., & Hinode Review Team (2019). "Achievements of Hinode in the First Eleven Years (Nanoflare Heating: Observations and Theory)," *Publications of the Astronomical Society of Japan*, *71*(5), R1. doi: 10.1093/pasj/psz084.

Klimchuk, J. A., & Luna, M. (2019). *The Astrophysical Journal*, *884*, 68.

Klimchuk, J. A., Patsourakos, S., & Cargill, P. J. (2008). *The Astrophysical Journal*, *682*, 1351. doi: 10.1086/589426

Knizhnik, K. J., Uritsky, V. M., Klimchuk, J. A., & DeVore, C. R. (2018). *The Astrophysical Journal*, *853*, 82.

Knizhnik, K. J., Antiochos, S. K., Klimchuk, J. A., & DeVore, C. R. (2019). *The Astrophysical Journal*, *883*, 26.

Ko, Y.-K., Young, P. R., Muglach, K., Warren, H. P., & Ugarte-Urra, I. (2016). *The Astrophysical Journal*, *826*, 126.

Kochhar, R. K. (1991). *Journal of the British Astronomical Association*, *101*(2), 95–100.

Krieger, A. S., Timothy, A. F., & Roelof, E. C. (1973). A coronal hole and its identification as the source of a high velocity solar wind stream. *Solar Physics*, *29*, 505.

Krishna Prasad, S., Banerjee, D., & Gupta, G. R. (2011). *Astronomy & Astrophysics*, *528*, L4.

Krishna Prasad, S., Jess, D. B., Van Doorsselaere, T., Verth, G., Morton, R. J., Fedun, V. et al. (2017). *The Astrophysical Journal*, *847*, 5.

Krucker, S., & Benz, A.O. (1998). *Astrophysical Journal Letters*, *501*, L213.

Kudoh, T., & Shibata, K. (1999). *The Astrophysical Journal*, *514*, 493.

Kuhar, M., Krucker, S., Glesener, L., Hannah, I. G., Grefenstette, B. W., Smith, D. M. et al. (2018). *Astrophysical Journal Letters*, *856*, 2.

Kuperus, M. (1969). The Heating of the Solar Corona. *Space Science Reviews, 9*, 713.

Kuridze, D., Verth, G., Mathioudakis, M., Erdélyi, R., Jess, D. B., Morton, R. J., et al. (2013). *The Astrophysical Journal*, *779*, 82.

Kuridze, D., Morton, R. J., Erdélyi, R., Dorrian, G. D., Mathioudakis, M., Jess, D. B., et al. (2012). *The Astrophysical Journal*, *750*, 51.

Laming, M. J. (2015). *Living Reviews in Solar Physics*, 12(2). doi 10.1007/lrsp-2015-2.

Leake, J. E., Arber, T. D., & Khodachenko, M. L. (2005). *Astronomy & Astrophysics*, *442*, 1091.

Leake, J. E., Daldorff, L. K. S., & Klimchuk, J. A., (2020), *The Astrophysical Journal*, *891*, 62.

Lee, M. A., & Roberts, B. (1986). *The Astrophysical Journal*, *301*, 430.

Lenz, D. D., DeLuca, E. E., Golub, L., Rosner, R., & Bookbinder, J. A. (1999). Temperature and emission-measure profiles along long-lived solar coronal loops observed with the transition region and coronal explorer. *The Astrophysical Journal*, *517*, L155.

Lin, R. P., Schwartz, R. A., Kane, S. R., Pelling, R. M., & Hurley, K. C. (1984). *The Astrophysical Journal*, *283*, 421

Lionello, R., Linker, J. A., & Mikic´, Z. (2009). *The Astrophysical Journal*, *690*, 902. doi: 10.1088/0004-637X/690/1/902.

Lionello, R., Velli, M., Downs, C., Linker, J. A., Mikić, Z., & Verdini, A. (2014). *The Astrophysical Journal*, *784*, 120. doi: 10.1088/0004-637X/784/2/120.

Liu, J., McIntosh, S. W., De Moortel, I., Threlfall, J., & Bethge, C. (2014). *The Astrophysical Journal*, *797*, 7.

Longbottom, A. W., Rickard, G. J., Craig, I. J. D., & Sneyd, A. D. (1998). Magnetic flux braiding: Force-free equilibria and current sheets. *The Astrophysical Journal*, *500*, 471–482. doi:10.1086/305694.

López Fuentes, M., & Klimchuk, J. A. (2015). *The Astrophysical Journal*, *799*, 128.

Lu, E. T., Hamilton, R. J., McTiernan, J. M., & Bromund, K. R. (1993). *The Astrophysical Journal*, *412*, 841.

Luna, M., Karpen, J. T., & DeVore, C. R. (2012). *The Astrophysical Journal*, *746*, 30.

Lundquist, L. L., Fisher, G. H., Metcalf, T. R., Leka, K. D., & McTiernan, J. M. (2008). *The Astrophysical Journal*, *689*, 1388. doi: 10.1086/592760.

Magyar, N., Van Doorsselaere, T., Goossens, M. (2017). *NatSR*, *7*, 14820.

Mariska, J. T., & Muglach, K. (2010). *The Astrophysical Journal*, *713*, 573–583.

Martens, P. C. H., Kankelborg, C. C., & Berger, T. E. (2000). *The Astrophysical Journal*, *537*, 471.

Mandrini, C. H., De´moulin, P., & Klimchuk, J. A. (2000). *The Astrophysical Journal*, *530*, 999. doi: 10.1086/308398.

Marsh, M. S., De Moortel, I., & Walsh, R. W. (2011). *The Astrophysical Journal*, *734*, 81.

Marsh, A. J., Smith, D. M., Glesener, L., Klimchuk, J. A., Bradshaw, S. J., Vievering, J., et al. (2018). *The Astrophysical Journal*, *864*, 5. DOI https://doi.org/10.3847/1538-4357/aad380

Martinez-Sykora, J., De Pontieu, B., Hansteen. V. H., Rouppe van der Voort, L., Carlsson, M., & Pereira, T. M. D. (2017). *Science*, *356*, 1269.

Martinez-Sykora, J., Rouppe van der Voort, L., Carlsson, M., De Pontieu, B., Pereira, T. M. D., Boerner, P., et al. (2015). *The Astrophysical Journal*, *803*, 44.

Mason, E. I., Antiochos, S. K., and Viall, N. M. (2019). *Astrophysical Journal Letters*, *874*, L33.

Moraitis, K., Toutountzi, A., Isliker, H., Georgoulis, M., Vlahos, L., & Chintzoglou, G. (2016). *Astronomy & Astrophysics*, *596*, 56.

Matthaeus, W. H., & Velli, M. (2011). *Space Science Reviews*, *160*, 145.

Matthaeus, W. H., Zank, G. P., Oughton, S., Mullan, D. J., & Dmitruk, P. (1999). *The Astrophysical Journal*, *523*, L93–L96.

Mathioudakis, M., Jess, D. B., & Erdélyi, R. (2013). *Space Science Reviews*, *175*, 1–27.

Matsumoto, T., & Suzuki, T. K. (2012). *The Astrophysical Journal*, *749*, 8.

Matsumoto, T., & Suzuki, T. K. (2014). *Monthly Notices of the Royal Astronomical Society*, *440*, 971.

McClements, K. G., Harrison, R. A., & Alexander, D. (1991). *Solar Physics*, *131*, 41.

McIntosh, S. W., De Pontieu, B., Carlsson, M., Hansteen, V., Boerner, P., & Goossens, M. (2011). *Nature*, *475*, 477–480.

McIntosh, S. W., & De Pontieu, B. (2012). *The Astrophysical Journal*, *761*, 138.

Mellow, C., Gerrard, C. L., Galsgaard, K., Hood, A. W., & Priest, E. R. (2005). Numerical simulations of the flux tube

tectonics model for coronal heating. *Solar Physics*, *227*, 39–60. doi:10.1007/s11207-005-1713-2.

Mendoza-Briceño, C. A., Sigalotti, L. D. G., & Erdélyi, R. (2005). *The Astrophysical Journal*, *624*, 1080–1092.

Mendoza-Briceño, C. A., & Erdélyi, R. (2006). *The Astrophysical Journal*, *648*, 722–731.

Meyer, K. A., Sabol, J., Mackay, D. H., & van Ballegooijen, A. A. (2013). *The Astrophysical Journal*, *770*, 18.

Mikić, Z., Schnack, D. D., & van Hoven, G. (1989). *The Astrophysical Journal*, *338*, 1148.

Mikić, Z., Lionello, R., Mok, Y., Linker, J. A., & Winebarger, A. R. (2013). *The Astrophysical Journal*, *773*, 94.

AQ18 Mikić, Z., Downs, C., Linker, J. A., Caplan, R. M., Mackay, D. H., Upton, L. A., et al. (2018). *Nature Astronomy*, *2*, 913. doi: 10.1038/s41550-018-0562-5.

Mok, Y., Mikić, Z., Lionello, R., Downs, C., & Linker, J. A. (2016). *The Astrophysical Journal*, *817*, 15. doi: 10.3847/0004-637X/817/1/15.

Moriyasu, S., Kudoh, T., Yokoyama, T., & Shibata, K. (2004). *The Astrophysical Journal*, *601*, L107–L110.

Morton, R. J., Erdélyi, R., Jess, D. B., & Mathioudakis, M. (2011). *The Astrophysical Journal*, *729*, L18.

Morton, R. J., & McLaughlin, J. A. (2013). *Astronomy & Astrophysics*, *553*, L10.

Morton, R. J., Tomczyk, S., & Pinto, R. F. (2015). *Nature Communications*, *6*, 7813.

Morton, R. J., Tomczyk, S., & Pinto, R. F. (2016). *The Astrophysical Journal*, *828*, 89.

Morton, R. J., Weberg, M. J., & McLaughlin, J. A. (2019). *Nature Astronomy*, ~~in press~~.

Morton, R. J., Verth, G., Jess, D. B., Kuridze, D., Ruderman, M. S., Mathioudakis, M. et al. (2012). *Nature Communications*, *3*, 1315.

Morton, R. J., Verth, G., Hillier, A., & Erdélyi, R. (2014). *The Astrophysical Journal*, *784*, 29.

Müller, D. A. N., Peter, H., & Hansteen, V. H. (2004). Catastrophic cooling and high-speed downflows in solar coronal loops. In A. K. Dupree & A. O. Benz (Eds.), *Stars as Suns: Activity, evolution and planets: Proceedings of the 219th symposium of the International Astronomical Union held during the IAU General Assembly XXV*, Sydney, Australia, 21–25 July 2003. San Francisco, CA: Astronomical Society of the Pacific (ASP).

Müller, D. A. N., De Groof, A., Hansteen, V. H., & Peter, H. (2005). *Astronomy & Astrophysics*, *436*, 1067.

Narain, U., & Ulmschneider, P. (1990). *Space Science Reviews*, *54*, 377.

Narain, U., & Ulmschneider, P. (1996). *Space Science Reviews*, *75*, 453.

Nakariakov, V. M., Ofman, L., DeLuca, E. E., Roberts, B., & Davila, J. M. (1999). *Science*, *285*, 862–864.

Nakariakov, V. M., & Verwichte, E. (2005). *Living Reviews in Solar Physics*, 2(3).

AQ19 Nita, G. M., Viall, N. M., Klimchuk, J. A., Loukitcheva, M. A., Gary, D. E., Kuznetsov, A. A., et al. (2018). *The Astrophysical Journal*, *853*, 66. doi: 10.3847/1538-4357/aaa4bf.

Ofman, L., Davila, J. M., & Steinolfson, R. S. (1994). *GeoRL*, *21*, 2259.

Ofman, L., Davila, J. M., & Steinolfson, R. S. (1995). *The Astrophysical Journal*, *444*, 471–477.

Ofman, L., Klimchuk, J. A., & Davila, J. M. (1998). *The Astrophysical Journal*, *493*, 474.

Ofman, L., Romoli, M., Poletto, G., Noci, G., & Kohl, J. L. (1997). *The Astrophysical Journal*, *491*, L111.

Okamoto, T. J., Tsuneta, S., Berger, T. E., Ichimoto, K., Katsukawa, Y., Lites, B. W., et al. (2007). *Science*, *318*, 1577.

Okamoto, T.J., De Pontieu, B. (2011), *The Astrophysical Journal*, *736*, 24, doi:10.1088/2041-8205/736/2/L24

Okamoto, T. J., Antolin, P., De Pontieu, B. Uitenbroek, H., Van Doorsselaere, T., & Yokoyama, T. (2015) *The Astrophysical Journal*, *809*, 71, doi 10.1088/0004-637X/809/1/71

Oran, R., Landi, E., van der Holst, B., Lepri, S. T., Vásquez, A. M., Nuevo, F. A., et al. (2015). *The Astrophysical Journal*, *806*, 55, doi: 10.1088/0004-637X/806/1/55

O'Shea, E., Banerjee, D., & Poedts, S. (2003). *Astronomy & Astrophysics*, *400*, 1065.

Pagano, P., & De Moortel, I. (2017). *Astronomy & Astrophysics*, *601*, A107.

Pagano, P., Pascoe, D. J., & De Moortel, I. (2018). *Astronomy & Astrophysics*, *616*, 125.

Pagano, P., & De Moortel, I. (2019). *Astronomy & Astrophysics*, *623*, A37.

Palmieri, L. (1881). La riga dell'Helium apparsa in una recente sublimazione vesuviana [The line of helium appeared in a recently sublimated material [from Mt.] Vesuvius.]. *Rendiconto dell'Accademia delle Scienze Fisiche e Matematiche* (Naples, Italy), *20*, 223, retrieved June 2019.

Parenti, S., del Zanna, G., Petralia, A., Reale, F., Teriaca, L., Testa, P., et al. (2017), *The Astrophysical Journal*, *846*, 25.

Parenti, S., Buchlin, E., Cargill, P. J., Galtier, S., & Vial, J.-C. (2006). *The Astrophysical Journal*, *651*, 1219.

Parenti, S., & Young, P. R. (2008), *Astronomy and Astrophysics*, *492*, 857. doi: 10.1051/0004-6361:200809928

Parker, E. N. (1988). Nanoflares and the Solar X-ray corona. *The Astrophysical Journal, 330*, 474.

Parker, E. N. (1991). *The Astrophysical Journal*, *376*, 355.

Parnell, C. E., & De Moortel, I. (2012). *Philosophical Transactions of the Royal Society A*, *370*, 3217–3240.

Parnell, C. E. & Galsgaard, K. (2004) *Astronomy and Astrophysics*, *428*, 595. doi: 10.1051/0004-6361:20034350

Parnell, C. E., & Jupp, P. E. (2000), *The Astrophysical Journal*, *529*, 554.

Parnell, C. E. & Priest, E. R. (1995), *Geophysical and Astrophysical Fluid Dynamics*, *80*, 255 DOI: 10.1080/03091929508228958

Patsourakos, S., & Klimchuk, J. A.(2006). *The Astrophysical Journal*, *647*, 1452.

Patsourakos, S., & Klimchuk, J. A. (2009). *The Astrophysical Journal*, *696*, 760.

Peter, H. (2010). *Astronomy & Astrophysics*, *521*, A51.

Peter, H., & Dwivedi, B. N. (2014). *Frontiers in Astronomy and Space Sciences*, *1*, 2. doi: 10.3389/fspas.2014.00002.

Peter, H., & Judge, P. G. (1999). *The Astrophysical Journal*, *522*, 1148.

Peter, H., Tian, H., Curdt, W., Schmit, D., Innes, D., De Pontieu, B., et al. (2014). *Science*, *346*, 6207. doi: 10.1126/science.1255726

Peres G., & Vaiana, G. S. (1990) . X-ray observations, scaling laws and magnetic fields. *Memorie della Societa Astronomica Italiana 61*, 401.
Poedts S., Goossens M., & Kerner W. (1989). *Solar Physics*, *123*, 83–115.
Poedts, S., Goossens, M., & Kerner, W. (1990). *The Astrophysical Journal*, *360*, 279–287.
Pontin, D. I., Galsgaard, K., Hornig, G., & Priest, E. R., (2005). *Physics of Plasmas*, *12*, 052307.
Porter, L. J., Klimchuk, J. A., & Sturrock, P. A. (1994). *The Astrophysical Journal*, *435*, 482–501.
Porter, L. J., & Klimchuk, J. A. (1995). *The Astrophysical Journal*, *454*, 499.
Poletto, G., Vaiana, G. S., Zombeck, M. V., Krieger, A. S., & Timothy, A. F. (1975). a comparison of coronal X-ray structures of ARs with magnetic fields computed from photospheric observations. *Solar Physics, 44*, 83.
Priest, E. R., & De'moulin, P. (1995). *Journal of Geophysical Research*, *100*, 23,443–23,463.
Priest, E. R., Parnell, C. E., & Martin, S. F. (1994). *The Astrophysical Journal*, *427*, 459. doi: 10.1086/174157
Priest, E. R. (1996). Coronal heating by magnetic reconnection. *Astrophysics and Space Science, 237*, 49.
Priest, E. R. (1999). Heating the solar corona by magnetic reconnection. *Astrophysics and Space Science*, *264*, 77.
Priest, E. R., & Forbes, T. G. (2000). *Magnetic Reconnection*. Cambridge University Press.
Priest, E. R., Hornig, G., & Pontin, D. I. (2003). *Journal of Geophysical Research*, *108*, 1285.
Priest, E. R., Chitta, L. P., & Syntelis, P. (2018). *Astrophysical Journal Letters*, *862*(2), L24.
Priest, E. R., Heyvaerts, J. F., & Title, A. M. (2002). A flux-tube tectonics model for solar coronal heating driven by the magnetic carpet. *The Astrophysical Journal*, *576*, 533–551. doi:10.1086/341539.
Pereira, T. M. D., Rouppe van der Voort, L., Hansteen, V. H., & De Pontieu, B. (2018). *Astronomy & Astrophysics*, *611*, L6, 4.
Rappazzo, A. F., Velli, M., Einaudi, G., & Dahlburg, R. B. (2008). *The Astrophysical Journal*, *677*, 1348.
Rappazzo, A. F., Velli, M., & Einaudi, G. (2010). *The Astrophysical Journal*, *722*, 65.
Rajaguru, S. P., Sangeetha, C. R., & Tripathi, D. (2019). *The Astrophysical Journal*, *871*, 155.
Reale, F., & Ciaravella, A. (2006), *Astronomy and Astrophysics*, *449*, 1177.
Reale, F., Orlando, S., Guarrasi, M., Mignone, A., Peres, G., Hood, A. W., et al. (2016). *The Astrophysical Journal*, *830*(1), article id. 21, 15 pp.
Reale, F., Parenti, S., Reeves, K. K., Weber, M., Bobra, M. G., Barbera, M., et al. (2007). *Science*, *318*, 1582.
Reale, F., Testa, P., Klimchuk, J. A., & Parenti, S., (2009b). *The Astrophysical Journal*, *698*, 756.
Reale, F. (2014). *Living Reviews in Solar Physics*, *11*, 4
Reale, F., McTiernan, J. M., & Testa, P. (2009a). *The Astrophysical Journal Letters*, *704*, L58
Reale, F., Nigro, G., Malara, F., Peres, G., & Veltri, P. (2005), *The Astrophysical Journal*, *633*, 489.
~~Reale, F. (2014). *Living Reviews in Solar Physics*, *11*, 4.~~
Reep, J. W., Bradshaw, S. J., & Klimchuk, J. A. (2013). *The Astrophysical Journal*, *764*, 193.
Reid, A., Mathioudakis, M., Doyle, J. G., Scullion, E., Nelson, C. J., Henriques, V., et al. (2016). *The Astrophysical Journal*, *823*, 110.
Rempel, M. (2017). *The Astrophysical Journal*, *834*, 10. doi: 10.3847/1538-4357/834/1/10.
Robbrecht, E., Verwichte, E., Berghmans, D., Hochedez, J. F., Poedts, S., & Nakariakov, V. M. (2001). *Astronomy & Astrophysics*, *370*, 591–601.
Roberts, B., Edwin, P. M., & Benz, A. O. (1984). On coronal oscillations. *The Astrophysical Journal*, *279*, 857–865.
Rosenberg, H. (1970). *Astronomy & Astrophysics*, *9*, 159.
Rosner, R., Tucker, W. H., & Vaiana, G. S. (1978). Dynamics of the quiescent solar corona. *The Astrophysical Journal*, *220*, 643.
Rouppe van der Voort, L., de Pontieu, B., Pereira, T. M. D., Carlsson, M., & Hansteen, V. (2015). *Astrophysical Journal Letters*, *799*, L3.
Rouppe van der Voort, L., De Pontieu, B., Scharmer, G. B., de la Cruz Rodríguez, J., Martínez-Sykora, J., Nóbrega-Siverio, D., et al. (2017). *Astrophysical Journal Letters*, *851*, 1.
Rouppe van der Voort, L. H. M., Rutten, R. J. & Vissers, G. J. M. (2016), *Astronomy & Astrophysics*, *592*, 100, DOI: 10.1051/0004-6361/201628889
Ruderman, M. S., & Roberts, B. (2002). *The Astrophysical Journal*, *577*, 475.
Ruderman, M. S., & Erdélyi, R. (2009). *Space Science Review*, *149*, 199–228.
Ruderman, M. S., Berghmans, D., Goossens, M., & Poedts, S. (1997a). *Astronomy & Astrophysics*, *320*, 305–318.
Ruderman, M. S., Goossens, M., Ballester, J. L., & Oliver, R. (1997b). *Astronomy & Astrophysics*, *328*, 361–370.
Sakao, T., Kano, R., Narukage, N., Kotoku, J., Bando, T., DeLuca, E. E., et al. (2007). *Science*, *318*, 1585–1588.
Sakurai, T., Ichimoto, K., Raju, K. P., & Singh, J. (2002). *Solar Physics*, *209*, 265.
Sakamoto, Y., Tsuneta, S., & Vekstein, G. (2008), *The Astrophysical Journal*, *689*, 1421.
Schmelz, J. T., Christian, G. M., & Matheny, P. O. (2016). *The Astrophysical Journal*, *833*, 2.
Schmelz, J. T., Scopes, R. T., Cirtain, J. W., Winter, H. D., & Allen, J. D. (2001). *The Astrophysical Journal*, *556*, 896S.
Schrijver, C. J. (2001). *Solar Physics*, *198*, 325. doi: 10.1023/A:1005211925515
Schrijver, C. J., Title, A. M., Berger, T. E., Fletcher, L., Hurlburt, N. E., Nightingale, R. W., et al. (1999). *Solar Physics*, *187*, 261.
Schrijver, C. J., Sandman, A. W., Aschwanden, M. J., & De Rosa, M. L. (2004). *The Astrophysical Journal*, *615*, 512. doi: 10.1086/424028.
Schwarzschild, M. (1948). *The Astrophysical Journal*, *107*, 1.
Skogsrud, H., Rouppe van der Voort, L., De Pontieu, B., & Pereira, T. M. D. (2015). *The Astrophysical Journal*, *806*, 170.
Shibata, K., Nakamura, T., Matsumoto, T., Otsuji, K., Okamoto, T. J., Nishizuka, N., et al. (2007). *Science*, *318*, 5856, 1591. https://doi.org/10.1126/science.1146708.
Shibasaki, K., Alissandrakis, C. E., & Pohjolainen, S. (2011). *Solar Physics*, *273*, 309. https://doi.org/10.1007/s11207-011-9788-4

Song, P., & ~~Vasylunas~~, V. M. (2011). *Journal of Geophysical Research*, *116*, A09104.

Song, D., Chae, J., Kwak, H., Kano, R., Yurchyshyn, V., Moon, Y.-J., et al. (2017). *Astrophysical Journal Letters*, *850*, 2, L33. doi10.3847/2041-8213/aa9a36.

Sokolov, I. V., van der Holst, B., Oran, R., Downs, C., Roussev, I. I., Jin, M., et al. (2013). *The Astrophysical Journal*, *764*, 23.

AQ20 Spitzer, L. (1962). *Physics of Fully Ionized Gases*.

Stangalini, M., Giannattasio, F., Erdélyi, R., Jafarzadeh, S., Consolini, G., Criscuoli, S., et al. (2017). *The Astrophysical Journal*, *840*, 19.

Stein, R. F., & Leibacher, J. (1974). Waves in the solar atmosphere. *Annual Review of Astronomy and Astrophysics*, *12*, 407–435.

Saint-Hilaire, P., Vilmer, N., & Kerdraon, A. (2013). *The Astrophysical Journal*, *762*, 1.

Suzuki, T. K., & Inutsuka, S. (2005). *The Astrophysical Journal*, *632*, L49–L52.

Syntelis, P., Priest, E. R., & Chitta, L. P. (2019). *The Astrophysical Journal*, *872*, 32.

Tam, K. V., Hood, A. W., Browning, P. K., & Cargill, P. J. (2015). *Astronomy & Astrophysics*, *580*, 122.

Taroyan, Y., Erdélyi, R., Doyle, J. G., & Bradshaw, S. J. (2007). *Astronomy & Astrophysics*, *462*, 331–340.

Taroyan, Y., & Erdélyi, R. (2009). *Space Science Reviews*, *149*, 229–254.

Tataronis, J. A., & Grossman, W. (1973). *Zeitschrift für Physik*, *261*, 203.

Terradas, J., Andries, J., Goossens, M., Arregui, I., Oliver, R., & Ballester, J. L. (2008). *Astrophysical Journal Letters*, *687*, L115.

Terzo, S., Reale, F., Miceli, M., Klimchuk, J. A., Kano, R., & Tsuneta, S. (2011), *The Astrophysical Journal*, *736*, 111.

Testa, P., Reale, F., Landi, E., DeLuca, E. E., & Kashyap, V. (2011), *The Astrophysical Journal*, *728*, 30

Testa, P., De Pontieu, B., Allred, J., Carlsson, M., Reale, F., Daw, A., et al. (2014). Evidence of nonthermal particles in coronal loops heated impulsively by nanoflares. *Science*, *346*, 1255724 doi: 10.1126/science.1255724.

Thurgood, J. O., Morton, R. J., & McLaughlin, J. A. (2014). *Astrophysical Journal Letters*, *790*, L2.

Tian, H., McIntosh, S. W. & De Pontieu, B. (2011). *The Astrophysical Journal*, *727*, L37.

Tian, H., Delica, E. E., Cranmer, S. R., De Pontieu, B., Peter, H. Martinez-Sykora, J., et al. (2014). *Science*, *346B*, 315.

Tian, H., Zhu X., Peter, H., Zhao, J., Samanta, T., & Chen, Y. (2018) *The Astrophysical Journal, 854*, 2, doi10.3847/1538-4357/aaaae6

Titov V. S. (2007) *The Astrophysical Journal*, *660*, 863

Titov, V. S., Hornig, G., & Démoulin, P. (2002). Theory of magnetic connectivity in the solar corona. *Journal of Geophysical Research*, *107*, 1164. doi:10.1029/2001JA000278.

Tomczyk, S., & McIntosh, S. W. (2009). *The Astrophysical Journal*, *697*, 1384–139.

Tomczyk, S., McIntosh, S. W., Keil, S. L., Judge, P. G., Schad, T., Seeley, D. H., et al. (2007). *Science*, *317*, 1192.

Tripathi, D., Mason, H. E., Dwivedi, B. N., Del Zanna, G., & Young, P. R. (2009). *The Astrophysical Journal*, *694*, 1256.

Trottet, G., Pick, M., & Heyvaerts, J. (1979). *Astronomy & Astrophysics*, *79*, 164–168.

Tsubaki, T. (1988). Observations of periodic oscillations or waves in the solar corona and prominences. In Solar and stellar coronal structure and dynamics. *Proceedings of the Ninth Sacramento Peak Summer Symposium*, Sunspot, NM, 17–21 August 1987, pp. 140–149. Sunspot, NM: National Solar Observatory.

Tucker, W. H. (1973). *The Astrophysical Journal*, *186*, 285.

Tu, J., & Song, P. (2013). *The Astrophysical Journal*, *777*, 53.

Uchida, Y. (1970). *Publications of the Astronomical Society of Japan*, *22*, 341–364.

Uchimoto, E., Strauss, H. R., & Lawson, W. S. (1991). *Solar Physics*, *134*, 111.

Ugarte-Urra, I., & Warren, H. P. (2012). *The Astrophysical Journal*, *761*, 21.

Ugarte-Urra, I., & Warren, H. P. (2011). *The Astrophysical Journal*, *730*, 37.

Ugarte-Urra, I., Warren, H. P., Upton, L. A., & Young, P. R. (2017). *The Astrophysical Journal*, *846*, 165. doi: 10.3847/1538-4357/aa8597.

Ugarte-Urra, I., Warren, H. P., & Brooks, D. H. (2009), *The Astrophysical Journal*, *695*, 642.

Usmanov, A. V., Matthaeus, W. H., Goldstein, M. L., & Chhiber, R. (2018). *The Astrophysical Journal*, *865*, 25. doi: 10.3847/1538-4357/aad687

Vaiana, G. S., Reidy, W. P., Zehnpfennig, T., van Speybroeck, L., Giacconi, R. (1968). X-ray structures of the Sun during the importance 1N Flare of 8 June 1968. *Science 161*, 564.

Vaiana, G. S., Krieger, A. S., Timothy, A. F. (1973). Identification and Analysis of Structures in the Corona from X-Ray Photography. *Solar Physics 32*, 81.

van Ballegooijen, A. A. (1988a). Force free fields and coronal heating Part 1. The formation of current sheets. *Geophysical & Astrophysical Fluid Dynamics*, *41*, 181–211. doi:10.1080/03091928808208850.

van Ballegooijen, A. A., Asgari-Targhi, M., Cranmer, S. R., & DeLuca, E. E. (2011). *The Astrophysical Journal*, *736*, 3.

van Ballegooijen A. A., Asgari-Targhi M., & Berger M. A. (2014). *The Astrophysical Journal*, *787*, 87.

van Ballegooijen, A. A., Asgari-Targhi, M., & Voss, A. (2017). *The Astrophysical Journal*, *849*, 46.

van der Holst, B., Sokolov, I. V., Meng, X., Jin, M., Manchester, W. B., IV, Tóth, G., & Gombosi, T. I. (2014). *The Astrophysical Journal*, *782*, 81. doi: 10.1088/0004-637X/782/2/81.

Vanspeybroeck, L. P., Krieger, A. S., & Vaiana, G. S. (1970). *Nature*, *227*, 818. https://doi.org/10.1038/227818a0.

Verdini, A., & Velli, M. (2007). *The Astrophysical Journal*, *662*, 669–676.

Vernazza, J. E., Foukal, P. V., Noyes, R. W., Reeves, E. M., Schmahl, E. J., Timothy, J. G., et al. (1975). *The Astrophysical Journal Letters*, *199*, L123–L126.

Verwichte, E., Marsh, M., Foullon, C., Van Doorsselaere, T., De Moortel, I., Hood, A. W., et al. (2010). *The Astrophysical Journal*, *724*, L194–L198.

Viall, N. M., & Klimchuk, J. A. (2011). *The Astrophysical Journal*, *738*, 24.

Viall, N. M., & Klimchuk, J. A. (2012). *The Astrophysical Journal*, *753*, 35. doi: 10.1088/0004-637X/753/1/35.

Viall, N. M., Klimchuk, J. A. (2015). *The Astrophysical Journal*, *799*, 58.
Viall, N. M., & Klimchuk, J. A. (2016). *The Astrophysical Journal*, *828*, 76.
Viall, N. M., & Klimchuk, J. A. (2017). *The Astrophysical Journal*, *842*, 108.
Vlahos, L., Georgoulis, M., Kluiving, R., & Paschos, P. (1995). *Astronomy & Astrophysics*, *299*, 897.
Vlahos, L., Pisokas, T., Isliker, H., Tsiolis, V., & Anastasiadis, A. (2016). *The Astrophysical Journal*, *827L*, 3.
Vourlidas, A., Klimchuk J. A., Korendyke, C. M., Tarbell, T. D., & Handy, B. N. (2001). *The Astrophysical Journal*, *563*, 374.
Vourlidas, A., Sanchez Andrade-Nuño, B., Landi, E., Patsourakos, S., Teriaca, L., Schühle, U., et al. (2010). *Solar Physics*, *261*, 53. doi: 10.1007/s11207-009-9475-x
Walsh, R. W., & Ireland, J. (2003). *The Astronomy and Astrophysics Review*, *12*, 1.
Walsh, R. W., & Galtier, S. (2000). *Solar Physics*, *197*, 57.
Wang, T. J., Ofman, L., Davila, J. M., & Mariska, J. T. (2009). *Astronomy & Astrophysics*, *503*, L25–L28.
Warren, H. P., & Winebarger, A.R. (2006) *The Astrophysical Journal*, *645*, 711.
Warren, H. P., Brooks, D. H., & Winebarger, A. R. (2011), *The Astrophysical Journal*, *734*, 90.
Warren, H. P., Ugarte-Urra, I., & Landi, E. (2014), *The Astrophysical Journal Supplement Series*, *213*, 11.
Warren, H. P., Winebarger, A. R., & Brooks, D. H. (2012), *The Astrophysical Journal*, *759*, 141.
Warren, H. P., Ugarte-Urra, I., Doschek, G. A., Brooks, D. H., & Williams, D. R. (2008). *The Astrophysical Journal*, *686*, 131.
Wedemeyer, S., Bastian, T., Brajša, R., Hudson, H., Fleishman, G., Loukitcheva, M., et al. (2016). *Space Science Reviews*, *200*, 1.
Wedemeyer-Böhm, S., & Rouppe van der Voort, L. (2009). *Astronomy & Astrophysics*, *507*, L9.
Wedemeyer-Böhm, S., & Wöger, F. (2008). Small-scale structure and dynamics of the lower solar atmosphere. *In IAU Symposium*, vol. *247*, pp. 66–73
Wedemeyer-Böhm, S., Lagg, A., & Nordlund, A. (2009). *Space Science Reviews*, *144*(1), 317. doi10.1007/s11214-008-9447-8
Wentzel, D. G. (1974). *Solar Physics*, *39*, 129–140.
Wentzel, D. G. (1976). *Solar Physics*, *50*, 343–360.
Wiegelmann, T., Thalmann, J. K., & Solanki, S. K. (2014). The magnetic field in the solar atmosphere. *The Astronomy and Astrophysics Review*, *22*(1), 78. doi10.1007/s00159-014-0078-7.
Wiegelmann, T., & Sakurai, T. (2012). *Living Reviews in Solar Physics*, 9(5). https://doi.org/10.12942/lrsp-2012-5.
Wiegelmann, T., Solanki, S. K., Borrero, J. M., Peter, H., Barthol, P., Gandorfer, A., et al. (2013). *Solar Physics*, *283*, 253.
Wikstøl, Ø., Hansteen, V. H., Carlsson, M., & Judge, P. G. (2000). *The Astrophysical Journal*, *531*, 1150–1160.
Wilhelm, K., Dwivedi, B. N., & Teriaca, L. (2004). *Astronomy & Astrophysics*, *415*, 1133.
Wilmot-Smith, A. L. (2015). An overview of flux braiding experiments. *Philosophical Transactions of the Royal Society A: Mathematical, Physical and Engineering Sciences. 373*, 20140265, http://doi.org/10.1098/rsta.2014.0265.
Wilmot-Smith, A. L., Pontin, D. I., Yeates, A. R., & Hornig, G. (2011). Heating of braided coronal loops. *Astronomy & Astrophysics*, *536*, A67. doi:10.1051/0004-6361/201117942.
Wilmot-Smith, A. L., & De Moortel, I. (2007). Magnetic reconnection in flux tubes undergoing spinning footpoint motions. *Astronomy & Astrophysics*, *473*, 615–623. doi:10.1051/0004-6361:20077455.
Winebarger, A. R., Lionello, R., Downs, C., Mikić, Z., Linker, J., & Mok, Y. (2016). *The Astrophysical Journal*, *831*, 172. doi: 10.3847/0004-637X/831/2/172.
Winebarger, A. R., & Warren, H.P. (2005). *The Astrophysical Journal*, *626*, 543.
Withbroe, G. L., & Noyes, R. W. (1977). Mass and energy flow in the solar chromosphere and corona. *Annual Review of Astronomy and Astrophysics*, *15*, 363–387.
Wright, P. J., Hannah, I. G., Grefenstette, B. W., Glesener, L., Krucker, S., Hudson, H. S., et al. (2017). *The Astrophysical Journal*, *844*, 2.
Yang, S. H., Zhang, J., Jin, C. L., Li, L. P., & Duan, H. Y. (2009). *Astronomy & Astrophysics*, *501*(2), 745–753.
~~Yung, M., Mikić, Z., Lionello, R., Downs, C., & Linker, J. A. (2016). *The Astrophysical Journal*, *817*, 15.~~
Zaqarashvili, T. V. (2003). *Astronomy & Astrophysics*, *399*, L15.
Zaqarashvili, T. V., & Erdélyi, R. (2009). *Space Science Reviews*, *149*, 355.
Zirker, J. B. (1993). *Solar Physics*, *148*, 43.